MONTANA STATE UNIVERSITY

Determination of elastic and optical properties of thin plates and investigation of the mechanisms involved in the laser generation of ultrasound
by David Howard Hurley

A thesis submitted in partial fulfillment of the requirements for the degree of Master of Science in Mechanical Engineering
Montana State University

Abstract:
The focus of this paper is two-fold. First, the shear wave velocity, Poisson's ratio, and optical absorption coefficient of a thin glass plate will be estimated using a Nd: YAG pulsed laser. Second, the combined influence that an ablative and thermoelastic source has on the elastic wave form generated by a pulsed laser will be investigated.

Thermoelastic waves are introduced into a sample when a portion of the laser's energy is optically absorbed along the depth of the specimen causing a steep thermal gradient. Neglecting the effects of heat conduction, the thermoelastic displacements are determined by solving the uncoupled displacement equations of thermoelasticity.

As the laser's energy is increased, a thin layer of atoms at the sample's surface is vaporized. The momentum transferred to the sample from the vaporized atoms constitutes the second generation mechanism and is termed ablation. The ablative mechanism, which is modeled as a normal force, in conjunction with the differential equations of isothermal elasticity is used to determine the displacement due to ablation.

The stress free boundary conditions of both the thermoelastic and ablative problems lead to the Rayleigh-Lamb frequency equation, the solution of which represents the various modes of propagation present in an infinite plate. For a given frequency bandwidth there is a plate thickness below which only the first symmetric (s0) and first asymmetric (a0) modes of propagation will be observed. Thus, by considering only thin plates, all but the first two modes of propagation are eliminated, resulting in a waveform with characteristics that are easy to distinguish.

To simplify the problem of determining the elastic constants and the optical absorption coefficient in a thin glass film, it is desired to generate only thermoelastic waves. This restriction is achieved by simply decreasing the power of the Nd: YAG laser. By adjusting the size of the laser beam radius, the Rayleigh velocity and the group velocity of the s0 mode at zero wavenumber can be measured experimentally. Measurement of these two velocities leads to an estimation of the elastic constants. The estimated elastic constants are refined by comparing experimental and theoretical velocity data for the a0 mode. Next, the amplitude of the theoretical and experimental velocity data for the a0 mode are compared, which allows the optical absorption coefficient to be determined.

Ablation occurs when the sample's surface reaches its melting point; therefore, ablation must be accompanied by thermoelastic waves. For the a0 mode, this experimental reality is modeled theoretically by simply combining the thermoelastic and ablative solutions. For specimens with large optical absorption coefficients, the thermoelastic and ablative solutions add constructively. This theoretical result, while verified in copper and brass samples, is not witnessed in stainless steel samples. Stainless steel shows what is thought to be a small time delay between the thermoelastic and ablative waves. The theoretical solution closely resembles the experimental data if a 160 ns time delay

is included between the thermoelastic and ablative solution. This phenomenon might be attributed to thermal shielding due to the formation of plasma during ablation.

DETERMINATION OF ELASTIC AND OPTICAL PROPERTIES OF THIN PLATES AND INVESTIGATION OF THE MECHANISMS INVOLVED IN THE LASER GENERATION OF ULTRASOUND

by

David Howard Hurley

A thesis submitted in partial fulfillment
of the requirements for the degree

of

Master of Science

in

Mechanical Engineering

MONTANA STATE UNIVERSITY
Bozeman, Montana

June 1991

APPROVAL

of a thesis submitted by

David Howard Hurley

This thesis has been read by each member of the thesis committee and has been found to be satisfactory regarding content, English usage, format, citations, bibliographic style, and consistency, and is ready for submission to the College of Graduate Studies.

6/17/91
Date

R. Jay Conant
Chairperson, Graduate Committee

Approved for the Major Department

6/18/91
Date

Robert J. Colwell
Head, Major Department

Approved for the College of Graduate Studies

July 9, 1991
Date

Henry L. Parsons
Graduate Dean

STATEMENT OF PERMISSION TO USE

In presenting this thesis in partial fulfillment of the requirements for a master's degree at Montana State University, I agree that the Library shall make it available to borrowers under rules of the Library. Brief quotations from this thesis are allowable without special permission, provided that accurate acknowledgment of source is made.

Permission for extensive quotation from or reproduction of this thesis may be granted by my major professor, or in his absence, by the Dean of Libraries when, in the opinion of either, the proposed use of the material is for scholarly purposes. Any copying or use of the material in this thesis for financial gain shall not be allowed without my written permission.

Signature David A Hurley

Date 6-21-91

ACKNOWLEDGEMENTS

I would like to thank Dr. R. Jay Conant for his guidance and the many useful discussions concerning the theoretical development of this project.

This work was supported by the Department of Interior's Bureau of Mines under Contract No. JO134035 through Department of Energy Contract No. DEACO7-76IDO1570. I would like to thank the Association of Western Universities for sponsoring my research during the summers of 1989 and 1990. I would also like to thank the Nondestructive Evaluation team at Idaho National Engineering Laboratory, in particular Dr. K.L. Telschow, for their assistance and guidance concerning the experimental development of this project.

TABLE OF CONTENTS

TABLE OF CONTENTS -Continued

LIST OF TABLES

LIST OF FIGURES

LIST OF FIGURES-Continued

LIST OF FIGURES-Continued

ABSTRACT

The focus of this paper is two-fold. First, the shear wave velocity, Poisson's ratio, and optical absorption coefficient of a thin glass plate will be estimated using a Nd:YAG pulsed laser. Second, the combined influence that an ablative and thermoelastic source has on the elastic wave form generated by a pulsed laser will be investigated.

Thermoelastic waves are introduced into a sample when a portion of the laser's energy is optically absorbed along the depth of the specimen causing a steep thermal gradient. Neglecting the effects of heat conduction, the thermoelastic displacements are determined by solving the uncoupled displacement equations of thermoelasticity.

As the laser's energy is increased, a thin layer of atoms at the sample's surface is vaporized. The momentum transferred to the sample from the vaporized atoms constitutes the second generation mechanism and is termed ablation. The ablative mechanism, which is modeled as a normal force, in conjunction with the differential equations of isothermal elasticity is used to determine the displacement due to ablation.

The stress free boundary conditions of both the thermoelastic and ablative problems lead to the Rayleigh-Lamb frequency equation, the solution of which represents the various modes of propagation present in an infinite plate. For a given frequency bandwidth there is a plate thickness below which only the first symmetric (s_o) and first asymmetric (a_o) modes of propagation will be observed. Thus, by considering only thin plates, all but the first two modes of propagation are eliminated, resulting in a waveform with characteristics that are easy to distinguish.

To simplify the problem of determining the elastic constants and the optical absorption coefficient in a thin glass film, it is desired to generate only thermoelastic waves. This restriction is achieved by simply decreasing the power of the Nd:YAG laser. By adjusting the size of the laser beam radius, the Rayleigh velocity and the group velocity of the s_o mode at zero wavenumber can be measured experimentally. Measurement of these two velocities leads to an estimation of the elastic constants. The estimated elastic constants are refined by comparing experimental and theoretical velocity data for the a_o mode. Next, the amplitude of the theoretical and experimental velocity data for the a_o mode are compared, which allows the optical absorption coefficient to be determined.

Ablation occurs when the sample's surface reaches its melting point; therefore, ablation must be accompanied by thermoelastic waves. For the a_o mode, this experimental reality is modeled theoretically by simply combining the thermoelastic and ablative solutions. For specimens with large optical absorption coefficients, the thermoelastic and ablative solutions add constructively. This theoretical result, while verified in copper and brass samples, is not witnessed in stainless steel samples. Stainless steel shows what is thought to be a small time delay between the thermoelastic and ablative waves. The theoretical solution closely resembles the experimental data if a 160 ns time delay is included between the thermoelastic and ablative solution. This phenomenon might be attributed to thermal shielding due to the formation of plasma during ablation.

CHAPTER 1

INTRODUCTION

The use of ultrasonic techniques as an interrogative probe for characterizing material properties has been a successful reality for the past 35 years. Ultrasonic testing was first used for locating material flaws in plates, forgings, and welds. Since the early days, ultrasonic testing has lent itself to an ever widening array of applications. These applications include characterization of porosity distribution in ceramics, evaluation of microstructural properties, such as grain size in metals, and ultrasonic testing to determine the stress distribution in load bearing structures.

The appeal of ultrasonic testing over other characterization techniques, such as tension tests and hardness tests, is that ultrasound can be used non-destructively. Another advantage of this non-destructive technique is its ability to detect microstructural flaws. Therefore, with growing emphasis on conservation of exotic materials and safety of sophisticated structures, ultrasonic testing has become an ideal tool to characterize material properties.

While there are a large number of ultrasonic techniques, the governing concept of all the techniques is the same. This concept consists of generating ultrasonic waves in a material, and then analyzing this disturbance after it has passed through the material. Tiny cracks and voids, as well as the elastic properties of the material itself, can alter the form and characteristics of the traveling wave as it passes through the material. With

the use of a suitable theory, the researcher can analyze this altered ultrasonic disturbance to determine various material properties. The material property of interest dictates to a large extent the theory and experimental procedure used.

Generation Mechanism of Laser Generated Ultrasound

Ultrasonic waves may be produced when a material is subjected to a laser pulse of sufficient intensity. There are two basic mechanisms responsible for producing ultrasound in this manner. The first mechanism that will be discussed can be described in a thermoelastic regime. As the laser irradiates the material, a portion of the laser's energy is optically absorbed along the depth of the specimen causing a steep thermal gradient, both spatially and temporally. This temperature gradient results in rapid thermal strains which in turn cause ultrasound to propagate through the material.

Valuable insight may be gained by giving a microscopic view of the above thermoelastic process. The laser pulse is composed of photons (quanta of light) which all have the same energy. These photons are absorbed by the material causing atoms that make up the material to rise to a higher energy state. A portion of the excited atoms release their energy in the form of kinetic energy to surrounding atoms. It is this rise in kinetic energy to the surrounding atoms that was classically described above by a rapid increase in temperature.

While a portion of the laser's energy was optically absorbed into the specimen, the remaining energy is either reflected from the surface or responsible for vaporizing a thin layer of atoms at the sample's surface. Vaporization of a thin layer of atoms at

the specimen's surface constitutes the second generation mechanism. Atoms at the surface that are given a sufficient amount of energy to escape the attractive forces of the material are said to be vaporized. As the vaporized atoms leave the surface they transfer a portion of their momentum to the surface resulting in the generation and propagation of ultrasonic waves through the specimen. This generation mechanism is known as ablation.

The experimental procedure used to generate ultrasonic waves takes advantage of coherent, monochromatic, and directionality properties of a Nd:YAG pulsed laser. These distinguishing features enable a narrow beam of high intensity light to be directed over large distances without dispersing. Upon striking the sample's surface, this high intensity beam generates ultrasound in accordance with the generation mechanisms listed above.

Objective

The overall objective of this thesis is two-fold. The first objective will be to estimate the elastic constants and the optical absorption coefficient of a thin glass film using laser generated ultrasound. Secondly, the combined influence that an ablative and a thermoelastic source have on the elastic wave form generated by a pulsed laser will be examined.

The first step in meeting the above objectives is to design an experiment that is capable of both producing and detecting ultrasound in thin glass and metallic samples. While the apparatus and experimental setup for similar experiments were provided by Idaho National Engineering Laboratory (INEL), the details pertinent to this experiment

still needed to be furnished. A thorough discussion of the experimental procedure will be presented in chapter two of this document.

The next step involves the development of a reliable theory that predicts the amplitude and time characteristics of the laser generated elastic waves. This theory has to accurately model the generation source while accounting for the geometry of the specimen. Theoretical details will be discussed in chapter three.

Literature Review

The generation of high frequency ultrasonic pulses by absorption of electromagnetic radiation was first demonstrated by White[1] in 1963. Later White[2] used a *Q*-switched ruby laser to produce Rayleigh surface waves in piezoelectric and nonpiezoelectric solids. Mechanical comb transducers were employed to detect surface waves on nonpiezoelectric specimens, while interdigital electrode transducers were used for piezoelectric substances. In this paper he proposed that the efficiency of generating surface waves could be increased by periodically distributing heat sources along the surface of the sample.

In 1980 Aindow *et al.*[3] reported the effects of ablation on elastic waves generated by an Nd:YAG laser. Their study showed that in the ablation regime the plasma formed causes a reduction in lateral thermal gradients which in turn serves to decrease both lateral and normal gradients in the acoustic source. The momentum transfer due to ablation partially camouflages the thermal shielding caused by the plasma, resulting in an enhancement of the longitudinal pulse.

Measurement of thin metallic film thickness using laser generated ultrasound was first described by Dewhurst et al.[4] in 1987. The method involved using a high power pulsed laser to generate both symmetric and asymmetric Lamb waves. A Michelson interferometer in conjunction with a He-Ne laser was used to detect these waves. By obtaining time-of-flight measurements and determining the velocity of the ultrasonic disturbance, the thickness of the material was ascertained.

Later Hutchins and Lundgren[5] demonstrated that the film thickness and the elastic constants could be estimated by using a wide bandwidth and well-defined source and receiver locations. For a given frequency bandwidth, there is a plate thickness below which only two Lamb modes will be detected (first asymmetric and symmetric mode). The first symmetric mode for very thin materials is virtually dispersionless and has velocity (C_e). By measuring the velocity (C_e) and fitting an approximate dispersion relation for the first asymmetric mode to the dispersion curve obtained experimentally, an estimation of the film thickness and elastic constants is obtained.

Recently Roy[6] has studied the influence that optical absorption and diffusivity have on the elastic wave form generated by a pulsed laser. His one dimensional solution consists of solving the heat conduction equation and then solving the uncoupled thermoelastic wave equation to obtain an expression for displacement. The solution predicts that for moderate values of absorptivity (10^4 - 10^5 cm^{-1}) the magnitude and the time characteristic of the waveform remain relatively unchanged for wide variations in diffusivity.

CHAPTER 2

EXPERIMENT

The experimental setup that is used to generate and detect ultrasound in thin glass and metallic samples is shown in Fig. 1. The primary components of this setup are an Nd:YAG pulsed laser, an Argon constant wave (cw) laser, a confocal Fabry Perot interferometer, and signal conditioning equipment. The Nd:YAG laser is responsible for generating ultrasound, while the detection of ultrasound is achieved by modulation of the Argon laser beam as it is reflected from the surface of the vibrating sample. The interferometer is employed to demodulate the Argon beam. The demodulated signal leaving the interferometer is then conditioned as it passes through an array of signal conditioning equipment. These components serve to divide the experimental procedure into four main categories.

The first category involves the generation of ultrasound in thin elastic samples (Lamb waves). The generation of Lamb waves is accomplished by irradiating the sample with high intensity light from an Nd:YAG pulsed laser. For this experiment the Nd:YAG laser has a pulse rate of 10 Hz, a pulse duration of 10 ns, and a typical power of 10 mj/pulse.

The source/receiver separation, shown in Fig. 2, is regulated by moving the generation beam (laser pulses) while keeping the receiver location fixed. An optical stage and lens apparatus, Fig. 2, is utilized to move the generation beam perpendicular

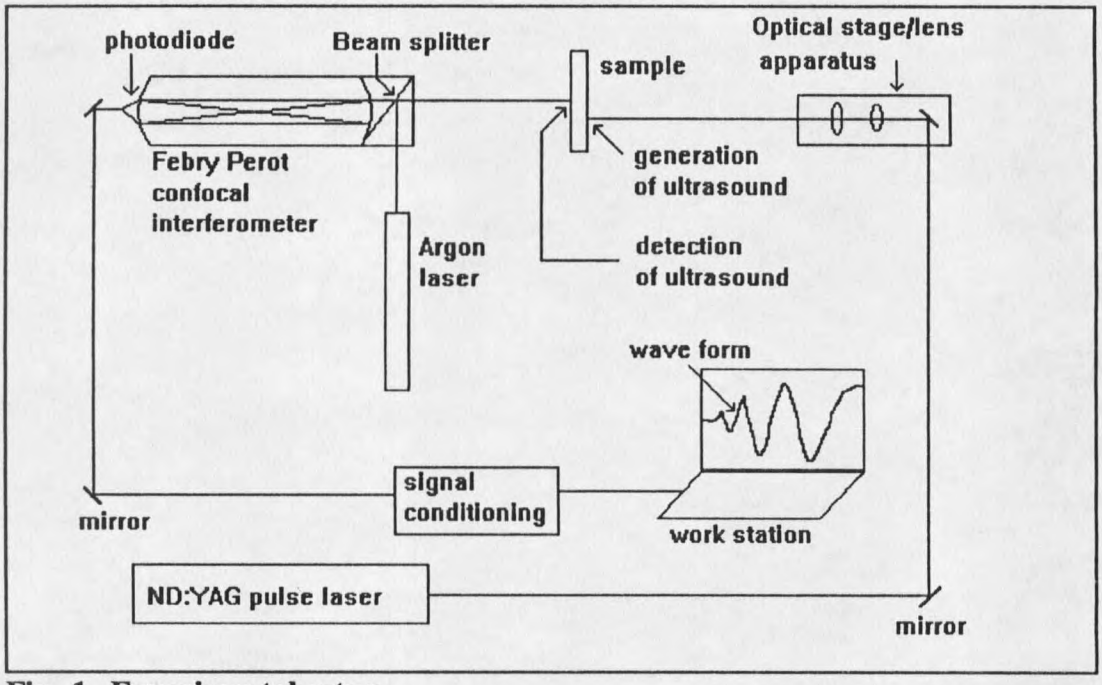

Fig. 1. Experimental setup

to the surface of the sample. By moving the generation beam in this manner the radial profile of laser pulses as projected on the sample is preserved. The location of the generation beam relative to the receiver location is then determined. This is done by replacing the specimen with a photographic film, and then exposing the film with both the Argon and Nd:YAG lasers, as demonstrated in Fig. 2. The film is examined under a microscope to accurately determine the source/receiver separation.

The next category concerns the detection of Lamb waves using an Argon laser. The first step in this procedure is to direct the Argon beam through a polarizing beam-splitter, shown in Fig. 1. One beam is use as a reference beam, while the other beam is steered towards the vibrating sample. Upon reflection from the vibrating surface, the laser light experiences a shift in frequency due to the Doppler effect. This modulated

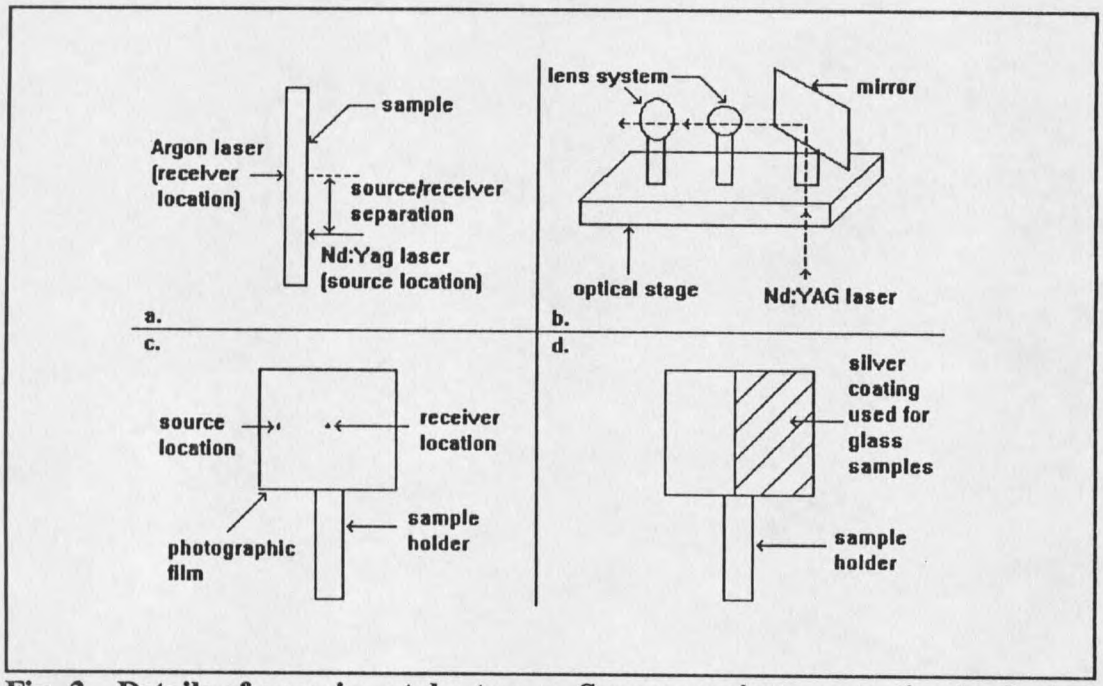

Fig. 2. Details of experimental setup. a. Source receiver separation b. Optical stage/lens apparatus. c. Photographic film. d. Silver coating used for glass samples.

beam contains the amplitude and time characteristics of the vibrating surface, information that will be deciphered by demodulating the Argon beam.

It should be noted that this detection scheme is noncontacting, thus lending itself to environments that would be hostile to contacting transducers. However, this noncontacting method requires that semi-transparent films, such as glass, undergo special preparation in order for this method to work. This difficulty is due to the dual reflection that would be encountered when the Argon beam is reflected from a semi-transparent film. A portion of the beam would reflect off the front surface while the remaining portion would reflect off the back surface of the sample, resulting in the combination of time and amplitude characteristics of both the front and back vibrating surfaces. This

problem is circumvented by sputtering a silver coating on the detection side of the sample, as displayed in Fig. 2, resulting in a single reflection.

The third category entails demodulating the doppler shifted Argon beam by passing it through the Fabry Perot interferometer. This is performed by setting the cavity of the interferometer on the slope of one of its response peaks shown in Fig. 3. The response of the interferometer in this region is linear, thus giving an output intensity that is proportional to the frequency shift of the Argon laser, and hence proportional to the velocity of the vibrating sample.

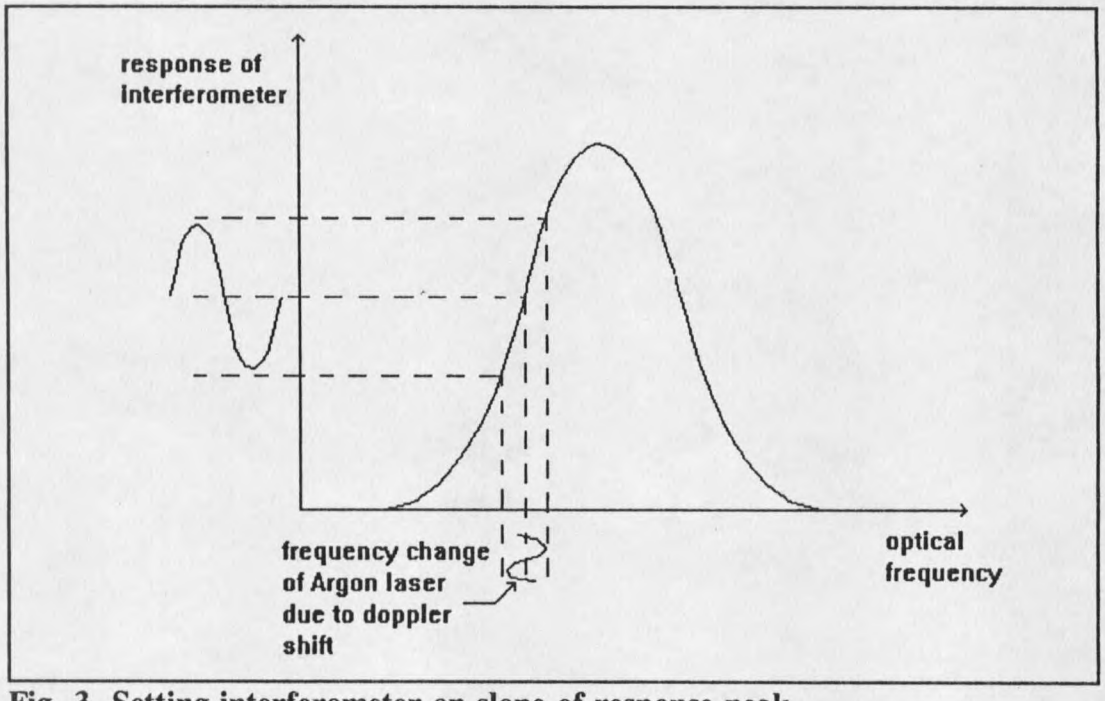

Fig. 3. Setting interferometer on slope of response peak.

The last category involves the conditioning of the demodulated signal exiting from the interferometer. The response of the interferometer is received by a photodiode placed at the back of the interferometer cavity. The signal from the photodiode is then

passed through an assortment of signal conditioning equipment which includes a band-pass filter and a digitizer (20 ns period).

Due to the response frequency of the interferometer, the upper limit of band-pass filter is confined to frequencies above 1 Mhz. It is the upper limit of the band-pass filter in conjunction with the plate thickness ($\sim .1$ mm) that allows only the first symmetric and asymmetric modes of propagation to be observed. This is graphically demonstrated in Fig. 4. This graph displays the relationship between dimensionless frequency and dimensionless wavenumber for the first four modes of propagation in a copper plate with stress free boundary conditions (Rayleigh-Lamb frequency spectrum). The dimensionless frequency is expressed as, $\omega h/c_t$, where ω is the dimensional frequency, h is the half plate thickness, and c_t is the shear wave velocity. Figure 4 illustrates that for dimensionless frequency less than ~ 1.5, only the first two modes of propagation will be observed. Thus, for a copper plate with a shear wave velocity of 2.24 mm/μs, the half plate thickness must be less than ~ 0.53 mm in order to exclude all but the first two modes.

The elimination of all but the first two modes of propagation results in a waveform with characteristics that are easy to distinguish. A typical waveform for a thin copper plate is shown in Fig. 5. The significant features of this waveform are the first symmetric mode, s_o, and asymmetric mode, a_o. The s_o mode is virtually dispersionless

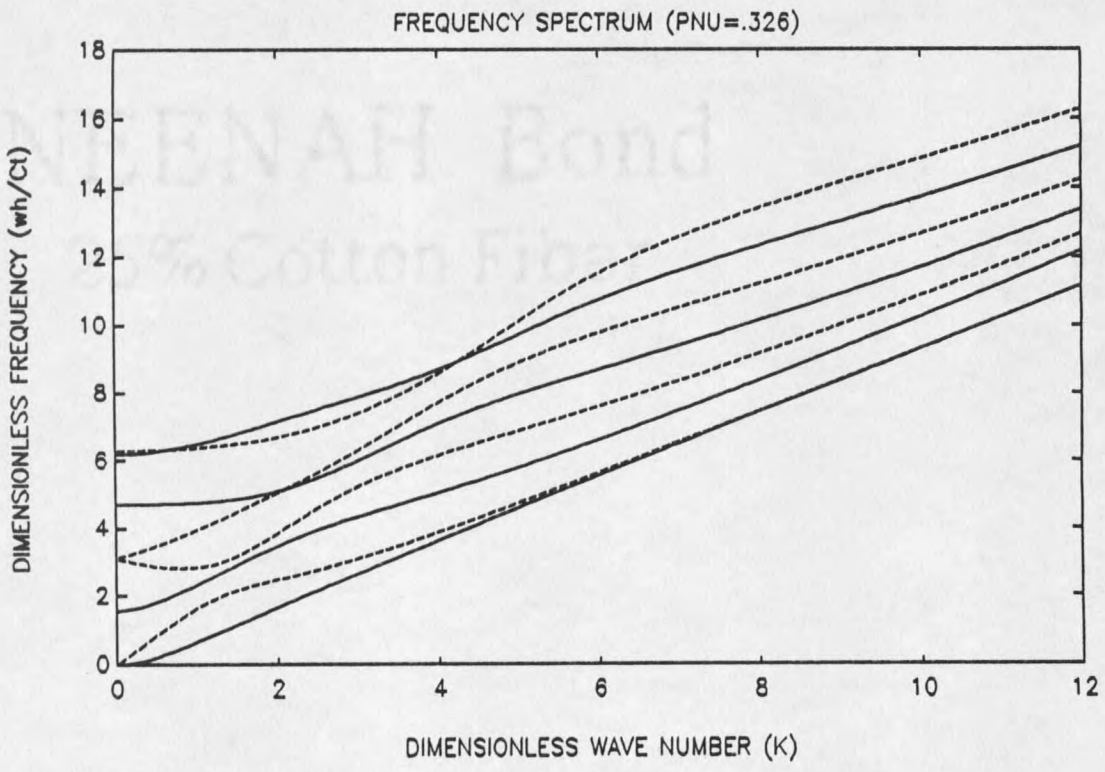

Fig. 4. Rayleigh-Lamb frequency spectrum for copper. Dashed and solid lines represent symmetric and asymmetric modes respectively.

and arrives at about 3.5 μs. The later arriving a_o mode dominates the waveform and is very dispersive. Waveforms of this nature (consisting of the first symmetric and asymmetric modes of propagation) will be the focus of this document.

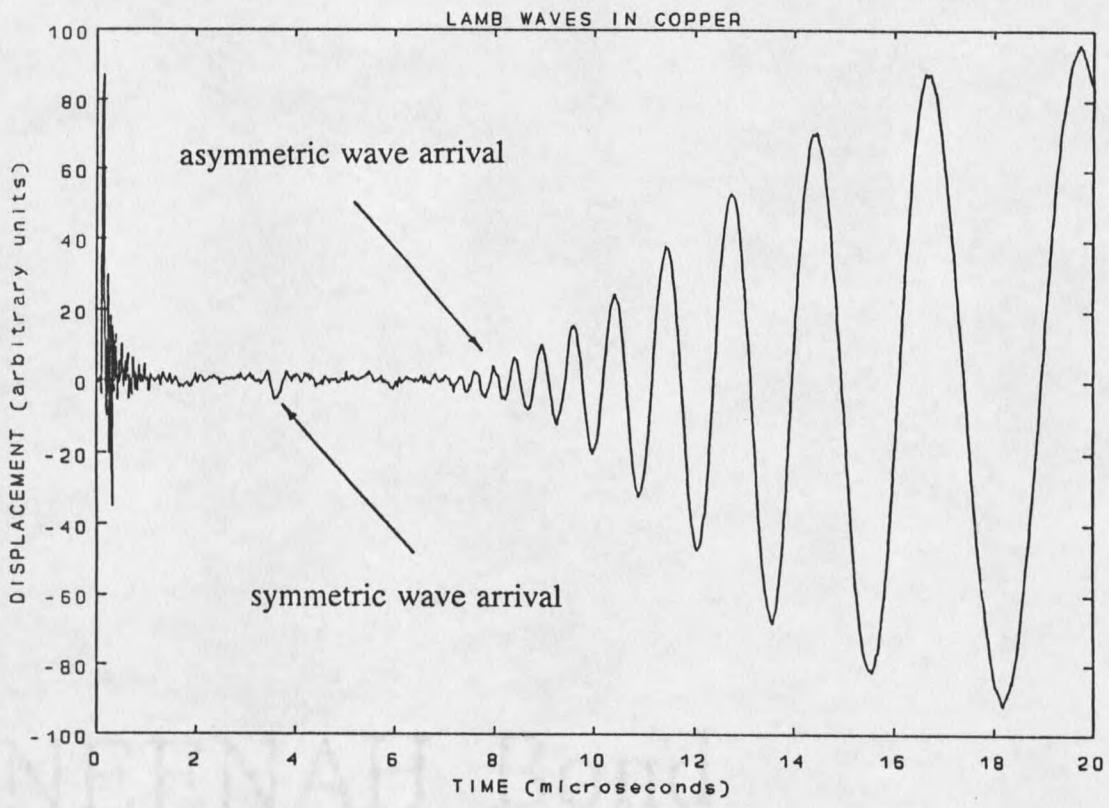

Fig. 5. Transient Lamb waveforms. The s_o wave arrives before the a_o wave.

CHAPTER 3

FORMULATION OF THE PROBLEM

In this chapter various assumptions pertinent to the experiment are made, followed by a presentation of the governing differential equations. The assumptions made regarding the present problem serve two purposes. First, they enable an analytical solution to be formally obtained. It is this analytical portion of the solution that facilitates a physical understanding of the problem. Second, these simplifying assumptions help make the analytical solution more tractable, which in turn aids the researcher in fitting the theory to the experiment. The assumptions appropriate to the experiment can be categorized into three broad groups.

General Assumptions

i) The material is both isotropic and homogeneous. These properties reduce the number of independent elastic constants to two. These constants can be expressed as Poisson's ratio, υ, and the modulus of elasticity, E.

ii) The intensity of the pulse laser in the radial direction is Gaussian as shown in Fig. 6.

iii) The laser pulse is assumed to be axially symmetric. This assumption results in an axially symmetric solution for the thermoelastic and ablative problem.

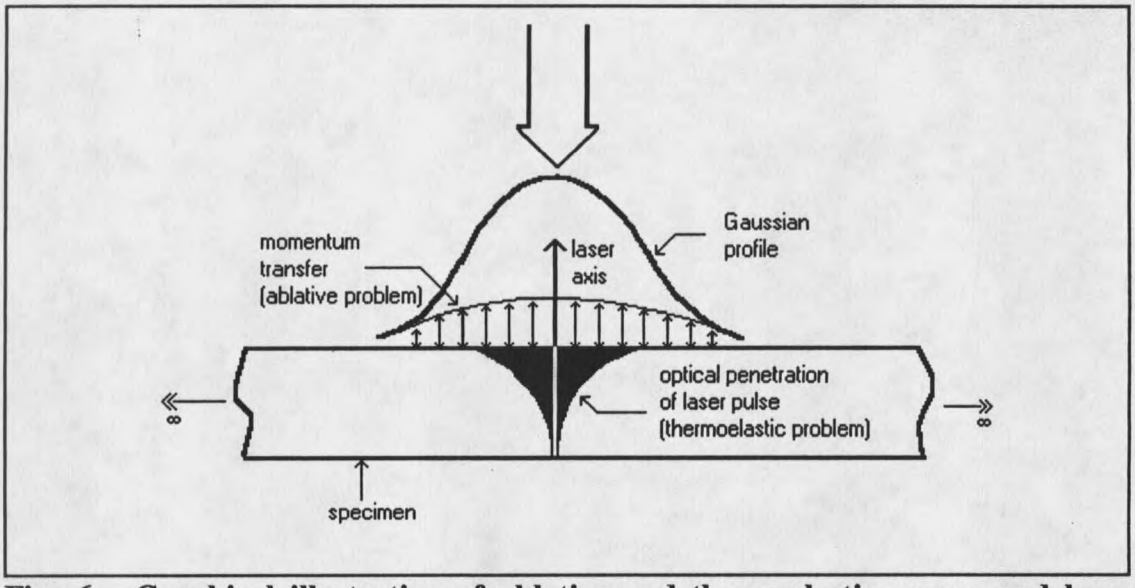

Fig. 6. Graphical illustration of ablative and thermoelastic source and laser profile.

iv) The specimen is considered to be infinite in the radial direction. This assumption is valid if $r_b/r_p << 1$, where r_b is the laser beam radius, and r_p is the plate radius.

Assumptions Regarding Thermoelastic Problem

i) The localized temperature increase caused by absorption of the laser's energy is small in comparison to the reference temperature. In addition the temperature increase will not produce an appreciable change in the material's structure.

ii) The above assumption is reinforced by another assumption regarding the magnitude of the deformation. The squares and products of the thermal strain, ϵ_{ij}, can be neglected as compared to ϵ_{ij}, resulting in a linear relation between strain and displacement.

iii) The influence of the strain rate is neglected; therefore, the governing equations are those of uncoupled thermoelasticity.

iv) Temporally, the heat source is represented as a Dirac delta function. The legitimacy of this assumption stems from the following two experimental realities. First, the laser's energy is considered to be instantaneously converted into thermal energy at the point at which the laser pulse is absorbed into the sample [7]. Second, the laser pulse duration is 20 ns while the time of interest for this problem is on the order of 40 μs.

v) Thermal diffusion is neglected; therefore, since the heat source is represented as a Dirac delta function, the temperature source can be represented temporally as a step function. This approximation is valid for wave travel times that are small in comparison with the thermal diffusion time.

Assumptions Regarding Ablative Problem

i) It is assumed that only a thin layer at the material's surface is vaporized; thus, the momentum transferred to the material has only one component. This component is normal to the surface and is responsible for producing ultrasonic waves. This assumption enables the ablative source to be modeled mechanically by utilizing a normal force solution [8]. This source is illustrated graphically in Fig. 6.

ii) The ablative source is represented temporally as a Dirac delta function. This assumption is valid since the time required for the plasma that is jettisoned from the sample's surface to reach its maximum velocity is on the order of 40 ns [7] and the time of interest for this problem is on the order of 40 μs.

Thermoelastic Formulation

Formulation of the thermoelastic problem follows that of Telschow and Conant[9], as well as Sve and Miklowitz[10]. The dimensionless coordinate system for this problem is shown in Fig. 7. (Dimensional quantities are primed.) All lengths are normalized with respect to the half layer thickness, h, and the shear wave velocity is used to nondimensionalize time, $t=(\mu/\rho)^{1/2}t'/h$.

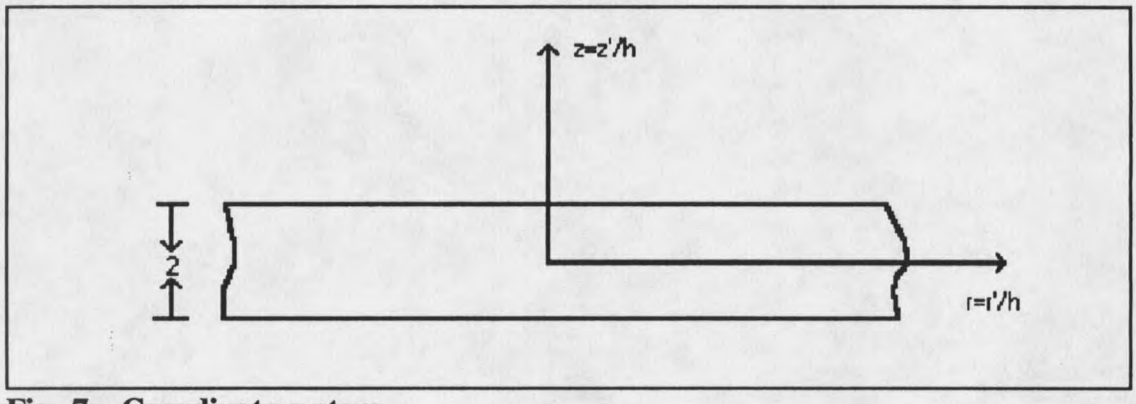

Fig. 7. Coordinate system.

Neglecting thermal diffusion, the temperature distribution generated by electromagnetic radiation can be represented as follows:

$$T(r,z,t)=T_{so}\exp[-r^2/a^2]\exp[-\eta(1+z)]H(t)\ , \qquad (3.1)$$

where $a=a'/h$ is the dimensionless Gaussian laser beam radius, and $\eta=bh$ is the dimensionless optical absorption coefficient. T_{so} is the surface temperature at $r=0$ and is given by

$$T_{so}=\frac{Q_o\eta}{\pi a^2\rho Ch^3(1-\exp(-2\eta))}\ , \tag{3.2}$$

where Q_o represents the total heat absorbed by the specimen. The uncoupled, dimensionless differential equations of thermoelasticity are [11]

$$\begin{aligned}\frac{1}{r}\frac{\partial}{\partial r}\left(r\frac{\partial\phi}{\partial r}\right)+\frac{\partial^2\phi}{\partial z^2}&=\left(\frac{C_t}{C_l}\right)^2\frac{\partial^2\phi}{\partial t^2}+\left(\frac{1+\nu}{1-\nu}\right)\alpha T\ ,\\ \frac{1}{r}\frac{\partial}{\partial r}\left(r\frac{\partial\psi}{\partial r}\right)-\frac{\psi}{r^2}+\frac{\partial^2\psi}{\partial z^2}&=\frac{\partial^2\psi}{\partial t^2}\ ,\end{aligned} \tag{3.3}$$

where ψ and ϕ are the Lamé potentials, α is the linear coefficient of thermal expansion, C_t and C_l are the transverse and longitudinal wave speed, respectively, and T is change in temperature. The dimensionless displacement in the z direction, w, is expressed in terms of the Lamé potentials by

$$w=\frac{w'}{h}=\frac{\partial\phi}{\partial z}+\frac{1}{r}\frac{\partial}{\partial r}(r\psi)\ , \tag{3.4}$$

where w' is the corresponding dimensional displacement.

Boundary/Initial Conditions for the Displacement Equation

The formulation is completed by assuming that the layer is initially at rest, and the faces of the layer are free from traction. These conditions are represented as follows:

$$u(r,z,0)=w(r,z,0)=\frac{\partial u}{\partial t}(r,z,0)=\frac{\partial w}{\partial t}(r,z,0)=0 \ ,$$
$$\sigma_z(r,\pm 1,t)=\sigma_{rz}(r,\pm 1,t)=0 \ , \qquad (3.5)$$

where u is the radial displacement, and σ_{zz} and σ_{rz} are the normal and shear stress, respectively.

Ablative Formulation

The formulation of the ablative problem will follow an approximate theory for plate flexural waves. The problem developed in this manner will not only make the ablative solution more tractable, but will provide valuable insight into the more complicated thermoelastic problem. This theory was first developed by Mindlin[12] and incorporates three essential features. First, the exact equations of elasticity are integrated over the plate thickness. Second, the deformation is restricted to finite degrees of freedom, thus excluding the thickness modes present in the exact theory. The last essential feature is the introduction of adjustment coefficients to bring the shear force proposed by this theory into agreement with the exact shear force.

The presentation of the above approximation in cylindrical coordinates will follow Graff's[13] presentation carried out in cartesian coordinates. The requirement that the displacement field is axially symmetric will not be implemented until the formulation is complete, therefore permitting a general development of Mindlin's plate theory in cylindrical coordinates.

All basic quantities such as length and time have the same nondimensional form as they did in the thermoelastic formulation; dimensional quantities are primed.

Plate Stress-Strain Relations

The nondimensional plate stresses M_r, M_θ, $M_{r\theta}$, Q_r, Q_θ as defined by classical plate theory for the element shown in Fig. 8 are

$$(M_r\ ,\ M_\theta\ ,\ M_{\theta r}) = \int_{-1}^{1} (\sigma_{rr}\ ,\ \sigma_{\theta\theta}\ ,\ \sigma_{r\theta}) z dz\ ,$$

$$(Q_r\ ,\ Q_\theta) = \int_{-1}^{1} (\sigma_{rz}\ ,\ \sigma_{\theta z}) dz\ , \tag{3.6}$$

where $\sigma_{ij} = 1/\mu(\sigma'_{ij})$. M_r and M_θ are identified with the bending moments per unit length about the θ axis and r axis respectively, while $M_{r\theta}$ is the twisting moment per unit length associated with the shear stress $\sigma_{r\theta}$.

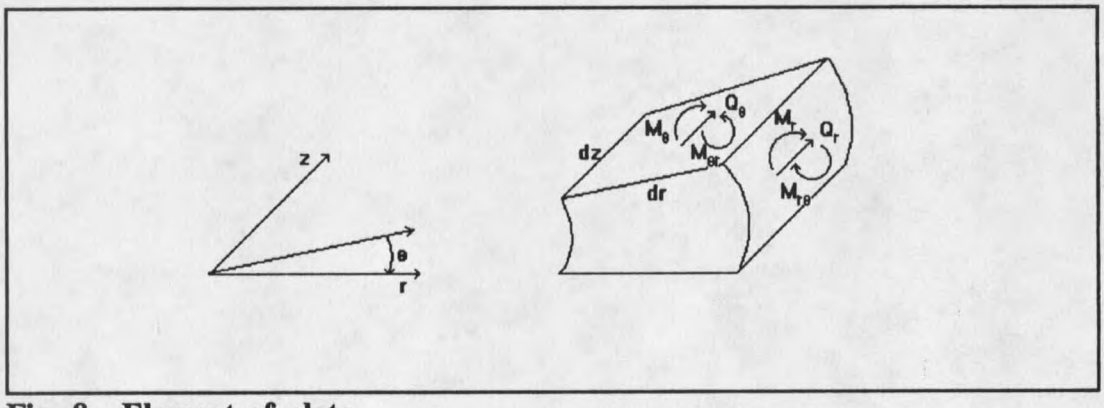

Fig. 8. Element of plate.

The five plate stresses may be defined in terms of five strain components, ϵ_{rr}, $\epsilon_{\theta\theta}$, $\epsilon_{r\theta}$, $\epsilon_{\theta z}$, and ϵ_{zr}. This is accomplished by first writing the stress-strain equations in cylindrical coordinates as follows:

$$\begin{aligned}
\sigma'_{rr}&=\lambda(\epsilon_{rr}+\epsilon_{\theta\theta}+\epsilon_{zz})+2\mu\epsilon_{rr}\ ,\\
\sigma'_{\theta\theta}&=\lambda(\epsilon_{rr}+\epsilon_{\theta\theta}+\epsilon_{zz})+2\mu\epsilon_{\theta\theta}\ ,\\
\sigma'_{zz}&=\lambda(\epsilon_{rr}+\epsilon_{\theta\theta}+\epsilon_{zz})+2\mu\epsilon_{zz}\ ,\\
\sigma'_{r\theta}&=2\mu\epsilon_{r\theta}\ ,\quad \sigma'_{\theta z}=2\mu\epsilon_{\theta z}\ ,\quad \sigma'_{zr}=2\mu\epsilon_{zr}\ .
\end{aligned} \tag{3.7}$$

The stress-strain equation for σ_{zz} can be rewritten in the form

$$\epsilon_{zz}=-\frac{\lambda}{\lambda+2\mu}(\epsilon_{rr}+\epsilon_{\theta\theta})+(\lambda+2\mu)^{-1}\sigma'_{zz}\ . \tag{3.8}$$

The strain component ϵ_{zz} is now eliminated from the first two of Eqs. (3.7), yielding

$$\begin{aligned}
\sigma'_{rr}&=\frac{4\mu(\lambda+\mu)}{(\lambda+2\mu)}\epsilon_{rr}+\frac{2\mu\lambda}{(\lambda+2\mu)}\epsilon_{\theta\theta}+\frac{\lambda}{(\lambda+2\mu)}\sigma'_{zz}\ ,\\
\sigma'_{\theta\theta}&=\frac{2\mu\lambda}{(\lambda+2\mu)}\epsilon_{rr}+\frac{4\mu(\lambda+\mu)}{(\lambda+2\mu)}\epsilon_{\theta\theta}+\frac{\lambda}{(\lambda 2\mu)}\sigma'_{zz}\ .
\end{aligned} \tag{3.9}$$

Using the relations

$$\frac{\lambda}{(\lambda+2\mu)}=\frac{\nu}{(1-\nu)}\ ,\quad \mu=\frac{E}{2(\nu+1)}\ , \tag{3.10}$$

the stress-strain equations may be rewritten as

$$\sigma'_{rr}=\frac{E}{1-\nu^2}(\epsilon_{rr}+\nu\epsilon_{\theta\theta})+\frac{\nu}{1-\nu}\sigma'_{zz},$$

$$\sigma'_{\theta\theta}=\frac{E}{1-\nu^2}(\epsilon_{\theta\theta}+\nu\epsilon_{rr})+\frac{\nu}{1-\nu}\sigma'_{zz}, \qquad (3.11)$$

$$\sigma'_{r\theta}=2\mu\epsilon_{r\theta}\ ,\ \sigma'_{\theta z}=2\mu\epsilon_{\theta z}\ ,\ \sigma'_{zr}=2\mu\epsilon_{zr}\ .$$

The plate stress-strain relations are obtained by substituting the above stress-strain equations into Eqs. (3.6). Using M_r as an example we have

$$M_r=\int_{-1}^{1}\frac{\sigma'_{rr}}{\mu}z\,dz=\int_{-1}^{1}\frac{E(\epsilon_{rr}+\nu\epsilon_{\theta\theta})}{\mu(1-\nu^2)}z\,dz+\int_{-1}^{1}\frac{\nu\sigma'_{zz}}{\mu(1-\nu)}z\,dz. \qquad (3.12)$$

Next, the integral contribution of σ'_{zz} is disregarded. Neglecting the weighted average of σ'_{zz} can be viewed as a generalization of classical plate theory, where σ'_{zz} itself is neglected.

$$M_r=\frac{E}{\mu(1-\nu^2)}\int_{-1}^{1}(\epsilon_{rr}+\nu\epsilon_{\theta\theta})z\,dz\ . \qquad (3.13)$$

By a similar procedure we get

$$M_\theta=\frac{E}{\mu(1-\nu^2)}\int_{-1}^{1}(\nu\epsilon_{rr}+\epsilon_{\theta\theta})z\,dz\ ,$$
$$M_{r\theta}=2\int_{-1}^{1}\epsilon_{r\theta}z\,dz\ . \tag{3.14}$$

It should be noted that Eq. (3.13) and the first of Eqs. (3.14) may have been obtained by setting $\sigma_{zz}=0$ at the onset. The present procedure reveals that the weighted average of σ_{zz} has been neglected and not σ_{zz} itself.

The plate shear forces given by Eq. (3.15) are treated in a similar manner to the Timoshenko beam. As a consequence of the kinematic assumptions that will be made shortly, the shear strains ϵ_{rz} and $\epsilon_{\theta z}$ are independent of z, and represent the shear strains at the mid-plane. Therefore, the shear forces that are obtained by integrating the shear strains over the thickness of the plate are inexact. This is compensated for by introducing an adjustment coefficient, γ^2, that bring the shear forces predicted by this theory into agreement with the exact shear forces:

$$Q_r=2\gamma^2\int_{-1}^{1}\epsilon_{zr}dz\ ,$$
$$Q_\theta=2\gamma^2\int_{-1}^{1}\epsilon_{\theta z}dz\ . \tag{3.15}$$

Kinematics of Deformation

By making assumptions regarding the kinematics of deformation, the displacements may be brought into this formulation. These assumptions are given by

$$\begin{aligned} u(r,\theta,z,t) &= z\psi_r(r,\theta,t) \ , \\ v(r,\theta,z,t) &= z\psi_\theta(r,\theta,t) \ , \\ w(r,\theta,z,t) &= w(r,\theta,t) \ , \end{aligned} \tag{3.16}$$

where u, v, and w represent physical displacements in the radial, tangential, and z directions respectively. ψ_r and ψ_θ represent arbitrary functions in r and θ. It should be noted that the thickness-stretch modes, allowed by the exact theory, will not be permitted by this approximation. This is due to the fact that thickness-stretch modes at zero wave number are dependent on z, while the displacement component, w, is independent of z. In addition, the assumed displacements represent asymmetric displacements with respect to the mid-plane of the plate; therefore, only asymmetric modes of propagation will be possible.

The plate stress-displacement relations are obtained by first writing the strain-displacement equations in cylindrical coordinates as follows:

$$\epsilon_{rr}=\frac{\partial u}{\partial r}\ ,\ \epsilon_{zz}=\frac{\partial w}{\partial z}\ ,$$

$$\epsilon_{\theta\theta}=\frac{1}{r}\frac{\partial v}{\partial \theta}+\frac{u}{r}\ ,$$

$$\epsilon_{\theta z}=\frac{1}{2}\left(\frac{\partial v}{\partial z}+\frac{1}{r}\frac{\partial w}{\partial \theta}\right)\ , \qquad \textbf{(3.17)}$$

$$\epsilon_{zr}=\frac{1}{2}\left(\frac{\partial w}{\partial r}+\frac{\partial u}{\partial z}\right)\ ,$$

$$\epsilon_{r\theta}=\frac{1}{2}\left(\frac{1}{r}\frac{\partial u}{\partial \theta}+\frac{\partial v}{\partial r}-\frac{v}{r}\right)\ ,$$

where u, v, and w are the assumed displacements given in Eqs. (3.16). Next, Eqs. (3.16) are substituted into Eqs. (3.17) giving

$$\epsilon_{rr}=z\frac{\partial \psi_r}{\partial r}\ ,\ \epsilon_{zz}=\frac{\partial w}{\partial z}\ ,$$

$$\epsilon_{\theta\theta}=\frac{z}{r}\frac{\partial \psi_\theta}{\partial \theta}+\frac{z\psi_r}{r}\ ,$$

$$\epsilon_{\theta z}=\frac{1}{2}\left(\psi_\theta+\frac{1}{r}\frac{\partial w}{\partial \theta}\right)\ , \qquad \textbf{(3.18)}$$

$$\epsilon_{zr}=\frac{1}{2}\left(\frac{\partial W}{\partial r}+\psi_r\right)\ ,$$

$$\epsilon_{r\theta}=\frac{1}{2}\left(\frac{z}{r}\frac{\partial \psi_r}{\partial \theta}+z\frac{\partial \psi_\theta}{\partial r}-\frac{z\psi_\theta}{r}\right)\ .$$

By inserting Eqs. (3.18) into Eqs. (3.13), (3.14) and (3.15), the plate stress-displacement relations can be defined as follows:

$$M_r=\frac{4}{3(1-\nu)}\left(\frac{\partial \psi_r}{\partial r}+\frac{\nu}{r}\left(\frac{\partial \psi_\theta}{\partial \theta}+\psi_r\right)\right),$$

$$M_\theta=\frac{4}{3(1-\nu)}\left(\nu\frac{\partial \psi_r}{\partial r}+\frac{1}{r}\left(\frac{\partial \psi_\theta}{\partial \theta}+\psi_r\right)\right),$$

$$M_{r\theta}=\frac{2}{3}\left(\frac{1}{r}\frac{\partial \psi_r}{\partial \theta}+\frac{\partial \psi_\theta}{\partial r}-\frac{\psi_\theta}{r}\right), \tag{3.19}$$

$$Q_r=2\gamma^2\left(\frac{\partial w}{\partial r}+\psi_r\right),$$

$$Q_\theta=2\gamma^2\left(\psi_\theta+\frac{1}{r}\frac{\partial w}{\partial \theta}\right).$$

Equations of Motion, Three Dimensional Elasticity

Next, consider the exact equations of motion in cylindrical coordinates, written nondimensionally as

$$\frac{1}{r}\frac{\partial}{\partial r}(r\sigma_{rr})+\frac{1}{r}\frac{\partial}{\partial \theta}\sigma_{r\theta}+\frac{\partial}{\partial z}\sigma_{rz}-\frac{\sigma_{\theta\theta}}{r}=\frac{\partial^2 u}{\partial t^2},$$

$$\frac{1}{r^2}\frac{\partial}{\partial r}(r^2\sigma_{\theta r})+\frac{1}{r}\frac{\partial}{\partial \theta}\sigma_{\theta\theta}+\frac{\partial}{\partial z}\sigma_{\theta z}=\frac{\partial^2 v}{\partial t^2}, \tag{3.20}$$

$$-\frac{1}{r}\frac{\partial}{\partial r}(r\sigma_{zr})+\frac{1}{r}\frac{\partial}{\partial \theta}\sigma_{z\theta}+\frac{\partial}{\partial z}\sigma_{zz}=\frac{\partial^2 w}{\partial t^2},$$

where the density has been nondimensionalized as $\rho=\rho' C_t^2/\mu = 1$. In order to transform the above equations into the plate-stress equations of motion, the first two equations

must be multiplied by z and integrated across the thickness of the plate. Demonstrating this procedure for the radial equation, we have

$$\frac{1}{r}\int_{-1}^{1}\frac{\partial(r\sigma_{rr})}{\partial r}zdz+\frac{1}{r}\int_{-1}^{1}\frac{\partial\sigma_{r\theta}}{\partial\theta}zdz+\int_{-1}^{1}\frac{\partial\sigma_{rz}}{\partial z}zdz-\int_{-1}^{1}\frac{\sigma_{\theta\theta}}{r}zdz=\rho\int_{-1}^{1}\frac{\partial^2 u}{\partial t^2}zdz. \qquad \textbf{(3.21)}$$

Using the plate stress relations given in Eqs. (3.6) and interchanging the order of integration and differentiation in the first, second, and fourth term of the above expression we have for these terms, respectively,

$$\frac{1}{r}\int_{-1}^{1}\frac{\partial}{\partial r}(r\sigma_{rr})zdz=\frac{1}{r}\int_{-1}^{1}(\sigma_{rr}+r\frac{\partial\sigma_{rr}}{\partial r})zdz=\frac{1}{r}M_r+\frac{\partial}{\partial r}M_r\ ,$$

$$\frac{1}{r}\int_{-1}^{1}\frac{\partial\sigma_{r\theta}}{\partial\theta}zdz=\frac{1}{r}\frac{\partial}{\partial\theta}M_{r\theta}\ , \qquad \textbf{(3.22)}$$

$$\int_{-1}^{1}\frac{\sigma_{\theta\theta}}{r}zdz=\frac{1}{r}M_\theta\ .$$

The third term in Eq. (3.21) can be integrated by parts giving

$$\int_{-1}^{1}\frac{\partial\sigma_{rz}}{\partial z}zdz=(z\sigma_{rz})_{-1}^{1}-\int_{-1}^{1}\sigma_{rz}dz=-Q_r\ . \qquad \textbf{(3.23)}$$

The shear stress boundary condition furnished in Eq. (3.5) is used to eliminate the first term on the right hand side of Eq. (3.23). With the first of Eqs. (3.16), the right hand side of (3.21) gives

$$\int_{-1}^{1} \frac{\partial^2 u}{\partial t^2} z dz = \frac{2}{3} \frac{\partial^2 \psi_r}{\partial t^2} . \tag{3.24}$$

The angular equation of motion is handled in the same manner. The remaining equation of motion is integrated directly:

$$\frac{1}{r}\int_{-1}^{1} \frac{\partial}{\partial r}(r\sigma_{rr})dz + \frac{1}{r}\int_{-1}^{1} \frac{\partial \sigma_{z\theta}}{\partial \theta} dz + \int_{-1}^{1} \frac{\partial \sigma_{zz}}{\partial z} dz = \int_{-1}^{1} \frac{\partial^2 w}{\partial t^2} dz. \tag{3.25}$$

The order of integration and differentiation can be interchanged for the first two terms in Eq. (3.25). The remaining integral yields

$$\int_{-1}^{1} \frac{\partial \sigma_{zz}}{\partial z} dz = (\sigma_{zz})_{-1}^{1} = q_2 - q_1 = q . \tag{3.26}$$

where q represents the distributed load on the plate. The resulting plate stress equations of motion are

$$\frac{1}{r}M_r+\frac{\partial M_r}{\partial r}+\frac{1}{r}\frac{\partial}{\partial\theta}M_{r\theta}-Q_r-\frac{M_\theta}{r}=\frac{2}{3}\frac{\partial^2\psi_r}{\partial t^2}\ ,$$

$$\frac{1}{r^2}(2rM_{r\theta}+r^2\frac{\partial M_{r\theta}}{\partial r})+\frac{1}{r}\frac{\partial M_\theta}{\partial\theta}-Q_\theta=\frac{2}{3}\frac{\partial^2\psi_\theta}{\partial t^2}\ , \qquad (3.27)$$

$$\frac{1}{r}Q_r+\frac{\partial Q_r}{\partial r}+\frac{1}{r}\frac{\partial Q_\theta}{\partial\theta}+q=2\frac{\partial^2 w}{\partial t^2}\ .$$

The plate stress-displacement equations given in Eq. (3.19) are substituted into Eq. (3.27) to give the nondimensional displacement equations of motion. At this point the assumption that the displacement field is axially symmetric will be used. In addition, since w is the displacement component of interest, only the first and third equations of motion will be needed. These equations are

$$\frac{\partial^2\psi_r}{\partial r^2}+\frac{1}{r}\frac{\partial\psi_r}{\partial r}-\frac{\psi_r}{r^2}-\frac{3\gamma^2(1-\nu)}{2}(\psi_r+\frac{\partial w}{\partial r})=(\frac{1-\nu}{2})\frac{\partial^2\psi_r}{\partial t^2}\ ,$$

$$\frac{\partial^2 w}{\partial r^2}+\frac{1}{r}(\frac{\partial w}{\partial r}+\frac{\partial}{\partial r}(r\psi_r)+\frac{q}{\gamma^2\mu}=\frac{1}{\gamma^2}\frac{\partial^2 w}{\partial t^2}\ . \qquad (3.28)$$

The dispersion relation resulting from Mindlin's approximate theory for the first asymmetric mode of propagation is [12]

$$\Omega^4-\Omega^2(\frac{2\kappa^2\gamma^2}{1-\nu}(\frac{1-\nu}{2}+\frac{1}{\gamma^2})+3\gamma^2)+\frac{2\gamma^2\kappa^4}{1-\nu}=0\ ,$$

$$\Omega=\frac{\omega' h}{C_t}\ ,\quad \kappa=\kappa' h\ , \qquad (3.29)$$

where Ω is the dimensionless frequency, and κ is the dimensionless wavenumber. Equation (3.29) is obtained by investigating the conditions under which straight-crested harmonic wave may propagate. This procedure, which has been carried out in great detail by Graff[13], provides a method for determining the adjustment coefficient, γ^2. Thus, by requiring that the phase velocity, $c = \Omega/\kappa$, converges to the Rayleigh velocity, c_R, as κ becomes large, we must have $\gamma^2 = (c_R/c_t)^2$. γ^2 is only a function of ν and can be obtained by solving Rayleigh's equation.

Before the boundary and initial conditions are presented, the functional form of the external loading will be constructed. The temporal profile of the loading function can be represented by a Dirac-delta function as mentioned earlier. Since the radial dependence of the laser pulse is assumed to be Guassian, the radial profile of the loading function will also have a Guassian dependence. Combining the radial and temporal profiles gives

$$q(r,t)=q_o\exp(\frac{-r^2}{a^2})\delta(t) \ , \qquad (3.30)$$

where a is the nondimensional Guassian beam radius, and q_o is the ablative source strength.

Boundary/Initial Conditions for Displacement Equation

The traction free boundary conditions for the exposed faces were implemented above when the exact equations of motion were integrated across the plates thickness.

The initial conditions for the ablative problem are given as:

$$w(r,0)=\frac{\partial w(r,0)}{\partial t}=\psi_r(r,0)=\frac{\partial \psi_r(r,0)}{\partial t}=0. \tag{3.31}$$

Equation (3.26) simply states that the plate is initially at rest. This completes the formulation of the problem.

CHAPTER 4

SOLUTION OF THE PROBLEMS

The differential equations that govern the displacement of a thin elastic plate that is subjected to high intensity laser radiation were developed in Chapter 3. Equations (3.3) were developed in a thermoelastic framework while Eqs. (3.28) were developed in an ablative framework. The solution of these equations will be the focus of this chapter. The solution techniques for both the thermoelastic and ablative problem will be similar. The structure of the displacement equations, (3.3) and (3.28) suggests Hankel transforms for the radial variable, while Laplace transforms will be used to eliminate dependence on time.

Solution of Thermoelastic Problem

The thermoelastic solution follows that of Sve and Miklowitz[10], except now only the first asymmetric mode of propagation is of importance. In addition, since the response of the interferometer is proportional to velocity, only dynamic displacements will be considered. The solution technique proceeds by applying Hankel and Laplace transforms to the Eqs. (3.3), and then solving the resulting ordinary differential equation in z. The inversion of the Laplace transform is accomplished by the use of residue theory. The transform expression for the displacement contains an infinite number of simple poles. As a result of the traction free boundary conditions and radial symmetry

these poles can be identified with the branches of the Rayleigh-Lamb frequency equation. Since the first asymmetric mode is of interest, only the lowest order pole will be used to compute the Laplace transform inversion. Radial dependence is recovered by converting the integral given in Eq. (4.1) into a Fourier integral and solving the resulting Fourier integral numerically. Formally the vertical displacement is given by

$$w(r,z,t)=\frac{(1+\nu)\exp(-\eta)T_{so}a^2\alpha}{2(1-\nu)}\int_0^{\infty} e^{\left(\frac{-\kappa^2a^2}{4}\right)}\kappa w_o(\kappa,z,t)J_o(\kappa r)d\kappa \ , \qquad (4.1)$$

where κ is the Hankel transform parameter and

$$w_o(\kappa,z,t)=-2M_a(\Omega_{na},\kappa,z)\cos(\Omega_{na}t) \ , \qquad (4.2)$$

where

$$M_a(\Omega,\kappa,t)=\frac{[M_{1a}(\Omega_{na})+M_{2a}(\Omega_{na})]}{[\eta^2-\kappa^2+(\Omega_{na}^2/\Delta^2)]\Omega_{na}^2D_a} \ . \qquad (4.3)$$

In the above expressions, the subscript, a, indicates the first asymmetric mode of propagation with respect to the midplane of the plate. The expressions M_{1a} and M_{2a} used to define M_a are defined as follows:

$$M_{1a}(\Omega_{ns}) = -\beta_1 G_3(\Omega_{na}) ch(\beta_1 z) \ ,$$
$$M_{2a}(\Omega_{ns}) = -2\kappa^2 G_4(\Omega_{na}) ch(\beta_2 z) \ , \tag{4.4}$$

where

$$G_3(\Omega_{na}) = 4\kappa^2 \eta \beta_2 sh(\beta_2) ch(\eta) - (\beta_2^2 + \kappa^2)^2 ch(\beta_2) sh(\eta) \ ,$$
$$G_4(\Omega_{na}) = (\beta_2^2 + \kappa^2)(\beta_1 ch(\beta_1) sh(\eta) - \eta sh(\beta_1) ch(\eta)) \ , \tag{4.5}$$

and

$$D_a = 4(\beta_2^2 + \kappa^2) sh(\beta_1) ch(\beta_2) + [\frac{(\beta_2^2 + \kappa^2)^2}{\beta_1 \Delta^2} - 4\beta_1 \kappa^2] ch(\beta_1) ch(\beta_2) +$$
$$[\frac{\beta_2^2 + \kappa^2)^2}{\beta_2} - \frac{4\beta_2 \kappa^2}{\Delta^2}] sh(\beta_1) sh(\beta_2) - 4\kappa^2 (\frac{\beta_2}{\beta_1 \Delta^2} + \frac{\beta_1}{\beta_2}) ch(\beta_1 sh(\beta_2) \ , \tag{4.6}$$

where β_1 and β_2 are defined as

$$\beta_1^2 = \kappa^2 - \Omega_{na}^2 / \Delta^2 \ ,$$
$$\beta_2^2 = \kappa^2 - \Omega_{na}^2 \ , \tag{4.7}$$
$$\Delta = c_l / c_t \ ,$$

and Ω_{na} is defined by the dispersion relation for asymmetric modes:

$$(\kappa^2+\beta_2^2)^2\cos(\beta_2)\sin(\beta_1)-4\kappa^2\beta_1\beta_2\cos(\beta_1)\sin(\beta_2)=0\ . \qquad (4.8)$$

Equations (4.4) are the same as the last two of Eqs. (48) of Ref[10] except that the factor $g(\kappa)$ appearing in the equations of Ref. [10] and defined by Eq. (18) of that paper has been incorporated explicitly in Eq. (4.1).

Through a change of variables, Eq. (4.1) will be converted into a Fourier integral. Converting Eq. (4.1) into a Fourier integral greatly facilitates modeling the frequency response of the photo diode and the signal conditioning equipment. The change of variables is accomplished by first writing Eq. (4.1) as

$$w(r,z,t)=\frac{1}{\sqrt{2\pi}}\int_0^\infty F(\kappa,z,t)\cos(\Omega_{na}t)d\kappa\ , \qquad (4.9)$$

where

$$F(\kappa,r,t)=-2\bar{T}\sqrt{2\pi}\exp(-\kappa^2a^2/4)\kappa J_o(\kappa r)M_a(\Omega_{na}(\kappa),\kappa,z)\ ,$$
$$\bar{T}=\frac{(1+\nu)\exp(-\eta)T_{so}a^2\alpha}{2(1-\nu)}\ . \qquad (4.10)$$

The variable κ and it's derivative can be expressed as

$$\kappa=\kappa(\Omega_{na})\ ,$$
$$d\kappa=\frac{\partial\kappa(\Omega_{na})}{\partial\Omega_{na}}d\Omega_{na}\ , \qquad (4.11)$$

where κ is related to Ω_{na} by Eq. (4.8). Now Eq. (4.9) can be expressed as

$$w(r,z,t)=\frac{1}{\sqrt{(2\pi)}}\int_{\Omega_{na}(0)}^{\Omega_{na}(\infty)} F(g(\Omega_{na}),z,t)\cos(\Omega_{na}t)\frac{\partial g(\Omega_{na})}{\partial \Omega_{na}}d\Omega_{na} \ . \tag{4.12}$$

Equations (4.7) and (4.8) reveal that $\Omega_{na} \to 0$ as $\kappa \to 0$ and $\Omega_{na} \to \infty$ as $\kappa \to \infty$, therefore; the upper and lower integration bounds in Eq. (4.12) can be replaced with ∞ and 0 respectively. Equation (4.12), which is now a Fourier transform of the displacement, will be inverted numerically. The numerical results will be presented in the next chapter.

Solution of Ablative Problem

The solution of the ablative problem will be carried out in much the same manner as the thermoelastic solution, except in greater detail. First, the dependence on time will be eliminated from Eqs. (3.28) by taking the Laplace transform of Eqs. (3.28), and applying the initial conditions, Eqs. (3.31), which gives

$$\begin{aligned} &\frac{\partial^2\Psi_r}{\partial r^2}+\frac{1}{r}\frac{\partial\Psi_r}{\partial r}-\frac{\Psi_r}{r^2}-\frac{3\kappa^2(1-\nu)}{2}\left(\Psi_r+\frac{\partial W}{\partial r}\right)=\frac{1-\nu}{2}p^2\Psi_r \ , \\ &\frac{1}{r}\frac{\partial W}{\partial r}+\frac{\partial^2 W}{\partial r^2}+\frac{1}{r}\frac{\partial}{\partial r}(r\Psi_r)+\frac{Q}{\gamma^2\mu}=\frac{1}{\gamma^2}p^2W(r,p) \ , \end{aligned} \tag{4.13}$$

where upper case quantities represent a Laplace transform with transform parameter p. The expression for the Laplace transform of the external loading function, Q, is defined by

$$Q(r,p)=q_o\exp(-r^2/a^2)\int_0^\infty \delta(t)\exp(-pt)dt=q_o\exp(\frac{-r^2}{a^2}) \ , \qquad (4.14)$$

where the last term on the right hand side of Eq. (4.14) follows from the definition of the Dirac-delta function.

Next, the radial dependence will be eliminated by taking the Hankel transform of Eqs. (4.13), which leads to

$$\begin{aligned} -\kappa^2\Psi_{r1}-\frac{3\gamma^2(1-\nu)}{2}(\Psi_{r1}-\kappa W_o)&=\frac{p^2(1-\nu)}{2}\Psi_{r1} \ , \\ -\kappa^2 W_o+\kappa\Psi_{r1}+\frac{Q_o}{\gamma^2\mu}&=\frac{p^2}{\gamma^2}W_o \ . \end{aligned} \qquad (4.15)$$

The Hankel transform of order n, denoted by subscript n, used to produce Eqs. (4.15) is defined by

$$f_n(\kappa)=\int_0^\infty rF(r)J_n(\kappa r)dr \ , \qquad (4.16)$$

where κ is the Hankel transform parameter, and J_n represents a Bessel function of the first kind of order n. The Hankel transform of the external loading function is defined by

$$Q_0(\kappa)=q_o\int_0^\infty \exp(\frac{-r^2}{a^2})J_o(\kappa,r)rdr=q_o\frac{a^2}{2}\exp(\frac{-\kappa^2a^2}{4}) \quad . \tag{4.17}$$

It should be noted that in obtaining the Hankel transform of Eq. (4.13) it was assumed that the expressions rW(r,p), rW'(r,p), rΨ(r,p), and rΨ(r,p)' tend to zero as r tends to zero or infinity. This assumption greatly increases the utility of the Hankel transform and in this case is not overly restrictive.

Solving for $\Psi(\kappa,p)$ in the first of Eqs. (4.15) gives

$$\Psi_{rl}(\kappa,p)=\frac{3\gamma^2(1-\nu)\kappa}{2\kappa^2+3\gamma^2(1-\nu)+p^2(1-\nu)}W_o(\kappa,p) \quad . \tag{4.18}$$

Next Eq. (4.18) is substituted into the second of Eqs. (4.15). After simplification this results in

$$W_o(\kappa,p)=\frac{Q_o}{\gamma^2\mu}\left\{\frac{\frac{2\gamma^2\kappa^2}{1-\nu}+3\gamma^4+p^2\gamma^2}{H_a(\kappa,p)}\right\} , \tag{4.19}$$

where $H_a(\kappa,p)$ is defined by

$$H_a(\kappa,p)=p^4+p^2[\frac{2\kappa^2\gamma^2}{1-\nu}(\frac{1-\nu}{2}+\frac{1}{\gamma^2})+3\gamma^2]+\frac{2\gamma^2\kappa^4}{1-\nu} , \tag{4.20}$$

The next step in the solution procedure is the Laplace inversion of Eq. (4.19). The formal procedure furnishes

$$\mathcal{L}^{-1}\{W_o(\kappa,p)\}=W_o(\kappa,t)=\frac{1}{2\pi i}\int_{Br} W_o(\kappa,p)\exp(pt)dp \ , \qquad (4.21)$$

where Br is the Bromwich contour in the right half p-plane. With use of Cauchy's theorem and residue theory, the Laplace inversion, Eq. (4.21), can be rewritten as

$$\mathcal{L}^{-1}\{W_o(\kappa,p)\}=2\pi i\sum_{i=1}^{n} a_i \ , \qquad (4.22)$$

where a_i are the residues of $W_o(\kappa,p)\exp(pt)$. The poles of $W_o\exp(pt)$ are the four simple poles located at the zeros, d_i, of Eq. (4.20). The residues connected with these poles can be obtained by

$$a_i=\lim_{(p\to d_i)}(p-d_i)W_o(\kappa,p)\exp(pt) \ , \qquad i=1,2,3,4. \qquad (4.23)$$

The zeros, d_i, are given by

$$d_{1,2}=\pm\sqrt{\frac{-B(\kappa)+\sqrt{B(\kappa)^2-4C(\kappa)}}{2}} \ , \qquad d_{3,4}=\pm\sqrt{\frac{-B(\kappa)-\sqrt{B(\kappa)^2-4C(\kappa)}}{2}} \ , \qquad (4.24)$$

where $B(\kappa)$ and $C(\kappa)$ are defined by

$$B(\kappa)=\frac{2\kappa^2\gamma^2}{1-\nu}\left(\frac{1-\nu}{2}+\frac{1}{\gamma^2}\right)+3\gamma^2 ,$$
$$C(\kappa)=\frac{2\gamma^2\kappa^4}{1-\nu} . \qquad (4.25)$$

Note that since $0 < \gamma < 1$ and $-1 < \nu < .5$, it follows that $B(\kappa) > 0$ and $C(\kappa) \geq 0$. Thus, by Descartes' rule of signs, the roots given by Eq. (4.24) cannot be real. The nature of the roots, d_i, of H_a is further revealed by examining the quantity $B(\kappa)^2 - 4C(\kappa)$. This quantity, in expanded form, is given by

$$B(\kappa)^2-4C(\kappa)=\kappa^4\left(\gamma^2-\frac{2}{1-\nu}\right)^2+\kappa^2\left(\frac{12\gamma^2}{1-\nu}+6\gamma^4\right)+9\gamma^4 \qquad (4.26)$$

Since the Hankel inversion requires that κ be real and positive, the quantity $B(\kappa)^2 - 4\,C(\kappa)$ is positive which, through Eqs. (4.24), shows that the roots, d_i, must be purely imaginary. Inserting $p=i\Omega$ into Eq. (4.20) we have

$$H_a(\kappa,i\Omega)=\Omega^4-\Omega^2\left[\frac{2\kappa^2\gamma^2}{1-\nu}\left(\frac{1-\nu}{2}+\frac{1}{\gamma^2}\right)+3\gamma^2\right]+\frac{2\gamma^2\kappa^4}{1-\nu} ,$$
$$d_{1,2,3,4}=i\Omega_{1,2,3,4} , \qquad (4.27)$$

where Ω is given by Eq. (3.29). Since Eq. (4.27), is identical to Eq. (3.29), the expressions $\Omega_{1,2,3,4}$ can be identified as the branches of Mindlin's frequency equation. The branch associated with $\Omega_{3,4}$ has a cutoff frequency of $\gamma\sqrt{3}$, while the branch

associated with $\Omega_{1,2}$ has a cutoff frequency of zero. Since our interest lies in modeling the first asymmetric mode of propagation, the branch associated with $\Omega_{3,4}$ will not be considered. Thus, only the residues located at $d_{1,2}$ will be required to invert the Laplace transform. Inserting Eq. (4.19) into Eq. (4.23) we have

$$a_1=\lim_{(p\to d_1)}\frac{Q_o(\kappa)}{\mu\gamma^2}\left(\frac{N(\kappa,p)(p-i\Omega)\exp(pt)}{p^4+B(\kappa)p^2+C(\kappa)}\right),$$
$$a_2=\lim_{(p\to d_2)}\frac{Q_o(\kappa)}{\mu\gamma^2}\left(\frac{N(\kappa,p)(p+i\Omega)\exp(pt)}{p^4+B(\kappa)p^2+C(\kappa)}\right), \tag{4.28}$$

where $N(\kappa,p)$ is given by

$$N(\kappa,p)=\frac{2\gamma^2\kappa^2}{1-\nu}+3\gamma^4+p^2\gamma^2 . \tag{4.29}$$

Equations (4.28) must be evaluated using L'Hôpital's rule, which results in

$$a_1+a_2=\frac{Q_o(\kappa)}{\mu\gamma^2}\left(\frac{iN(\kappa,i\Omega)\exp(i\Omega t)-iN(\kappa,-i\Omega)\exp(-i\Omega t)}{4\Omega^3-2\Omega B(\kappa)}\right) . \tag{4.30}$$

Since $N(\kappa,p)$ is an even function of p, the Laplace inversion can be written as

$$W_o(\kappa,t)=\frac{Q_o(\kappa)}{\mu\gamma^2}\left(\frac{2\sin(\Omega t)N(\kappa,i\Omega)}{-4\Omega^3+2\Omega B(\kappa)}\right) . \tag{4.31}$$

The Hankel inversion of Eq. (4.31), is formally given by

$$w(r,t)=\int_0^\infty \kappa W_o(\kappa,t)J_o(\kappa,r)d\kappa \ . \qquad (4.32)$$

The remaining step in this solution procedure is to convert the Hankel transform given in Eq. (4.32) into a Fourier integral. As with the thermoelastic solution, the impetus for converting Eq. (4.32) into a Fourier integral is the ease with which the frequency response of the photodiode and signal conditioning equipment can be modeled. It should be noted that a Fourier transform could have been used to eliminate time from onset. The present problem utilizes a Laplace transform because, with the aid of residue theory, the inversion of the Laplace transform, as compared to the inversion of the Fourier transform, can be performed with relative ease. With reference to Eq. (4.31), Eq. (4.32) can be written as

$$w(r,t)=\frac{1}{\sqrt{2\pi}}\int_0^\infty F(\kappa,t)\sin(\Omega t)d\kappa \ , \qquad (4.33)$$

where F(κ,t) is defined by

$$F(\kappa,t)=\frac{2Q_o(\kappa)\sqrt{2\pi}\kappa J_o(\kappa,r)N(\kappa,i\Omega)}{\mu\gamma^2[-4\Omega^3+2\Omega B(\kappa)]} \ . \qquad (4.34)$$

The Hankel inversion parameter (κ) is related to the frequency by the first of Eqs. (4.24), which allows the differential dκ in Eq. (4.33) to be defined as follows:

$$d\kappa(\Omega)=\frac{\partial\kappa(\Omega)}{\partial\Omega}d\Omega=\frac{1}{4\sqrt{S}}[-\frac{\partial B}{\partial\kappa}+\frac{1}{2\sqrt{\bar{S}}}(2B\frac{\partial B}{\partial\kappa}-4\frac{\partial C}{\partial\kappa})]d\Omega\ , \tag{4.35}$$

where the expressions S and $\bar{S}$ are defined by

$$S=\sqrt{\frac{-B+\sqrt{\bar{S}}}{2}} \tag{4.36}$$

$$\bar{S}=\sqrt{B^2-4C}\ .$$

With the aid of Eq. (4.35), Eq. (4.33) can be written as

$$w(r,t)=\frac{1}{\sqrt{2\pi}}\int_{\Omega(0)}^{\Omega(\infty)}F(\Omega,t)\frac{\partial\kappa(\Omega)}{\partial\Omega}\sin(\Omega t)d\Omega\ . \tag{4.37}$$

Since, by the first of Eq. (4.24), $\Omega \to 0$ as $\kappa \to 0$ and $\Omega \to \infty$ as $\kappa \to \infty$, the upper and lower integration limits in Eq. (4.37) can be replaced with ∞ and 0 respectively. Equation (4.37), which now represents a Fourier integral for the displacement, must be solved numerically. The numerical results will be presented in chapter 6 of this paper.

CHAPTER 5

RESULTS/ANALYSIS OF THE THERMOELASTIC PROBLEM

The focus of the present chapter will be to compare the thermoelastic theory developed in Chapters 3 and 4 with experimental Lamb waves generated in a thin glass plate. This comparison will allow the elastic constants and the optical absorption coefficient of the glass film to be determined. First the elastic constants of the glass sample will be estimated by measuring the wave speeds of the first symmetric and asymmetric waves. Using the approximate elastic constants, the program COMBINATION will then be used to generate theoretical velocity data which will be compared to the experimental velocity data. This comparison will serve to fine tune the approximation of the elastic constants and will reveal the absorption coefficient.

Technique for Estimating Elastic Constants of Thin Glass Films

The Rayleigh-Lamb frequency spectrum for the first symmetric mode, s_o, and the first asymmetric mode, a_o, of a thin brass plate is shown in Fig 9. For small dimensionless wave number, κ, the s_o mode is linear and has phase velocity, C_e, equal to its group velocity. Therefore, since the group velocity is a measurable quantity, C_e can be determined experimentally. C_e is obtained by first rewriting Eq.(4.8) as

$$\frac{\tan(\beta_2)}{\tan(\beta_1)} = \frac{4\kappa^2\beta_1\beta_2}{(\kappa^2+\beta_2^2)^2} \quad . \tag{5.1}$$

For small κ, the small angle approximation for the tangent function can be used giving

$$\frac{\tan(\beta_2)}{\tan(\beta_1)} \approx \frac{\beta_2}{\beta_1} = \frac{-4\beta_1\beta_2\kappa^2}{(\kappa^2-\beta_2^2)^2} \quad . \tag{5.2}$$

With the aid of Eq. (4.7), Eq. (5.2) can be solved for C_e resulting in

$$C_e = \frac{\Omega}{\kappa} = 2C_t\sqrt{1-\frac{C_t^2}{C_L^2}} = 2C_t\sqrt{\frac{1}{2-2\nu}} \quad . \tag{5.3}$$

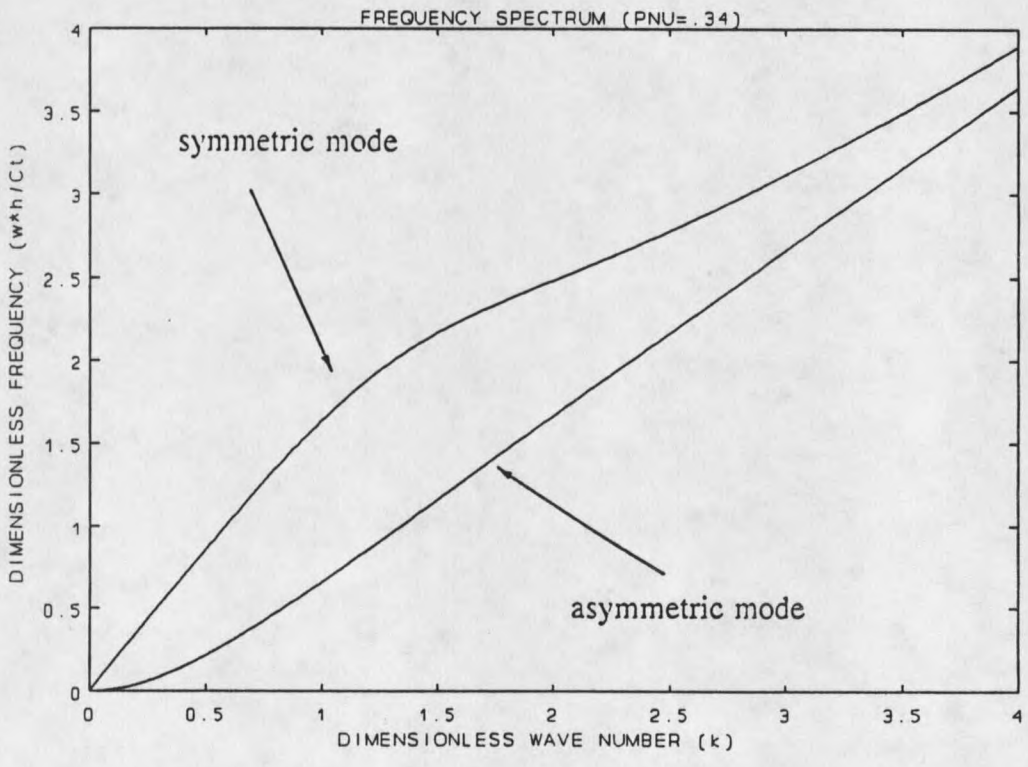

Fig. 9. First symmetric and asymmetric mode for .105 mm thick brass sample.

C_e is a function of υ and E; therefore, another relation is required to uniquely determine both υ and E. This relation may be obtained by considering the a_o mode. The phase velocity for this mode varies from zero at zero wave number to the Rayleigh velocity at very large wave number. In addition, for large wave number the a_o mode becomes linear; therefore, the high frequency components of the a_o mode are dispersionless and travel at the Rayleigh velocity. The Rayleigh velocity is expressed as

$$C_r=\gamma(\upsilon)C_t \ . \qquad (5.4)$$

where γ is the only root of the Rayleigh equation that satisfies the conditions required for the existence of surface waves. The Rayleigh equation is given by [14]

$$(C/C_t)^6-8(C/C_t)^4+(C/C_t)^2(24-\frac{16}{\Delta^2})-16(1-\frac{1}{\Delta^2})=0 \ , \qquad (5.5)$$

where Δ, defined in Eqs. (4.7), is the ratio of the longitudinal and shear wave velocities. Now Eq.(5.4) is substituted into Eq.(5.3) resulting in

$$\frac{C_e}{C_r}=\frac{2}{\gamma}\sqrt{1-\frac{1}{\Delta^2}} \ , \qquad (5.6)$$

which is only a function of ν, allowing ν to be uniquely determined. Next, C_t is obtained by substituting ν and C_e into Eq. (5.3). Before this procedure is used, the circumstances which will produce symmetric waves traveling with constant velocity, C_e, and asymmetric waves traveling at the Rayleigh velocity must be investigated.

As mentioned earlier, the symmetric mode of propagation has a well defined velocity, C_e, only for small wave number. In order to experimentally determine C_e, it would be desirable to manipulate the parameters of the experiment in such a way that only the low frequency dispersionless components of the s_o mode are excited. This goal is achieved by adjusting the nondimensional Guassian beam radius (GBR) of the Nd:YAG laser. Figure 10 shows the Fourier spectrum of the velocity for the first symmetric wave with GBR as a parameter. Figure 10 demonstrates that for large GBR, only the low frequency components of the s_o mode will be excited. Hence, for large GBR the group velocity of the s_o mode will equal its phase velocity allowing C_e to be determined experimentally.

The question still remains, how can high frequency asymmetric waves be generated so as to enable measurement of C_r? Once again, the answer involves adjustment of GBR. In Fig. 11 the Fourier spectrum versus frequency of the first asymmetric wave with GBR as a parameter has been plotted. From Fig. 11 it can been seen that as GBR is decreased, the higher frequency components of the a_o mode become more important. Owing to the strong dependence of the symmetric and asymmetric Fourier spectrums on GBR, the velocities C_e and C_r may be accurately determined by adjusting GBR and hence the elastic constants may be estimated.

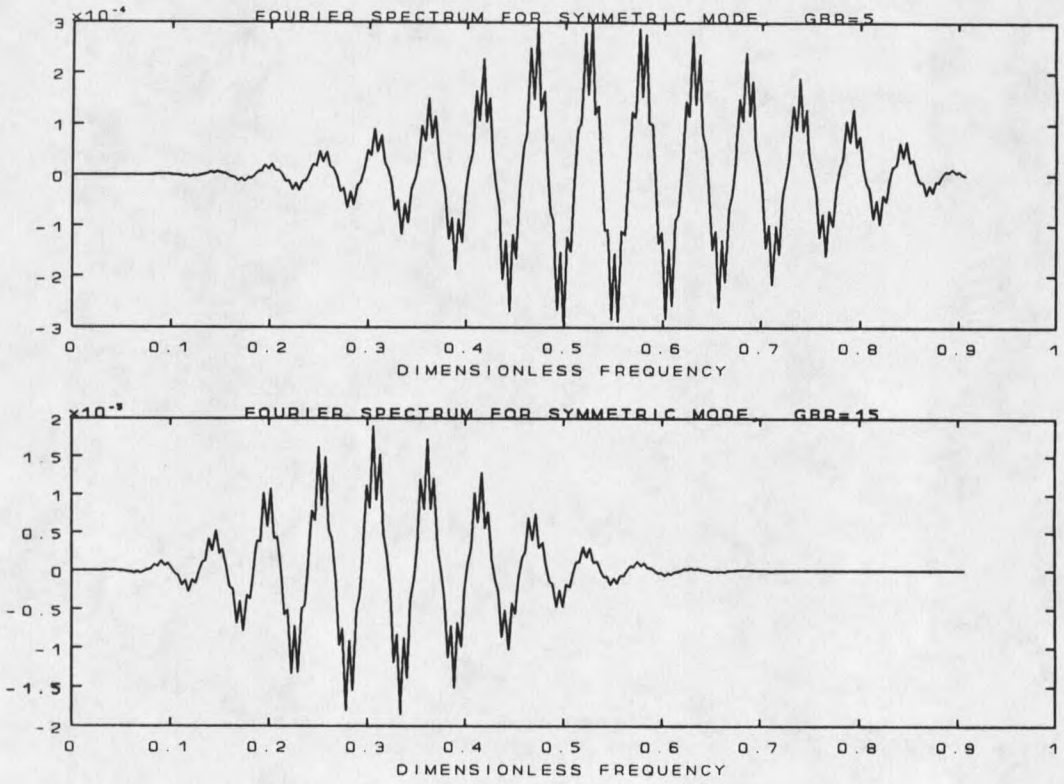

Fig. 10. Fourier spectrum of the velocity with the Gaussian beam radius (GBR) as a parameter.

Estimation of Elastic Constants for Brass Sample

The first test to which the above technique will be put is to estimate Poisson's ratio and the shear wave velocity of a specimen with known elastic constants and optical penetration depth. The specimen chosen was a thin brass plate. Figure 12 shows the experimental Lamb waves that were generated in a .105 mm thick brass sample. The nondimensional source receiver separation distance (R) was 253. The symmetric wave arrives at 3.5 μs and has a velocity of 3.79 mm/μs. The asymmetric wave can first be distinguished at 6.91 μs and has an approximate velocity of 1.92 mm/μs. The program

PNNNU was used to solve Eq. (5.6) numerically for the elastic constants. The results of this technique are listed in Table 1.

Table 1. Comparison between estimated elastic constants and published elastic constants.

	Estimated values	Published values	Percent Difference
Poisson's ratio	.393	.324	21.3%
Shear wave velocity (mm/μs)	2.04	2.166	5.8%

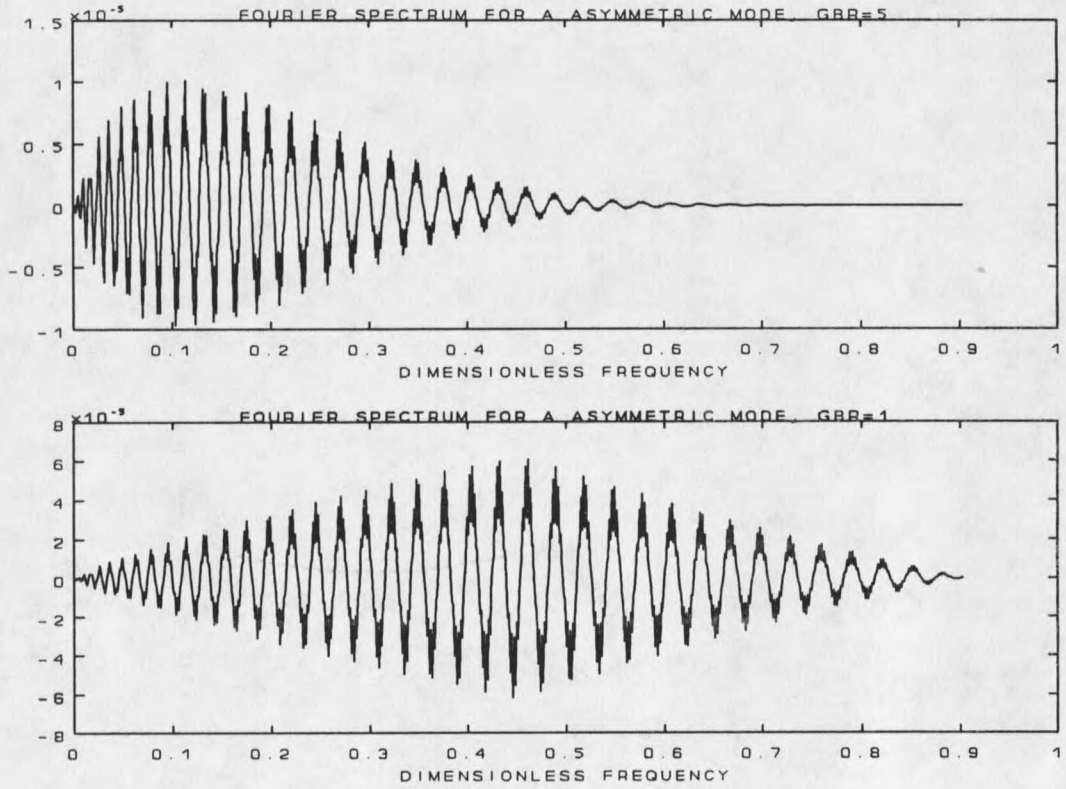

Fig. 11. Fourier spectrum of the velocity with the Gaussian beam radius (GBR) as a parameter.

The large uncertainty in the estimate of ν can be explained by considering the asymmetric wave speed. Had the magnitude of GBR been smaller, the higher frequency components of the asymmetric wave would have been stimulated, resulting in a more accurate estimate of ν.

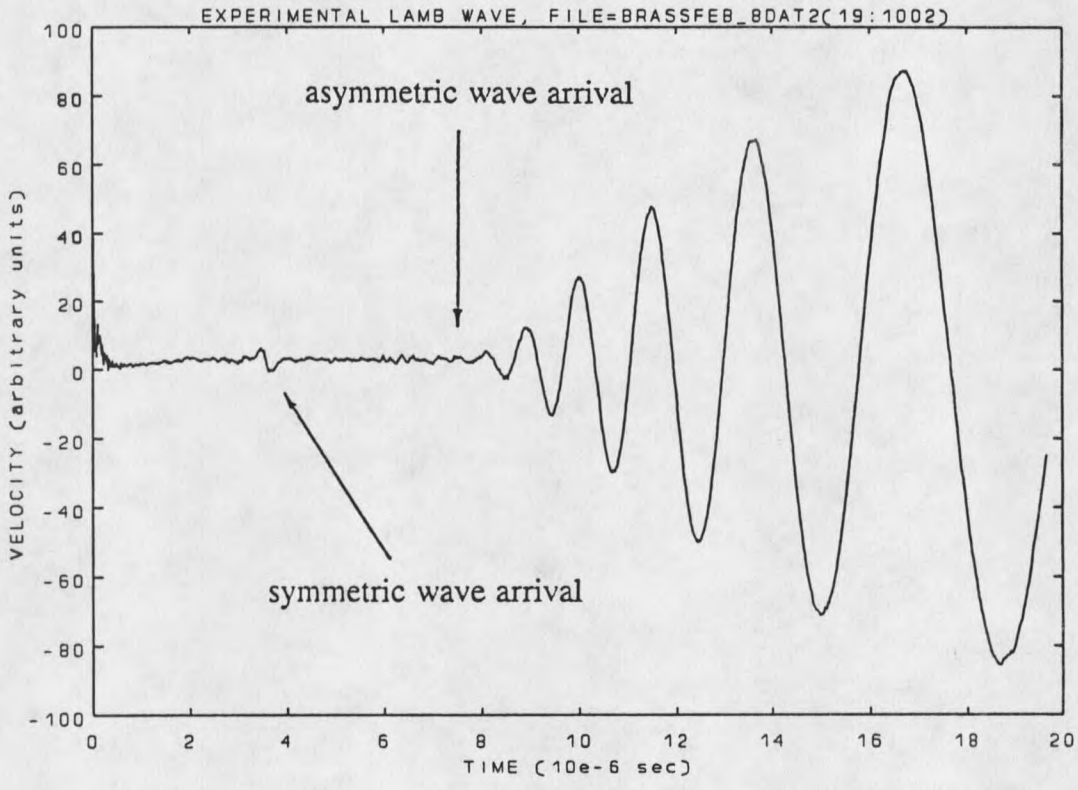

Fig. 12. Lamb waves in .105 mm thick brass sample.

Figure 9 demonstrates that for small dimensionless frequency, the asymmetric group velocity is less than C_r. Therefore, if the magnitude of GBR is too large the high frequency components of the a_o wave that are traveling at C_r will not be excited, resulting in an estimation of C_r that is smaller than the actual value. While this technique in its

present form (GBR too large) results in considerable uncertainty in υ, it serves as a upper limit for υ. This result is illustrated in Fig. 13 which shows a plot of C_e/C_r versus υ. An estimate of C_r that is smaller than the actual value will result in an initial estimate of υ that is larger than the actual value.

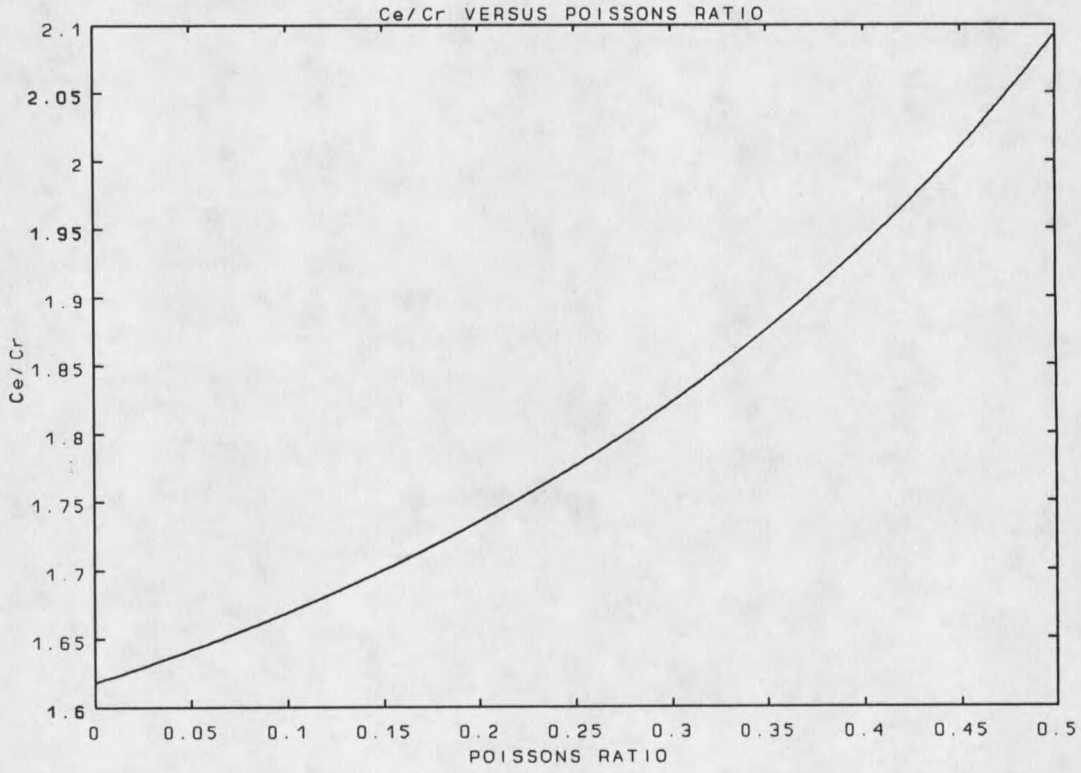

Fig. 13. Technique for estimating elastic constants serves as an upper limit on ν.

The results for the elastic constants may be brought into closer agreement with published values by comparing the theoretical velocity data generated using the estimated elastic constants to the experimental velocity data. This comparison is presented in Fig. 14, which shows that both the experimental and theoretical wave forms are similar in

shape but show a difference in phase. Now the question arises, changing which parameters will bring the theoretical data into agreement with the experimental data?

The parameters involved in the thermoelastic solution that have not been well defined are the Guassian laser beam radius, GBR, the optical absorption coefficient, ETA, and the shear wave velocity, C_t. Figure 15 illustrates that changing GBR has no effect on the phase of the asymmetric wave. In fact, decreasing GBR only adds high frequency components to the a_o wave, a result that was discovered earlier. Figure 16 shows that as ETA is decreased the amplitude of the a_o wave decreases but the phase remains the same. This dependence on ETA is expected since the asymmetric wave should vanish as ETA goes to zero. C_t is the only remaining parameter. Figure 17 demonstrates that changing C_t does in fact have an effect on the phase of the asymmetric wave. Since the time is nondimensionalized using C_t, an increase in C_t will cause the time scale used in the theoretical model to shrink relative to the experimental data. Conversely a decrease in C_t will cause the theoretical time scale to expand relative to the experimental data. Figure 14 reveals that expanding the theoretical time scale produces the desired result; thus, C_t must be made larger to bring the experiment and theory into agreement. Figure 18 establishes that for a given C_e, increasing C_t is tantamount to increasing C_r. Figure 13 displays that, for a given C_e, an increase in C_r results in a decrease in υ, which places the value of υ closer to the published data. Figure 19 compares both the experiment and the theory after many applications of the above process, and Table 2 shows a comparison of the elastic constants used to produce Fig 19 and the published elastic constants. While this procedure for determining elastic

constants is quite lengthy, it does produce accurate results and reveals the cause and effect nature of many of the parameters involved in the experiment.

Table 2. Comparison between estimated elastic constants and published elastic constants.

	Estimated values	Published values	Percent Difference
Poisson's ratio	.329	.324	1.5%
Shear wave velocity (mm/μs)	2.20	2.166	1.6%

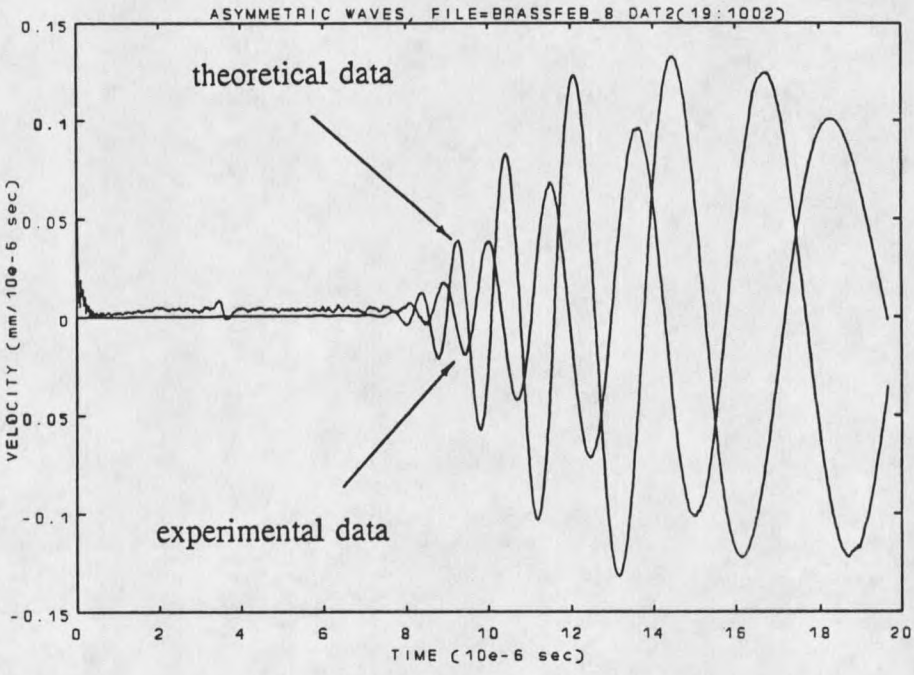

Fig. 14. Comparison between theoretical and experimental data.

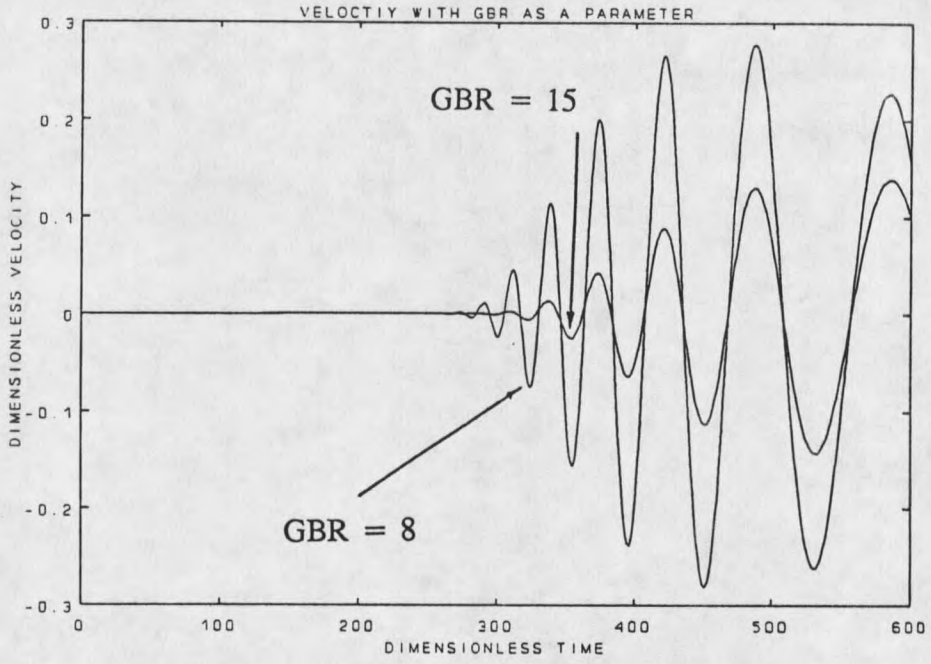

Fig. 15. Theoretical velocity data with GBR as a parameter.

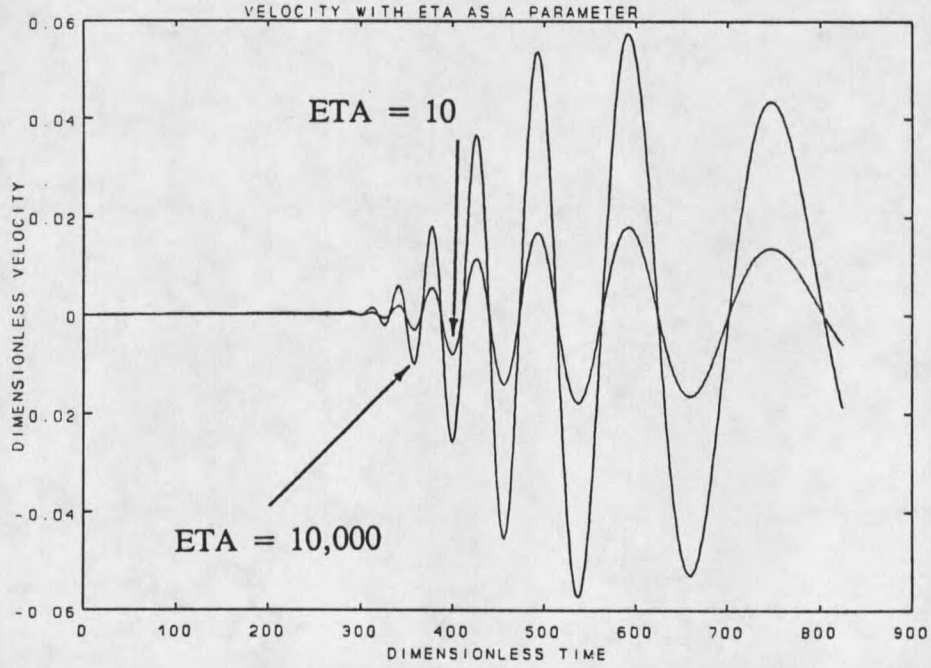

Fig. 16. Theoretical velocity data with ETA as a parameter.

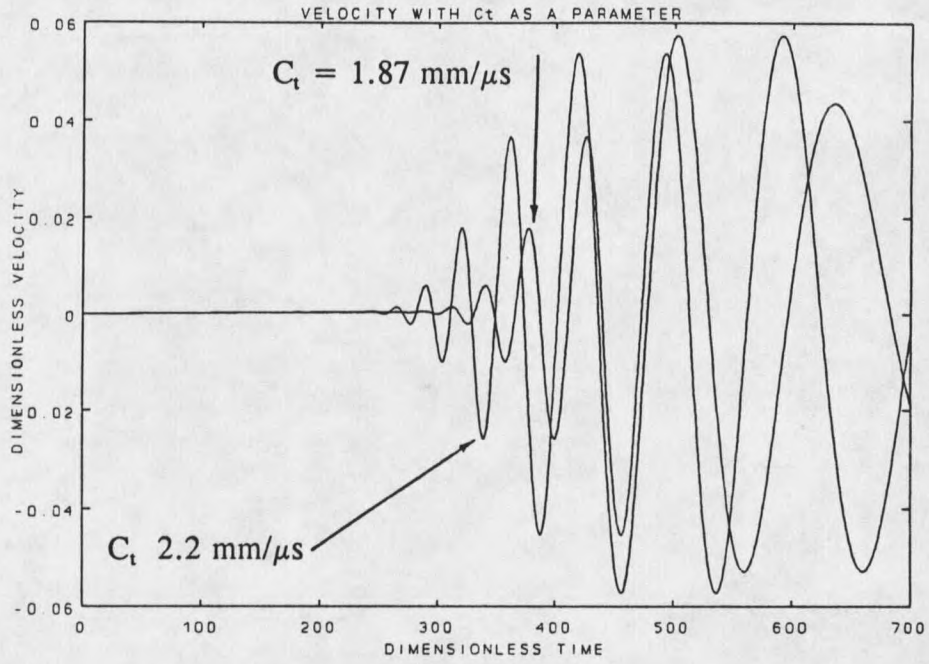

Fig. 17. Theoretical velocity data with C_t as a parameter.

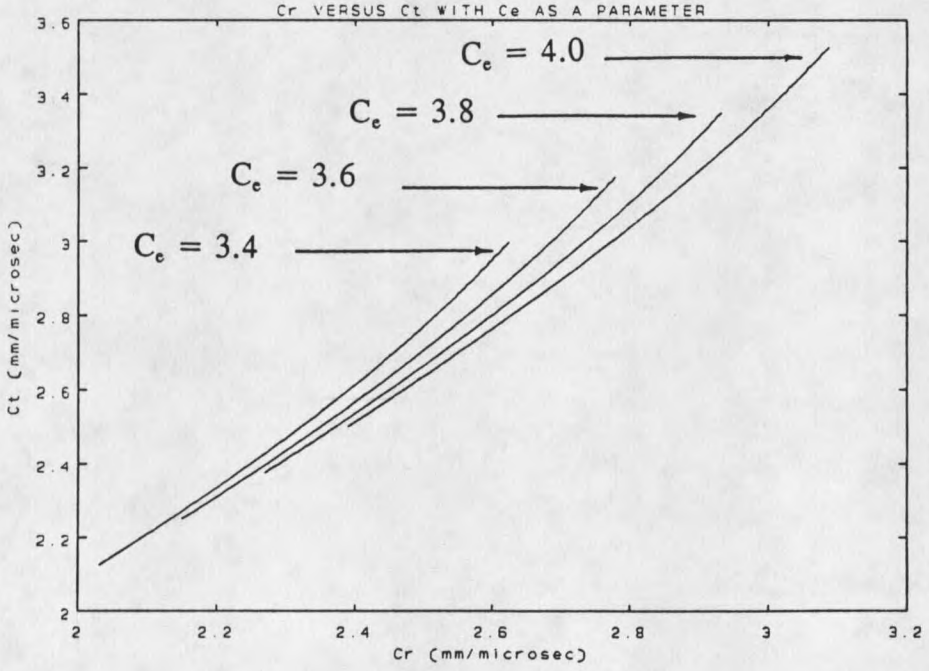

Fig. 18. For a given value of C_e, an increase in C_t results in an increase in C_r.

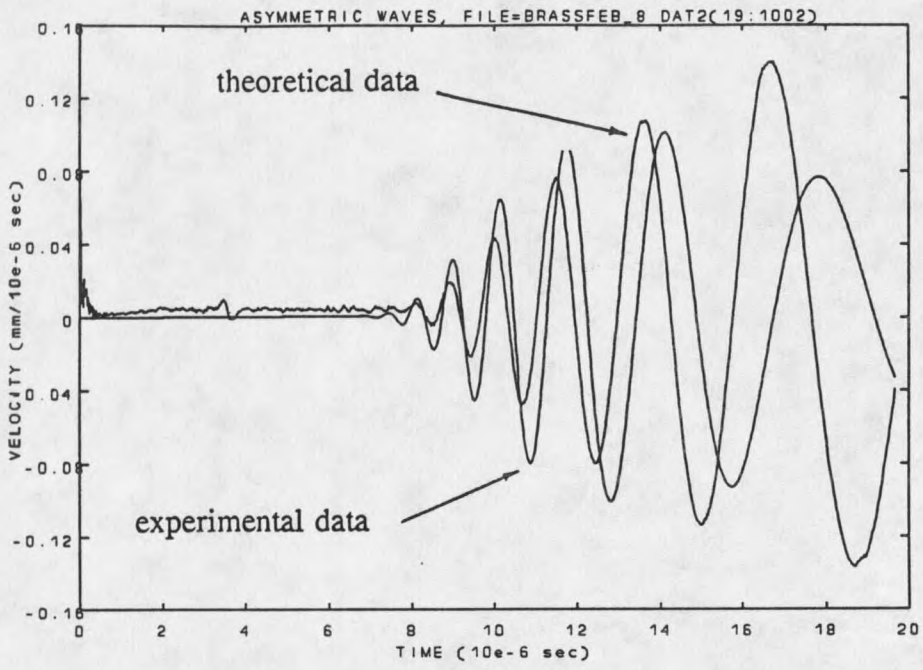

Fig. 19. Comparison between experimental and theoretical data after elastic constants have been fine tuned.

Estimation of Elastic Constants and Optical Absorption Coefficient for a Glass Sample

The same procedure used for the brass sample was carried out on a thin specimen of laser safety glass. Table 3 compares the estimated value of ν and C_t to the published data and Fig. 20 displays both the experimental and theoretical data. Once again the results are accurate. In addition to the elastic constants of this glass film, the dimensionless optical absorption coefficient (ETA) is of interest. By using the experimental results for the brass sample the response of the interferometer and signal conditioning equipment may be calibrated. Since the signal amplitude is dependent on the optical absorption coefficient, the amplitude of the theoretical data may be compared

to the calibrated experimental data revealing ETA. In Fig. 21, the maximum velocity for the first asymmetric wave has been plotted versus ETA. This figure demonstrates that for ETA less than about 7, the maximum velocity is very sensitive to changes in ETA; thus, the present technique of comparing the theoretical and experimental amplitudes to obtain ETA, is extremely sensitive in this region. Figure 21 also demonstrates that the sensitivity of the present technique drops off rapidly for ETA greater than 7.

Table 3. Comparison between estimated elastic constants and published elastic constants.

	Estimated values	Published values	Percent Difference
Poisson's ratio	.283	.245	15.5%
Shear wave velocity (mm/μs)	3.25	3.05	6.55%

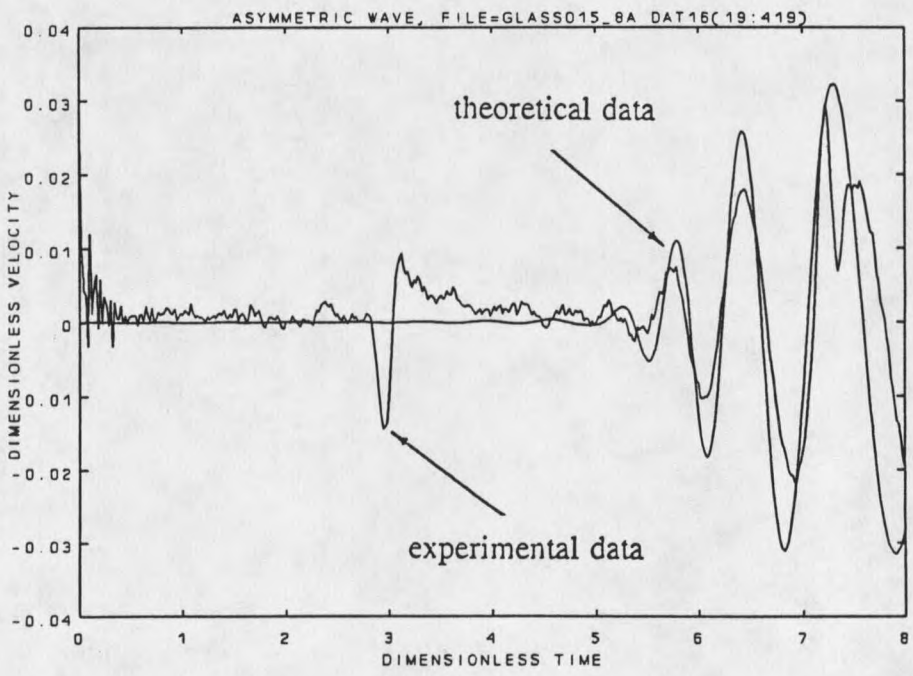

Fig. 20. Comparison between experimental and theoretical data for glass sample.

The system was calibrated using the .105 mm thick brass sample. The experimental Lamb wave shown in Fig 19 has a peak velocity of .132 mm/μs which corresponds to a peak amplified voltage of the photodiode of 97.8 mv. The attenuation used to produce Fig. 19 was 16 dβ. Thus, if the amplification of the signal is not changed, the peak velocity of the theory and the experiment may be compared. By adjusting the optical absorption coefficient, the theory is brought into agreement with the experimental data thus enabling an estimation of the optical absorption coefficient. The results of this process are compared to the experimentally determined optical absorption coefficient for the laser safety glass sample in Table 4.

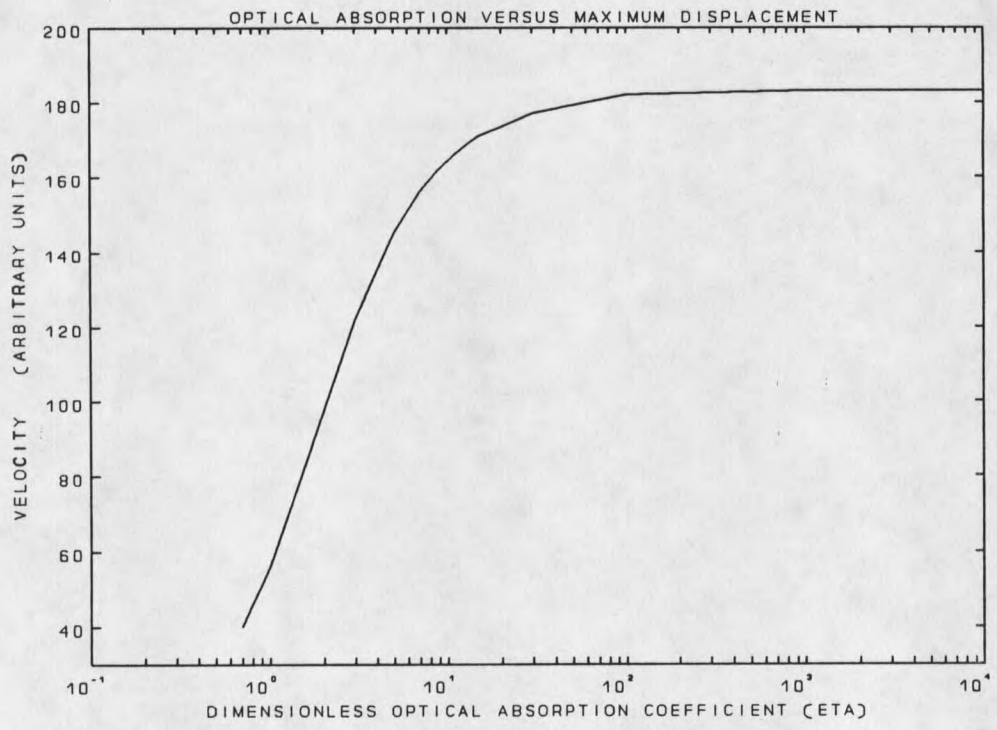

Fig. 21. Maximum velocity of asymmetric wave plotted versus optical absorption coefficient (ETA).

Table 4. Comparison between estimated and experimental optical absorption coefficient.

	Estimated values	Experimental value	Percent Difference
ETA	1.45	0.926	56.6%

Conclusion

In conclusion, this technique of comparing experimental and theoretical wave forms not only allows the determination of the elastic constants of thin glass films, but also permits the optical absorption coefficient to be estimated. Table 4 shows that the estimated value of ETA has a considerable uncertainty. This uncertainty is very sensitive to the thermal constants of the material, the linear coefficient of expansion, α, and the specific heat, C. Equations (3.2) and (4.1) illustrate that the signal amplitude is proportional to α/C; therefore, uncertainty in the thermal constants would result in uncertainty in the estimated value of ETA. Since the symmetric and asymmetric velocities have the same dependence on the thermal constants, this problem can be circumvented by comparing the ratio of the maximum symmetric and asymmetric velocities.

CHAPTER 6

RESULTS AND ANALYSIS OF THE ABLATIVE PROBLEM

In chapter 5, the elastic constants of a thin glass film were determined using ultrasound generated in a thermoelastic manner. The focus of the present chapter will be to examine the combined influence that an ablative and thermoelastic source have on the waveform generated in thin metallic samples. In order to facilitate this investigation, only the first asymmetric mode of propagation will be studied.

Since ablation takes place once the atoms on the sample's surface begin to vaporize, ablative waves must be accompanied by thermoelastic waves. This experimental reality is modeled theoretically by simply adding the ablative and thermoelastic solutions. Joining the solutions in this fashion is allowed since the differential equations describing both the thermoelastic and ablative problem are linear.

Investigation of the Accuracy of the Ablative Solution

Before combining the thermoelastic and ablative solutions, we must investigate how closely Mindlin's approximate plate theory, which was used to model the ablative problem, agrees with the exact theory, which was used to model the thermoelastic problem. As a result of the stress free boundary conditions, the exact frequency spectrum for both the thermoelastic and ablative problems is governed by the Rayleigh-frequency equation. This fact allows a comparison between the two theories to be

performed by comparing Mindlin's approximate frequency equation for the first asymmetric mode (a_o), given in Eq. (4.22), with the exact frequency equation for the a_o mode, given in Eq. (4.8). This comparison is graphically displayed in Fig. 22. The program MLABRT was used to produce the exact frequency spectrum, while the program MOMENTSPEC was used to produce Mindlin's frequency spectrum. Figure 22 shows that for dimensionless wave number less than 1.5 the approximate frequency relation cannot be distinguished from the exact frequency relation for the a_o mode. The discrepancy that starts to develop after a dimensionless wave number of 1.5 will not affect the solution since the bandpass filter employed in the experiment does not allow this portion of the frequency spectrum to be observed.

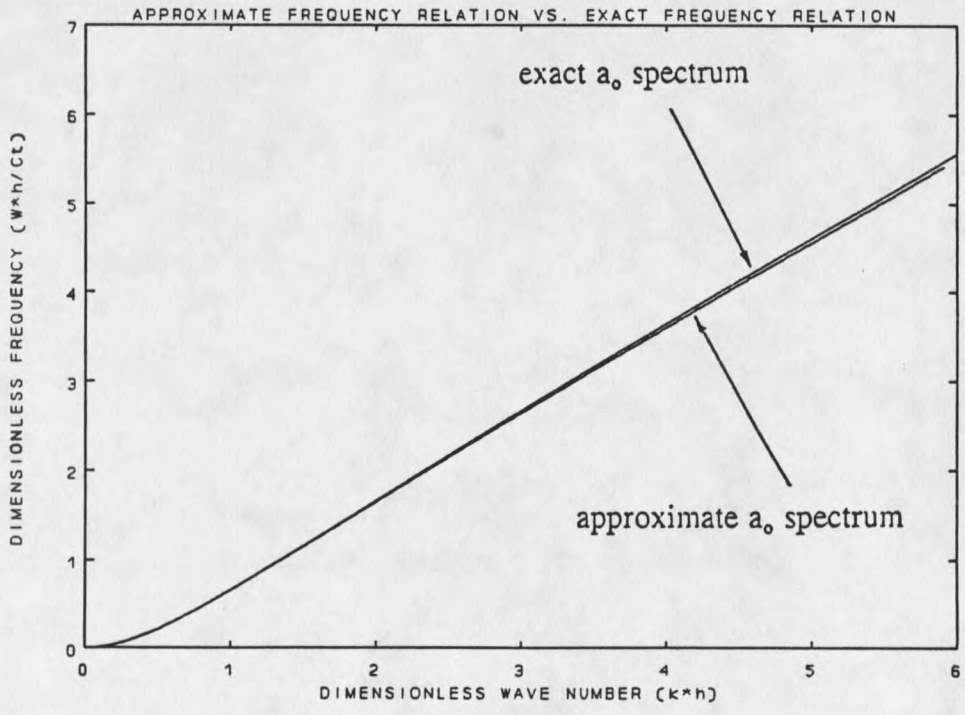

Fig. 22. Mindlin's frequency spectrum compared with the exact frequency spectrum for the a_o mode.

Combination of Thermoelastic and Ablative Solutions

Owing to the close comparison between the two theories, the thermoelastic and ablative solution will both utilize Mindlin's approximate frequency relation. Consolidating the solution in this manner reduces computer time since only one frequency relation must be calculated.

The top graph in Figs. 23 and 24 shows the ablative solution superimposed on the thermoelastic solution, while the bottom graph shows the two solutions added together. The ablative source strength, q_o, given in Eq. (3.25), has not been considered; therefore, the signal amplitude of the ablative and thermoelastic waves will remain arbitrary. The Gaussian laser beam radius (GBR), radial distance from epicenter (R), and Poisson's ratio (PNU) are the same for both solutions in each plot. The thermoelastic solution employs a dimensionless optical absorption coefficient of 10,000, which is a typical value for metals. Figures 23 through 24 illustrate that as the parameters GBR and R are varied, the two solutions behave in a coherent fashion. Thus for metals, ablative waves should constructively interfere with thermoelastic waves causing an increase in signal amplitude. By calculating the ablative source strength, the magnitude of this signal increase can be determined. Conversely, knowledge of the relative signal increase would facilitate the calculation of the ablative source strength.

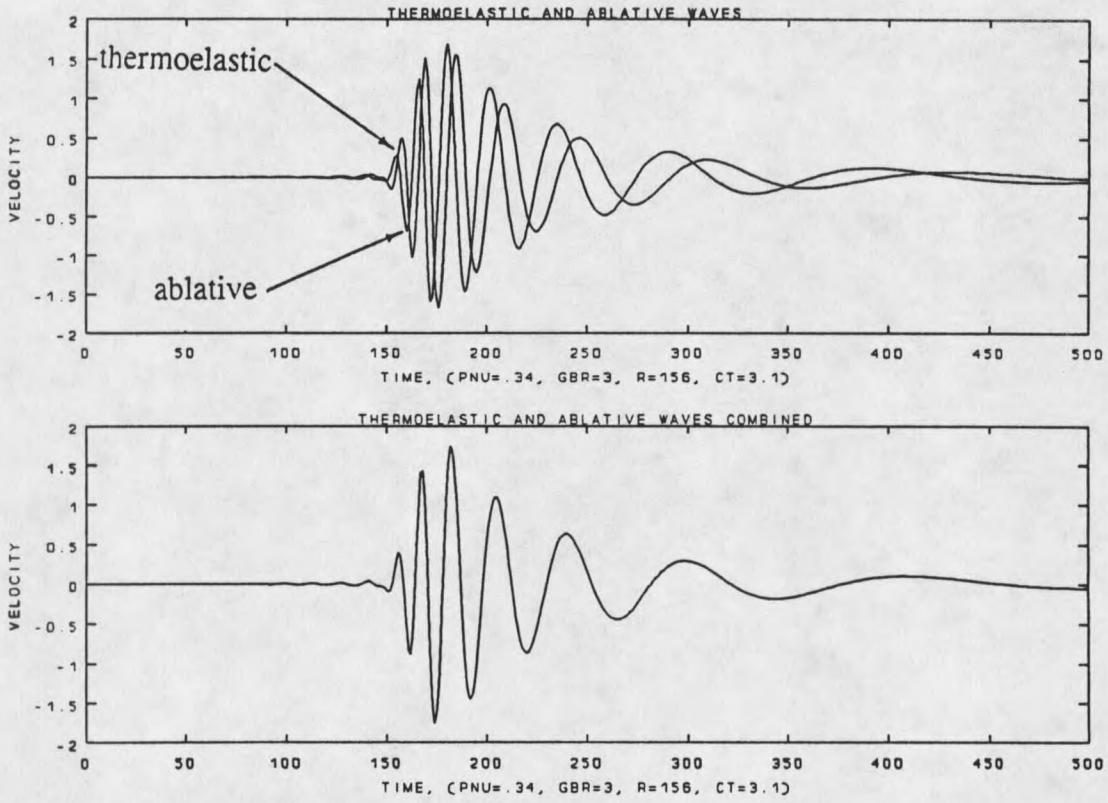

Fig. 23. Thermoelastic and ablative solutions compared. The parameters GBR and R are the same for both solutions.

Comparison to Experimental Data

Experimentally, the combined effects of thermoelastic and ablative waves were investigated for pure brass and stainless steel (SAE 304) samples. Figure 25 shows the variation in amplitude with increasing laser power density for the brass sample. At about 15mj/mm^2 the graph ceases to be linear indicating the formation of plasma[3].

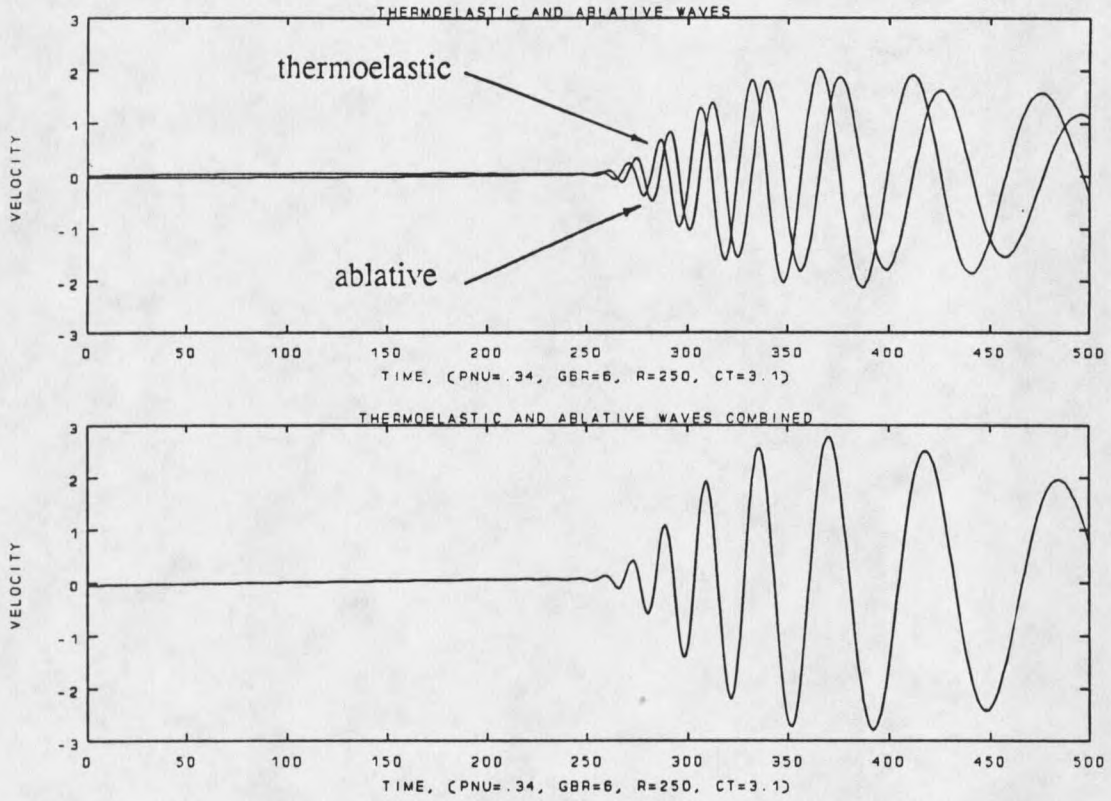

Fig. 24. Thermoelastic and ablative solutions compared. The parameters GBR, and R are the same for both solutions.

Shown in Fig. 26 are Lamb waves generated in a .105 mm thick brass sample. The Lamb waves displayed in the top graph were generated thermoelastically (power density = 12.5mj/mm^2), while the bottom graph displays Lamb waves in the same brass sample that were generated by a thermoelastic and an ablative source (power density = 16.3mj/mm^2). All parameters for both plots in Fig. 26 are the same except the laser power density. The experimental results presented in Fig. 26 seem to confirm the

theoretical results presented in Figs. 23 and 24, namely, ablative waves add constructively to the signal amplitude. If in fact the increase in signal amplitude encountered in the brass sample is due to ablative effects, then the ablative source strength could be experimentally determined by measuring the magnitude of the signal increase.

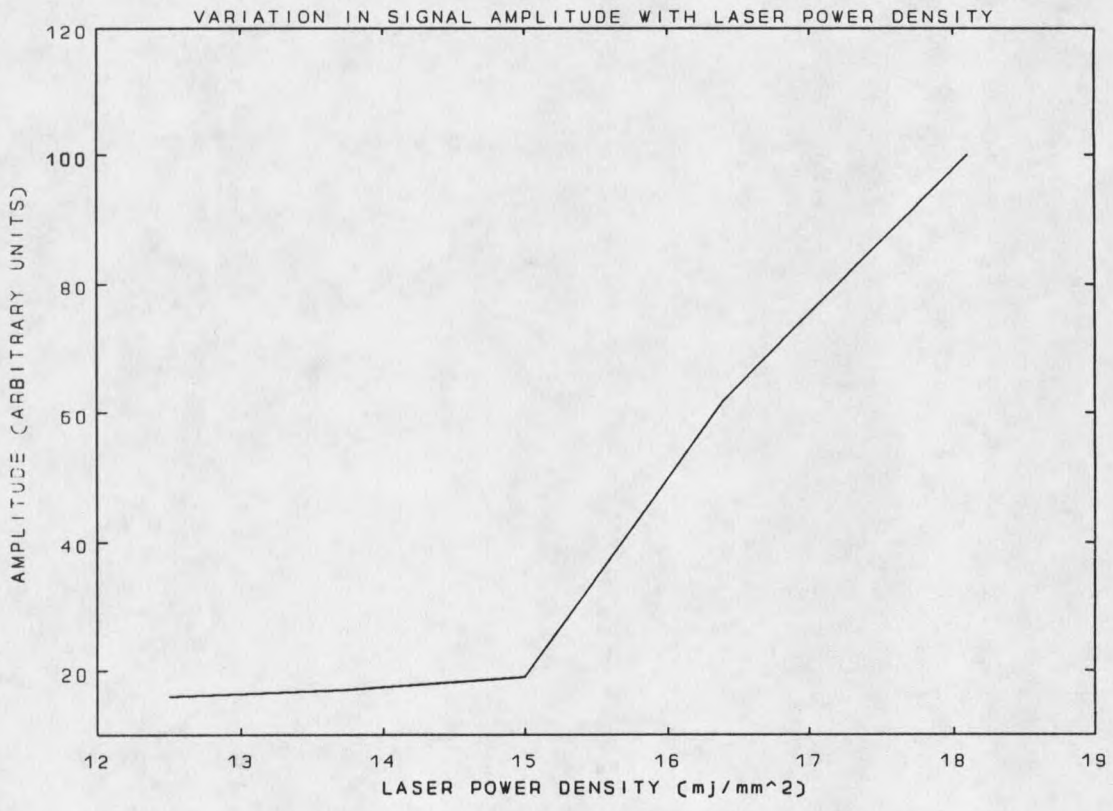

Fig. 25. Average laser power density versus signal amplitude. At 14 mj/mm^2 the graph ceases to be linear indicating the formation of plasma.

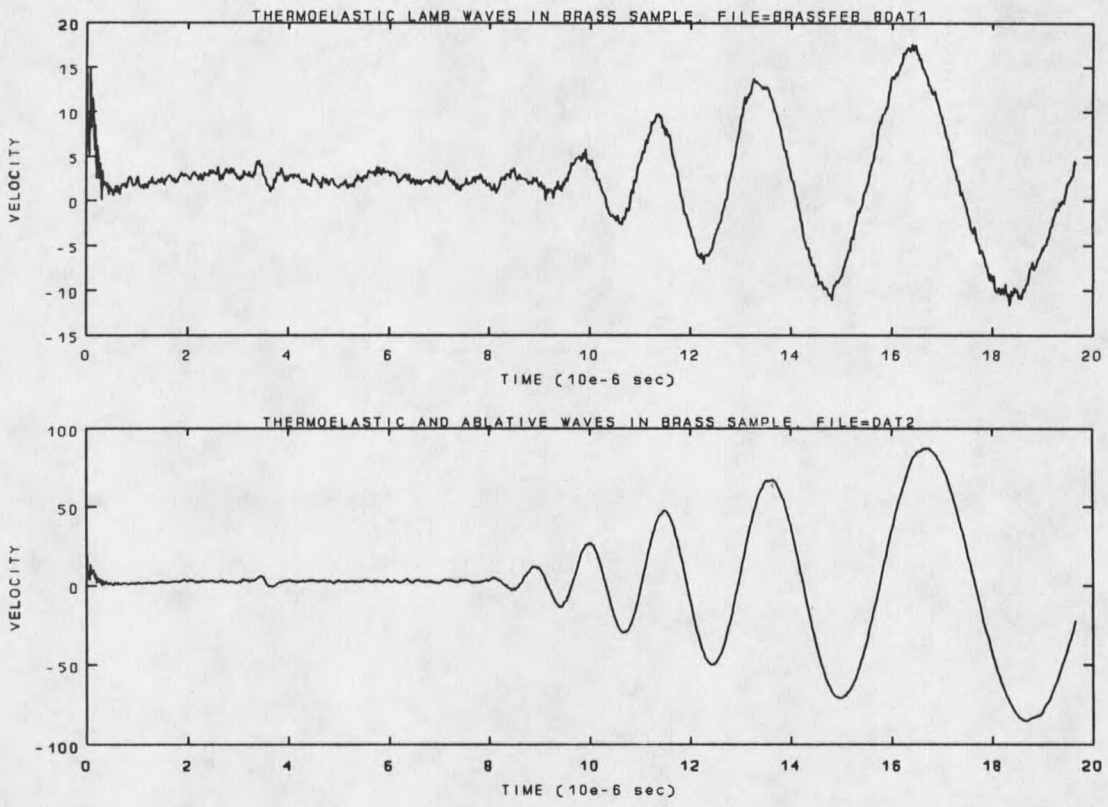

Fig. 26. (Top) Lamb waves produced thermoelastically. (Bottom) Lamb waves due to thermoelastic and ablative effects.

In Fig. 27 the variation in amplitude with increasing laser power for stainless steel has been plotted. For stainless steel, plasma is formed at 7mj. The top graph in Fig. 28 displays Lamb waves in a stainless steel sample that were produced thermoelastically, while the Lamb waves shown in the bottom graph are due to the combined effects of an ablative and a thermoelastic source. The bottom graph in Fig. 28 reveals that there is a wave packet arriving at 5 μs which is not observed in the Lamb waves that were

produced thermoelastically. This initial wave packet appears to destructively interfere with the later arriving larger amplitude wave packet at 7 μs.

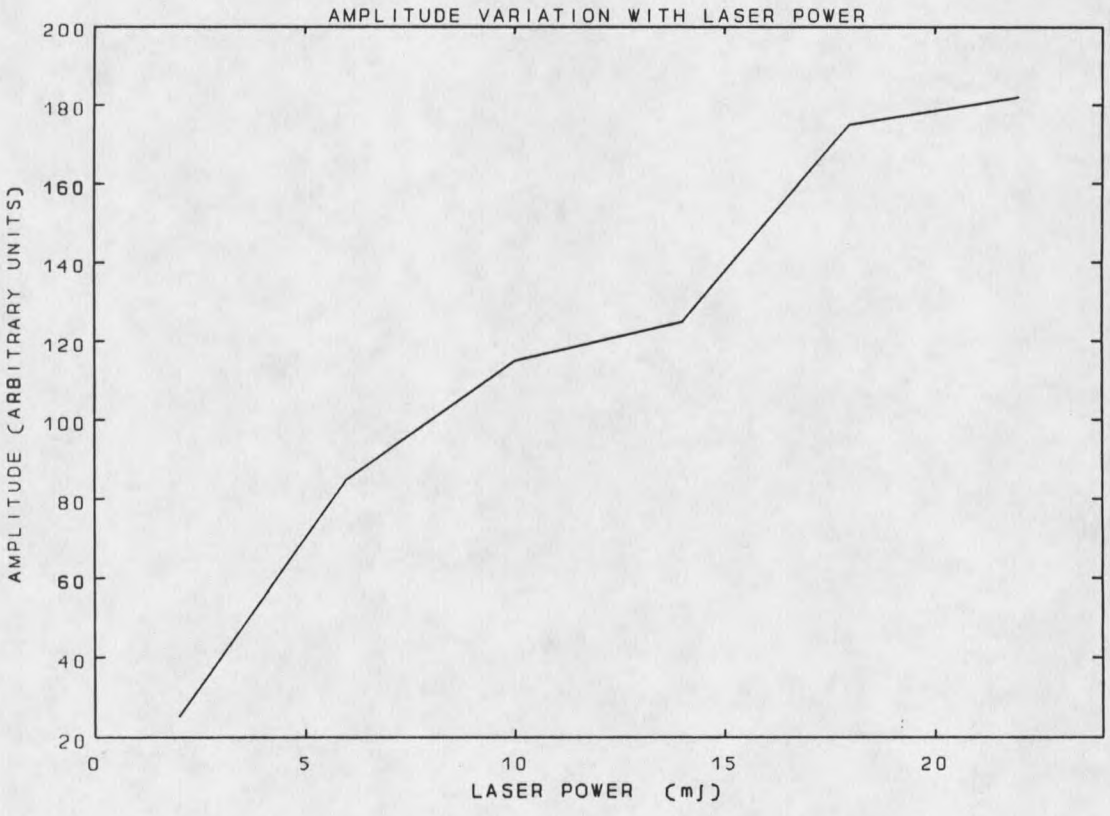

Fig. 27. Laser power density versus signal amplitude. Graph ceases to linear a 7 mj/mm^2 indicating the formation of plasma.

In Fig. 29 and 30 three sets of Lamb waves produced in the stainless steel sample have been plotted with laser power as a parameter. The two data sets shown in Fig. 29 were produced using a laser power of 2 and 10 mj, while the two data sets shown in Fig. 30 were produced using a laser power of 10 and 22 mj. Figures 29 and 30 illustrate that as the laser power is increased, the larger amplitude wave shown in the bottom of Fig.

28 is shifted forward in time. This observation suggests that the onset of ablation causes the thermoelastic wave to be shifted in time resulting in the thermoelastic wave destructively interfering with the ablative wave. This hypothesis is supported theoretically by including a 140 ns time delay for the thermoelastic solution and then combining it with the ablative solution. The theoretical solution prepared in this manner is presented in Fig. 31.

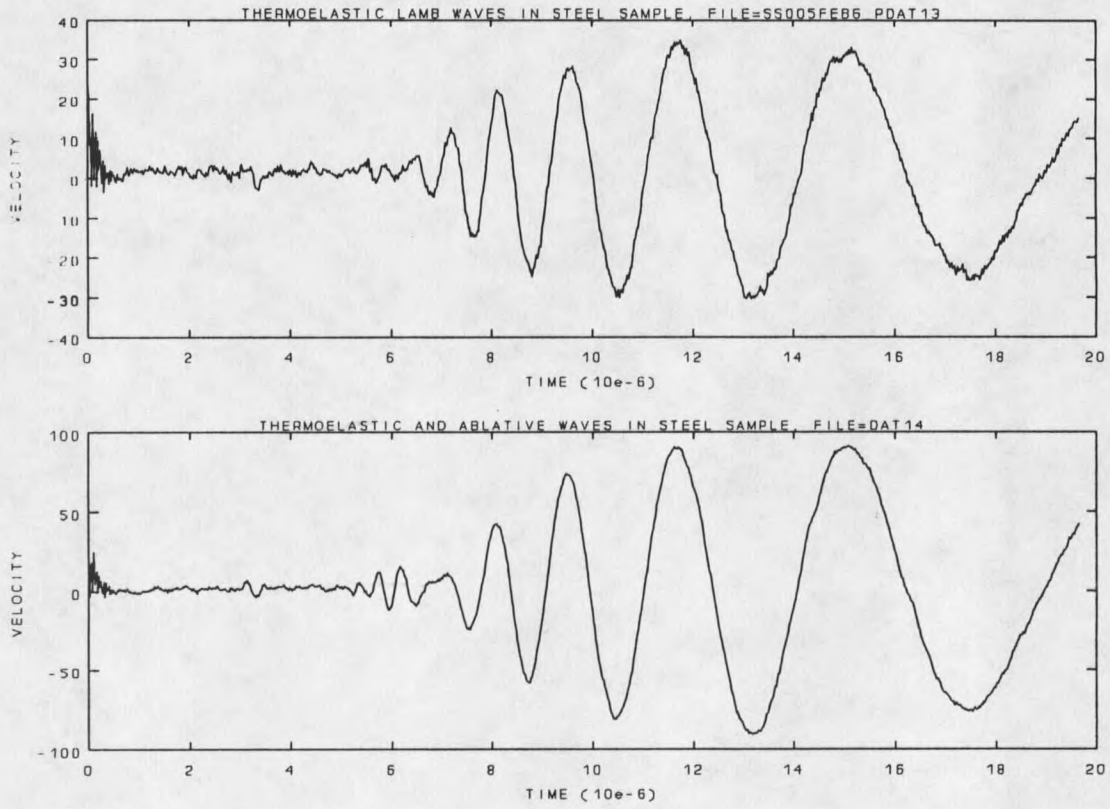

Fig. 28. (Top) Lamb waves produced thermoelastically. (Bottom) Lamb wave due to ablative and thermoelastic effects.

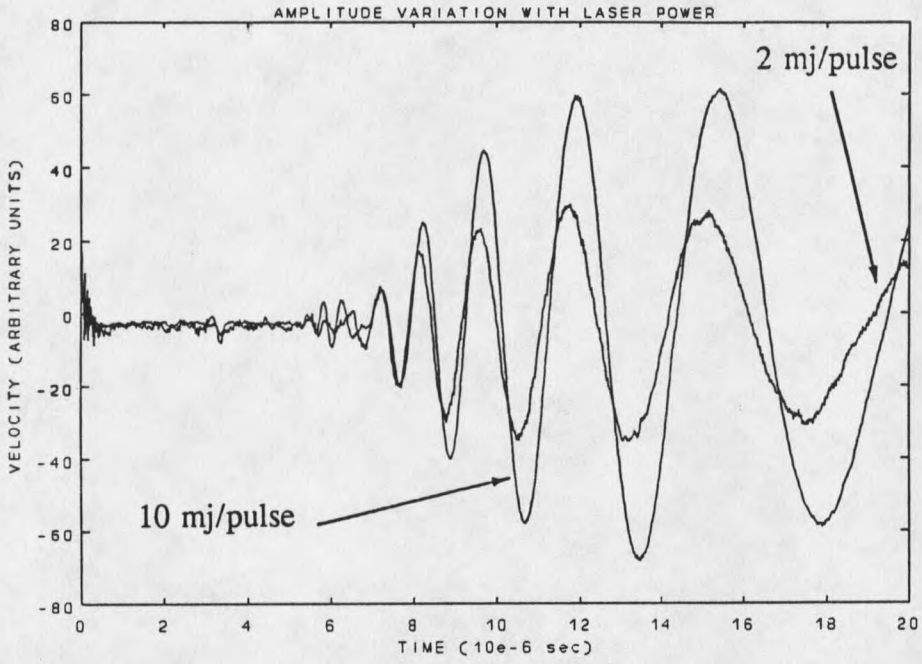

Fig. 29. Thermoelastic wave shifted in time with increase in laser power.

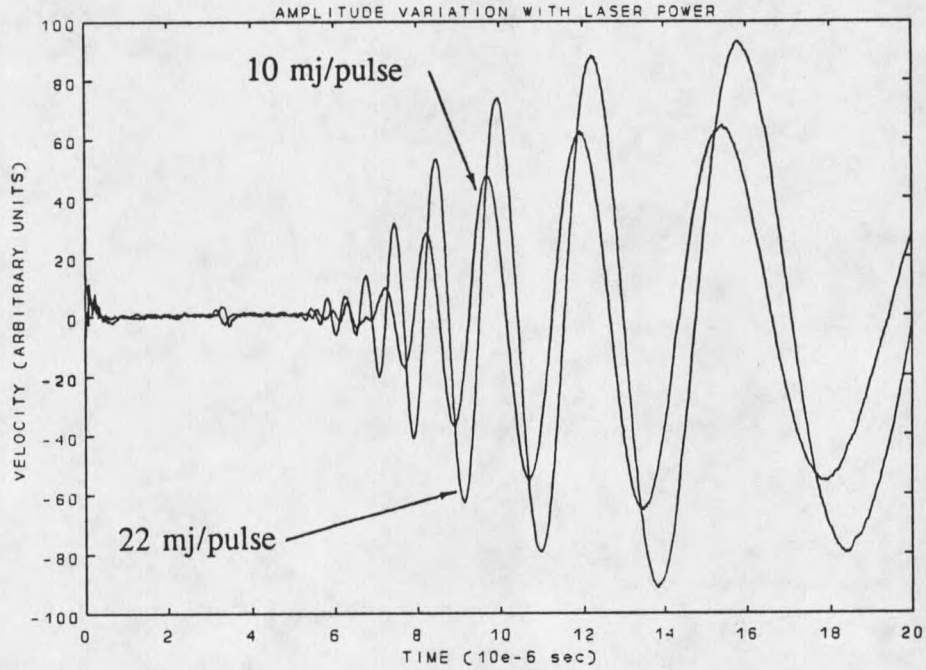

Fig. 30. Thermoelastic wave shifted in time with increase in laser power.

The thermoelastic and ablative solutions combined in Fig. 31 utilize a nondimensional Guassian beam radius of 6 and .1 respectively. The precursor wave packet is composed of high frequencies; thus, in order for the ablative solution to model the precursor wave packet the Guassian beam radius for the ablative solution must be extremely small. The dependence of the a_o Fourier spectrum on GBR was discussed in chapter 5.

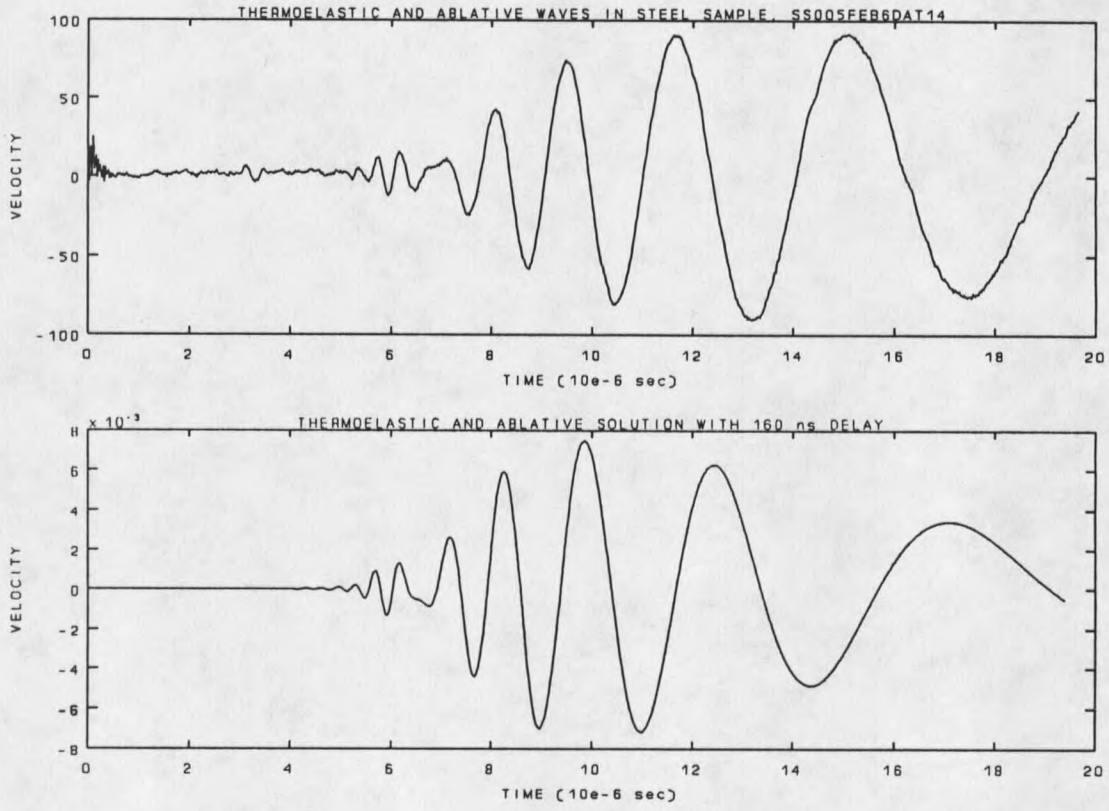

Fig. 31. (Top) Experimental data for stainless steel sample. (Bottom) Theoretical model with 140 ns delay in thermoelastic solution.

Conclusion

For samples such as brass, ablative waves add constructively to the signal, thereby increasing the signal to noise ratio. The onset of ablation in stainless steel samples results in a small precursor wave packet, composed of high frequencies, that destructively interferes with the larger amplitude thermoelastic wave. This peculiar behavior witnessed in stainless steel can be modeled theoretically by including 140 ns time delay for the thermoelastic solution and then combining it with the ablative solution. If in fact the thermoelastic wave is shifted in time, then this unusual phenomenon in stainless steel might be explained by thermal shielding. Thermal shielding results when the plasma produced during ablation impedes the optical absorption of the laser's energy into the specimen. Thus, the temperature increase required to produce thermoelastic waves results from heat conduction from the plasma to the sample instead of optical absorption of the laser's energy. The conduction time would then explain the time delay in the thermoelastic wave. This possible scenario is completed by assuming that the plasma produced in brass samples during ablation does not absorb the laser's energy to the same degree and hence the thermoelastic wave produced in brass results from optical absorption. Valuable insight into the nature of ablation and the plasma produced during ablation may be gained by further investigating the effect of ablation in stainless steel.

REFERENCES CITED

REFERENCES CITED

1. R.M. White, "Elastic Wave Generation by Electron Bombardment or Electromagnetic Wave Absorption", *Journal of Applied Physics*, **34**, 2123-2130 (1963).

2. R.M. White, "Excitation of Surface Elastic Waves by Transient Surface Heating", *Applied Physics Letters*, **12**, 12-15 (1963).

3. A.M. Aindow, R.J. Dewhurst, D.A. Hutchins, and S.B. Palmer, "Laser-Generated Ultrasonic Pulses at Free Metal Surfaces", *Journal of the Acoustical Society of America*, **69**, 449-455 (1981).

4. R.J. Dewhurst, C. Edwards, A.D. Mckie, and S.B. Palmer, "Estimation of the Thickness of Thin Metal Sheet Using Laser Generated Ultrasound", *Applied Physics Letters*, **51**, 1066-1068 (1987).

5. D.A. Hutchins and K. Lundgren, "Quantitative Studies of Lamb Waves in Thin Materials Using Laser Techniques",in *Review of Progress in Quantitative Nondestructive Evaluation*, edited by D.O. Thompson and D.E. Chimenti (Plenum, New York, 1088) **7A**, 79-83.

6. A. Roy, *The Effects of Thermal Diffusion and Optical Absorption on Laser Generated Ultrasonic Waves in a Solid*, M.S. Thesis, Mechanical Engineering, Montana State University (1989).

7. J.F. Ready, *Effects of High Power Laser Radiation*, Academic Press, New York (1971).

8. J.D. Aussel, A Le Brun, and J.C. Baboux, "Generation of Acoustics by Laser: Theory and Experimental Study of Emission Source", *Ultrasonics*, **26**, 245-255 (1988).

9. K.L. Telschow and R.J. Conant, "Optical and Thermal Parameter Effects on Laser-Generated Ultrasound", *Journal of the Acoustical Society of America*, **88**, 1494-1502 (1990).

10. C. Sve and J. Miklowitz, "Thermally Induced Stress Waves in an Elastic Layer", *Journal of Applied Mechanics*, **40**, 161-167 (1973).

REFERENCES CITED-CONTINUED

11. J.L. Nowinski, *Theory of Thermoelasticity with Applications*, Sijthoff and Nordhoff, The Netherlands (1978).

12. R. D. Mindlin, "Influence of Rotatory Inertial and Shear on Flexural Motions of Isotropic, Elastic Plates", *Journal of Applied Mechanics*, **18**, 31 (1951).

13. K.F. Graff, *Wave Motion in Elastic Solids*, Ohio State Press, Columbus (1975).

14. Y.C. Fung, *Foundation of Solid Mechanics*, Prentice-Hall, Englewood Cliffs (1965).

APPENDICES

APPENDIX A
PROGRAM NAME: CECA.M

Fig. 32. Program to calculate the ratio of Ce over Cr versus Poisson's ratio.

```
% THIS M FILES CALCULATES THE RATIO OF CE (SYMMETRIC GROUP VELOCITY AT ZERO
% WAVENUMBER) TO CR (RAYLEIGH VELOCITY) VERSUS POISSON'S RATIO.
%
% THIS M FILE WAS USED TO GENERATE FIGURE 13.
%
% LAST UPDATED 6/3/91

% PNU=POISSON'S RATIO
% CTCL=(SHEAR WAVE VELOCITY)/(LONGITUDINAL WAVE VELOCITY)
% COEF=COEFFICIENTS OF RAYLEIGH EQUATION
% ALPHA=RATIO OF CR (RAYLEIGH VELOCITY)/ CT (SHEAR WAVE VELOCITY)

pnu(1)=.5;
lk=1;
while pnu(lk) > 0
   lk=lk+1;
   pnu(lk)=pnu(lk-1)-.001;
   ctclsq=(1-2*pnu(lk))/(2*(1-pnu(lk)));
   ctcl=sqrt(ctclsq);
   coef=[1, 0, -8, 0, 24-16*ctclsq, 0, -16*(1-ctclsq)];
   rtss=roots(coef);
   alpha=rtss(5);
   ceca(lk-1)=2/alpha*(1-ctclsq)^.5;
end
```

APPENDIX B
PROGRAM NAME: COMBA.M

Fig. 33. Program to calculate the velocity for the ablative problem.

```
% THIS M-FILE CALCULATES THE HANKEL TRANSFORM INVERSION OF THE VELOCITY
% EQUATION AS DEVELOPED BY MINDLIN FOR THE FIRST ASYMMETRIC MODE OF PROPOGATION.
%
% THE FREQUENCY SPECTRUM RESULTING FROM THIS SOLUTION TECHNIQUE WILL USED
% TO INVERT THE HANKEL TRANSFORM IN THE THERMOELASTIC FORMULATION
%
% THIS M-FILE, THRU A CHANGE OF VARIABLES, TRANSFORMS THE HANKEL INVERSION
% INTO A FOURIER INVERSION.  THIS CHANGE OF VARIABLES ALLOWS THE USUAL
% FOURIER ANALYSIS TO BE PERFORMED ON THE RESULTING DISPLACEMENTS.
%
% THE SOURCE FOR THIS CASE IS A NORMAL FORCE AND REPRESENTS AN ABLATIVE SOURCE.
% THE SOURCE FUNCTION IS ASSUMED TO HAVE A DELTA FUNCTION REPRESENTATION
% IN TIME, AND A GUASSIAN DEPENDENCE IN THE RADIAL DIRECTION.
%
% NO ATTEMPT TO CALCULATE ABLATIVE SOURCE STRENGTH HAS BEEN MADE; THEREFORE
% THE AMPLITUDE OF THE ABLATIVE WAVES WILL BE ARBITRARY.

% ASSEMBLE INTEGRAND USING HURLEY'S NOTATION
% FTRANS=FOURIER TRANSFORM OF VELOCITY
N1=2*(alpha^2)*(k.^2)/(1-pnu);
N2=3*(alpha^4);
N3=-(omeg.^2)*(alpha^2);
Ek=(2*(k.^2)*(alpha^2)/(1-pnu))*((1-pnu)/2 + 1/(alpha^2)) + 3*(alpha^2);
N=(N1+N2+N3);
exxp=exp(-(gbra^2)*(k.^2)/4);
fbess=bessel(0,k*r).*wtta;
ftrans=k.*dado.*exxp.*fbess.*windowa'.*(N./((-4*omeg.^3)+2*omeg.*Ek));

% SUM OVER TIME TO CALCULATE ****VELOCITY****
tt=t0;
ntstep=tmax/tinc;
if round(ntstep)==ntstep
   ntstep=ntstep+1;
else
    if (ntstep-round(ntstep))<.5
       ntstep=round(ntstep)+1;
    else
       ntstep=round(ntstep);
    end  % END IF
end  % END IF
for tindex=1:ntstep
    wrt(tindex)=sum(ftrans.*omeg.*cos(omeg*tt));
    tt=tt+tinc;
end;  % END FOR
```

APPENDIX C
PROGRAM NAME: COMBINATION.M

Fig. 34. Program that links COMBA and COMBT and performs routines that are common to COMBA and COMBT.

```
% THIS M-FILE LINKs COMBT, THE M-FILE FOR THE THERMOELASTIC FORMULATION, AND
% COMBA, THE M-FILE FOR THE ABLATIVE FORMULATION.  ALL ROUTINES THAT
% COMMON TO BOTH PROGRAMS WILL BE PERFORMED IN THIS PROGRAM TO SAVE
% COMPUTING TIME.
% THESE ROUTINES INCLUDE:  1.) ASSIGNING AND FITTING PARAMETERS TO
%                              EXPERIMENT.
%                          2.) CALCULATING WINDOWS FUNCTIONS.
%                          3.) CALCULATING WEIGHTS FOR SIMPSONS METHOD.
%                          4.) GRAPHING VELOCITIES.


% ASSIGN PELIMINARY PARAMETERS.
% THESE PARAMETERS ARE DEFINED IN THE INPUT STATEMENTS GIVEN BELOW.
if exist('eta')~=1
   gbrt=.1;
   gbra=.1;
   r=156;
   tmax=310;
   tinc=.775;
   t0=0;
   z=-1;
   eta=.88;
   cle=19.6e-6;
   ccc=840;
   mmm=1;
   intg=1;
   rho=2.6;
   eng=4.82;
end

% FIT PARAMETERS TO EXPERIMENT
setup=1;
while setup~=0
   gbrttxt=num2str(gbrt);
   gbratxt=num2str(gbra);
   rtxt=num2str(r);
   tmaxtxt=num2str(tmax);
   tinctxt=num2str(tinc);
   t0txt=num2str(t0);
   ztxt=num2str(z);
   etatxt=num2str(eta);
   cletxt=num2str(cle);
   ccctxt=num2str(ccc);
   mmmtxt=num2str(mmm);
   intgtxt=num2str(intg);
   rhotxt=num2str(rho);
   engtxt=num2str(eng);


   % DISPLAY CURRENT PARAMETERS
   disp(' ')
   disp(['GBRT=',gbrttxt,'  ','R=',rtxt,'  ','Z=',ztxt,'  ','ETA=',etatxt,...
         '  ','GBRA=',gbratxt]);
   disp(['COEF OF LINEAR EXPANSION=',cletxt,'  ','HEAT CAPACITY=',ccctxt]);
   disp(['TINC=',tinctxt,'     ','T0=',t0txt,'     ','TMAX=',tmaxtxt]);
   disp(['WINDOW SELECTION=',mmmtxt,'  ','FORMULATION SELECTION=',intgtxt]);
   disp(['DENSITY=',rhotxt,'    ','Qo=',engtxt]);
   % PROMPTED FOR CHANGE IN PARAMETERS
   mm=menu('CHOSE PARAMETERS  { 0=CONTINUE }','GBRT',...
   'R','TMAX','TINC','T0','Z','ETA','COEF LINEAR','WINDOW SELECTION',...
   'FORMULATION SELECTION','HEAT CAPACITY','GBRA','RHO','Qo');
   if mm==1
        gbrt=input('DIMENSIONLESS BEAM RADIUS FOR THERMOELASTIC PROBLEM');
   elseif mm==2
        r=input('ENTER DIMENSIONLESS RADIAL POSITION ');
   elseif mm==3
```

Fig. 34. (continued)

```
        tmax=input('ENTER DIMENSIONLESS TIME OF DURATION ');
    elseif mm==4
        tinc=input('ENTER DIMENSIONLESS TIME INCREMENT ');
    elseif mm==5
        t0=input('ENTER DIMENSIONLESS STARTING TIME ');
    elseif mm==6
        z=input('ENTER TOP (-1) OR BOTTOM (1) FOR PLATE POSITION ');
    elseif mm==7
        eta=input('ENTER VALUE FOR DIMENSIONLESS ETA ');
    elseif mm==8
        cle=input('ENTER COEFF. OF LINEAR EXPANSION (1/degree celcius) ');
    elseif mm==9
        mmm=menu('CHOSE A WINDOW','BARTLETT','BLACKMAN','BOXCAR',...
        'HAMMING','HANNING','KAISER');
    elseif mm==10
        intg=menu('CHOSE FORMULATION','THERMOELASTIC','ABLATIVE','BOTH',...
        'THERMO AND ABLATIVE SOLUTIONS ADDED');
    elseif mm==11
        ccc=input('ENTER HEAT CAPAICITY (J/Kg.degree celcius) ');
    elseif mm==12
        gbra=input('DIMENSIONLESS BEAM RADIUS FOR ABLATIVE PROBLEM ');
    elseif mm==13
        rho=input('ENTER DENSITY (g/cm^3) ');
    elseif mm==14
        eng=input('ENTER Qo (J) ');
    elseif mm==0
        setup=0;
    end   % END IF
end   % END WHILE

% COMPUTE WINDOW FUNCTION
% WINDOWA=ASYMMETRIC WINDOWING FUNCTION
if mmm==1
   windowa=bartlett(numomeg);
elseif mmm==2
   windowa=blackman(numomeg);
elseif mmm==3
   windowa=boxcar(numomeg);
elseif mmm==4
   windowa=hamming(numomeg);
elseif mmm==5
   windowa=hanning(numomeg);
elseif mmm==6
   windowa=kaiser(numomeg);
end   % END IF

% ASSEMBLE WEIGHTS FOR SIMPSON'S METHOD
% WTTA=ASYMMETRIC WEIGHTING FUNCTION
wtta=ones(1,numomeg);
wtta(2)=4;
for l=3:(numomeg-1)
    wtta(l)=wtta(l-1)+(2*(-1)^l);
end  % END FOR
wtta=wtta.*(omeginc/3);

% CALCULATE SOURCE STRENGTH
% THERMAG=MAGNITUDE OF THERMOELASTIC SOURCE
tso=(eng*10e6)/((h^3)*pi*rho*ccc*(gbrt^2)*(1-exp(-2*eta)));
thermag=((1+pnu)*tso*(gbrt^2)*cle)/(2*(1-pnu));

% CALL THERMO AND ABLATIVE M-FILES, COMBT AND COMBA RESPECTIVELY
if intg==1
   COMBT
   time=0:tinc:tmax;
   plot(time,watdsp)
   title('THERMOELASTIC DISPLACEMENT')
```

Fig. 34. (continued)

```
elseif intg==2
   COMEA
   time=0:tinc:tmax;
   plot(time,wrt)
   title('ABLATIVE DISPLACEMENT')
elseif intg==3
   COMET
   COMEA
   time=0:tinc:tmax;
   subplot(211)
   plot(time,watdsp)
   title('THERMOELASTIC DISPLACEMENT')
   subplot(212)
   plot(time,wrt)
   title('ABLATIVE DISPLACEMENT')
elseif intg==4
   COMET
   COMEA
   time=0:tinc:tmax;
   plot(time,wrt+watdsp)
   title('THERMO PLUS ABLATIVE DISPLACEMENT')
end   % END IF
```

APPENDIX D
PROGRAM NAME: COMBT.M

Fig. 35. Program to calculate the velocity for the thermoelastic problem.

```
% THIS M-FILE CALCULATES THE HANKLE TRANSFORM INVERSION OF THE VELOCITY
% EQUATION AS DEVELOPED BY MIKLOWITZ AND SVE FOR LAMB WAVES IN PLATES.
% ONLY THIN FILM ARE CONSIDERED. ONLY THE FIRST ASYMMETRIC MODE WILL BE
% CONSIDERED.
% THIS M-FILE USES MINDLIN'S APPROX. DISPERSION RELATIONSHIP (SHEAR
% AND ROTARY INERTIA) TO COMPUTE THE HANKEL INVERSION
% THIS M-FILE THROUGH A CHANGE IN VARIALBES TRANSFORMS THE HANKLE INVERSION
% INTO A FOURIER INVERSION.

% COMPUTE COMMON QUANINTIES FOR INTEGRATION ROUTINE
delsq=(2*(1-pnu)/(1-2*pnu));
epsl=(1-1/delsq);

% ANTISYMMETRIC MODE CALCULATION (USING MIKLOWITZ'S NOTATION)

% CALCULATES BETA 1 & 2
b1a_sqr=(k.^2-omeg.^2./delsq);
b2a_sqr=(k.^2-omeg.^2);
b1a=sqrt(b1a_sqr);
b2a=sqrt(b2a_sqr);

% CALCULATE D's
da1=4*(b2a_sqr + k.^2).*sinh(b1a).*cosh(b2a);
da22=((b2a_sqr + k.^2).^2)./(b1a.*delsq) - 4.*b1a.*k.^2;
da2=da22.*cosh(b1a).*cosh(b2a);
da33=((b2a_sqr + k.^2).^2)./b2a - (4.*b2a.*k.^2)./delsq;
da3=da33.*sinh(b1a).*sinh(b2a);
da44=-4*(k.^2).*(b2a./(b1a.*delsq) + b1a./b2a);
da4=da44.*cosh(b1a).*sinh(b2a);
da=da1+da2+da3+da4;

% CALCULATE G's & M's
g33=(4.*k.^2).*b2a.*sinh(b2a).*(eta^2*(1+exp(-2*eta))/2);
g3=g33-((b2a_sqr+k.^2).^2).*cosh(b2a).*(eta*(1-exp(-2*eta))/2);
m1a=-b1a.*cosh(b1a.*z).*g3;
g44=b1a.*cosh(b1a).*(eta*(1-exp(-2*eta))/2);
g4=g44-sinh(b1a).*(eta^2*(1+exp(-2*eta))/2);
g4=g4.*(b2a_sqr+k.^2);
m2a=-2*(k.^2).*cosh(b2a.*z).*g4;

% PUT IT ALL TOGETHER
% FTNS=FOURIER TRANSFORM OF VELOCITY
denoma=(eta^2 - k.^2 + omeg.^2./delsq);
ma=(m1a+m2a)./(denoma.*(omeg.^2).*da);
wbjok=-2.*exp(-(k.*gbrt/2).^2).*ma.*bessel(0,k.*r).*k;
waintg=wbjok.*wtta.*dadc;
ftrns=omeg.*windowa'.*waintg;

% SUM OVER TIME TO CALCULATE VELOCITY
tt=t0;
ntstep=tmax/tinc;
if round(ntstep)==ntstep
   ntstep=ntstep+1;
else
   if ntstep-round(ntstep)<.5
      ntstep=round(ntstep)+1;
   else
      ntstep=round(ntstep);
   end  % END IF
end   %  END IF
for tindex=1:ntstep   % INTEGRATE ANTISYMMETRIC DYMANIC TERMS ONLY
    watdsp(tindex)=-sum(ftrns.*sin(omeg.*tt));
    watdsp(tindex)=watdsp(tindex)*thermag;
    tt=tt+tinc;
end % END FOR
```

APPENDIX E
PROGRAM NAME: CRCT.M

Fig. 36. Program that calculates the ratio of Cr to Ct for a given Ce.

```
% THIS M FILE CALCULATES CR (RAYLEIGH VELOCITY) VERSUS CT (SHEAR WAVE
% VELOCITY) FOR A GIVEN CE (GROUP VELOCITY OF SYMMETRIC MODE AT ZERO
% WAVENUMBER).
%
% THIS M FILE WAS USED TO GENERATE FIGURE 18.
%
% LAST UPDATED 6/3/91

% PNU=POISSON'S RATIO
% ALPHA=RATIO OF CR (RAYLEIGH VELOCITY)/ CT (SHEAR WAVE VELOCITY)
% COEF=COEFFICIENTS OF RAYLEIGH'S EQUATION

ce=input('ENTER SYMMETRIC WAVE VELOCITY');
pnu(1)=.5;
lk=1;
while pnu(lk) > 0
   ctclsq=(1-2*pnu(lk))/(2*(1-pnu(lk)));
   ctcl=sqrt(ctclsq);
   coef=[1, 0, -8, 0, 24-16*ctclsq, 0, -16*(1-ctclsq)];
   rtss=roots(coef);
   alpha=rtss(5);
   cr(lk)=(ce*alpha)/(2*sqrt(1-ctclsq));
   ct(lk)=ce/(2*sqrt(1-ctclsq));
   pnu(lk+1)=pnu(lk)-.005;
   lk=lk+1;
end
```

APPENDIX F
PROGRAM NAME: GTWYROOT.MEXG

Fig. 37. This program is the main gateway between MLABRT.FOR and MLABRT.MEXG.

```
C
C THIS PROGRAM MUST BE COMPILED USING G_FLOATING QUALIFIER
C
C THIS SUBROUTINE IS THE MAIN GATEWAY FROM MLABRT.FOR TO MLABRT.MEXG.
C WHEN MLABRT.MEXG IS EXECUTED, MATLAB CALLS THE USRFCN SUBROUTINE IN
C THE MLABRT.MEXG FILE. DO NOT MODIFY THIS SUBROUTINE DECLARATION.
C
      SUBROUTINE USRFCN(NLHS,PLHS,NRHS,PRHS)
      INTEGER NLHS,NRHS
      INTEGER*4 PLHS(*),PRHS(*)
C
C DECLARE MEX UTILITY FUNTIONS
C
      INTEGER*4 GETSTR
      INTEGER*4 CRTMAT,REALP,IMAGP,GETGLO,ALREAL,ALINT
      DOUBLE PRECISION GETSCA
C
C DECLARE VARIABLES FOR INTERFACING TO MATLAB
C
      INTEGER*4 PNUP,NMODEP,DELKP,NGQP,SKPAP
      INTEGER*4 KAPPAP,AUXFRQSP,AUXFRQAP
      INTEGER*4 M,N
C
C DECLARE LOCAL VARIABLES
C
      DOUBLE PRECISION PNU,NMODE,DELK,NGQ,SKPA
      DOUBLE PRECISION KAPPA(10000),AUXFRQS(10000),AUXFRQA(10000)
C
C CHECK INPUT AND OUTPUT AURGUMENTS
C
      IF (NRHS.NE.5) THEN
         CALL MEXERR('ROOTS REQUIRES 5 INPUT ARGUMENTS')
      ELSE IF (NLHS.NE.3) THEN
         CALL MEXERR('ROOTS REQUIRES 3 OUTPUT ARGUMENTS')
      END IF
C
C ASSIGN POINTERS TO THE VARIOUS PARAMETERS
C
      PNUP=REALP(PRHS(1))
      NMODEP=REALP(PRHS(2))
      DELKP=REALP(PRHS(3))
      NGQP=REALP(PRHS(4))
      SKPAP=REALP(PRHS(5))
C
C COPY INPUT DATA OUT OF MATLAB VARIABLES INTO LOCAL VARIABLES
C
      CALL CPOUT(PNUP,PNU,1)
      CALL CPOUT(NMODEP,NMODE,1)
      CALL CPOUT(DELKP,DELK,1)
      CALL CPOUT(NGQP,NGQ,1)
      CALL CPOUT(SKPAP,SKPA,1)
C
C NGQ AND NMODE ARE IMPLICITLY DECLARED AS TYPE INTEGER IN ROOT PROGRAM,
C BUT IN USRFNC SUBROUTINE THE VARIABLES ARE DECLARED AS DOUBLE PRECISION.
C INGQ AND INMODE WHERE CREATED TO MAKE PARAMETERS CONSISTANT
C
      INGQ=NGQ
      INMODE=NMODE
C
C CREATE MATICES FOR RETURN AURGUMENTS. THIS SECTION HAS TO COME AFTER
C CPOUT SECTION, BECAUSE INPUT AURGUMENTS DETERMINE DIMENSIONS OF
C OUTPUT MATICES.
C
      PLHS(1)=CRTMAT(INMODE,INGQ,0)
      PLHS(2)=CRTMAT(INMODE,INGQ,0)
      PLHS(3)=CRTMAT(INMODE,INGQ,0)
```

Fig. 37. (continued)

```
C
C ASSIGN POINTERS TO OUTPUT PARAMETERS. THIS MUST ALSO COME AFTER
C CPOUT SECTION.
C
      AUXFRQSP=REALP(PLHS(1))
      AUXFRQAP=REALP(PLHS(2))
      KAPPAP=REALP(PLHS(3))
C
C DO AUCTUAL COMPUTATIONS IN A ROOT SUBROUTINE
C
      CALL ROOT(AUXFRQS,AUXFRQA,KAPPA,PNU,INMODE,DELK,INGQ,SKPA)
C
C COPY DATA FROM THE LOCAL VARIABLES INTO MATLAB RETURN AURGUMENTS
C
      CALL CPIN(AUXFRQS,AUXFRQSP,INGQ*INMODE)
      CALL CPIN(AUXFRQA,AUXFRQAP,INGQ*INMODE)
      CALL CPIN(KAPPA,KAPPAP,INGQ*INMODE)
      RETURN
      END
```

APPENDIX G
PROGRAM NAME: MLABRT.FOR

Fig. 38. Fortran program that calculates the entire Rayleigh-Lamb frequency spectrum.

```
C THIS PROGRAM HAS TO BE COMPILED USING G_FLOATING QUALIFIER
C
C
C CHANGES WHERE MADE TO DR. CONANT'S PROGRAM, ROOT.FOR, IN ORDER TO
C INCORPORATE IT INTO A MEXG FILE.  THE CHANGES CAN BE OUTLINED AS FOLLOWS.
C
C   1.) CHANGED ROOT FROM A SELF CONTAINED PROGRAM TO A SUBROUTINE
C       IN ORDER FOR IT TO BE LINK WITH THE GATEWAY ROUTINE.
C   2.) PNU, NMODE, NGQ, AND DELK WERE CHOSEN AS INPUT AURGUMENTS
C   3.) CALLS TO OUTPUT AND INPUT FILES WERE ELIMINATED
C   4.) GQPOINTS,AND RDINPUT SUBROUTINES WITHIN ROOT SUBROUTINE WERE
C       ELIMINATED
C   5.) CREATE OUTPUT MATRICES AUXFRQS, AUXFRQA, KAPPA.
C
      SUBROUTINE ROOT(AUXFRQS,AUXFRQA,KAPPA,PNU,NMODE,DELK,NGQ,SKPA)
      IMPLICIT DOUBLE PRECISION (A-H, O-Z)
      DOUBLE PRECISION LASTKAPA, KAPPA(NMODE,NGQ), KSQ,FRQS,
     &                 FRQA,AUXFRQS(NMODE,NGQ),AUXFRQA(NMODE,NGQ)
      COMMON / CLCT / DEL, DELSQ
      COMMON / LLLL / LODDS, LEVNS, LODDA, LEVNA
      CHARACTER FLNAM*9
      DATA MAXITER / 40 /
C
C DR. CONANTS INPUT DATA THAT WAS INCORPORATED INTO ROOT.FOR
C
      GER=1.0
      XACC=.0001

      OPEN(10,FILE='OUTFL',STATUS='UNKNOWN')
      OPEN(20,FILE='LOGFILE',STATUS= 'UNKNOWN' )
C
C COMPUTE COMMON QUANTITIES AND INITIALIZE VARIABLES.
C
      FLNAM='OUTFL'
      DELSQ = 2.D0 * (1.D0 - PNU) / (1.D0 - 2.D0 * PNU)
      DEL = DSQRT(DELSQ)
      LODDS = 1
      LEVNS = 2
      LODDA = 1
      LEVNA = 2
      AUXFRQS(1,1) = 0.D0
      AUXFRQA(1,1) = 0.D0
      FRQS=0.D0
      FRQA=0.D0
C
C CALL QPOINTS, THIS SUBROUTINE CALCULATES KAPPA ARRAY
C
      CALL QPOINTS(SKPA, DELK, KAPPA, NGQ,NMODE,NDIM)
C
C COMPUTE FREQUENCY SPECTRUM.
C
      DO 5 MODE = 1, NMODE
         IF (MODE .NE. 1)THEN
            CALL FRQZERO(FRQS,FRQA)
            AUXFRQS(MODE,1)=FRQS
            AUXFRQA(MODE,1)=FRQA
         END IF
         LASTKAPA = 0.D0
         DO 10 I = 1, NGQ
            IF (KAPPA(MODE,I) .EQ. 0. .AND. MODE .EQ. 1) THEN
               AUXFRQS(MODE,I) = 0.D0
               AUXFRQA(MODE,I) = 0.D0
               GO TO 225
            ELSE
               CALL FSPECTRM (FRQS, FRQA, KAPPA(MODE,I), LASTKAPA, XACC,
     1                        SEMIBAND, MAXITER, MODE)
```

Fig. 38. (continued)

```
                AUXFRQS(MODE,I)=FRQS
                AUXFRQA(MODE,I)=FRQA
                GO TO 225
              END IF
  225         WRITE(10,215) KAPPA(MODE,I),AUXFRQS(MODE,I),AUXFRQA(MODE,I)
  215         FORMAT(3(2X,D22.15))
   10       CONTINUE
    5    CONTINUE
        CLOSE(10)
        RETURN
        END
C
C*******************************************************************************
C
      SUBROUTINE QPOINTS(SKPA, DELK, KAPPA, NGQ,NMODE, NDIM)
C
C ESTABLISHES NGQ EQUALLY SPACED INTEGRATION POINTS STARTING WITH SKPA
C AND WITH SPACING DELK.
C
      DOUBLE PRECISION SKPA, DELK, KAPPA(NMODE,NGQ)
C
C
C CHECK THAT NGQ IS ODD.
C
      NGQ2 = NGQ / 2
      IF (2 * NGQ2 .EQ. NGQ) THEN
         WRITE(*, *) 'NGQ = ', NGQ
         WRITE(*, *) 'NUMBER OF INTEGRATION POINTS MUST BE ODD.'
         STOP
      ELSE
      DO 20 K=1,NMODE
         KAPPA(K,1) = SKPA
         DO 10 I = 2, NGQ
            KAPPA(K,I) = KAPPA(K,(I - 1)) + DELK
   10    CONTINUE
   20 CONTINUE
      RETURN
      END IF
      END
C
C ROOT.FOR
C
C
C-------------------------------------------------------------------------------
C
      SUBROUTINE FRQZERO (FZROS, FZROA)
C
C       ********************************************************************
C       *                                                                  *
C       *   This subroutine calculates the frequencies corresponding       *
C       *   to a wavenumber of zero for the number of SYMMETRIC modes      *
C       *   specified and arranges them in a monotonically increasing      *
C       *   sequence.                                                      *
C       *                                                                  *
C       *                                                                  *
C       *      ********  ALL VARIABLES ARE DIMENSIONLESS  ********        *
C       *                                                                  *
C       *                                                                  *
C       *         DEL     = Ratio of longitudinal to transverse            *
C       *                   wave speed.                                    *
C       *                                                                  *
C       *         FZRO    = Array of frequencies corresponding to          *
C       *                   a wavenumber of zero.                          *
C       *                                                                  *
C       *         IMODE   = Current mode.                                  *
C       *                                                                  *
```

Fig. 38. (continued)

```
C       *         LEVN    = Counting index for "even" modes.          *
C       *                                                             *
C       *         LODD    = Counting index for "odd" modes.           *
C       *                                                             *
C       *         MAXMODE = Dimension of array FZRO.                  *
C       *                                                             *
C       *         NMODE   = Number of modes requested.                *
C       *                                                             *
C       ***************************************************************
C
      IMPLICIT DOUBLE PRECISION (A-H,O-Z)
      COMMON / CLCT / DEL, DELSQ
      COMMON / LLLL / LODDS, LEVNS, LODDA, LEVNA
      PI = 3.14159265358979
C
C Calculate FZROS for both an "odd" and an "even" mode and use the
C smaller of the two values as the next element in the sequence.
C
        IF (DEL * DFLOAT(LODDS) .LT. DFLOAT(LEVNS)) THEN
           FZROS = DEL * DFLOAT(LODDS) * PI / 2.D0
           LODDS = LODDS + 2
        ELSE
           FZROS = DFLOAT(LEVNS) * PI / 2.D0
           LEVNS = LEVNS + 2
        END IF
C
C Calculate FZROA for both an "odd" and an "even" mode and use the
C smaller of the two values as the next element in the sequence.
C
        IF (DEL * DFLOAT(LEVNA) .LT. DFLOAT(LODDA)) THEN
           FZROA = DEL * DFLOAT(LEVNA) * PI / 2.D0
           LEVNA = LEVNA + 2
        ELSE
           FZROA = DFLOAT(LODDA) * PI / 2.D0
           LODDA = LODDA + 2
        END IF
      RETURN
      END
C
C-------------------------------------------------------------------------------
C
      SUBROUTINE FSPECTRM (FRQS, FRQA, KAPPA, LASTKAPA, XACC, SEMIBAND,
     1           MAXITER, MODE)
C
C       ***************************************************************
C       *                                                             *
C       *   This subroutine calculates the frequency vs. wavenumber   *
C       *   curve for both SYMMETRIC and ANTISYMMETRIC modes.  Fre-   *
C       *   quencies for a given wavenumber are determined by         *
C       *   Newton's method.  Starting frequencies for Newton's       *
C       *   method are determined by a linear extrapolation of the    *
C       *   previous solution.                                        *
C       *                                                             *
C       *                                                             *
C       *      ********  ALL VARIABLES ARE DIMENSIONLESS  ********     *
C       *                                                             *
C       *                                                             *
C       *         DELSQ    = Square of the ratio of longitudinal to   *
C       *                    transverse wave speed.                   *
C       *                                                             *
C       *         DFDFREQ  = Partial derivative of f wrt frequency.   *
C       *                                                             *
C       *         DFDKPA   = Partial derivative of f wrt wavenumber.  *
C       *                                                             *
C       *         DKPA     = Wavenumber increment.                    *
```

Fig. 38. (continued)

```
C      *                                                                *
C      *         FREQ     = Roots of the frequency equation for a       *
C      *                    given wavenumber.                           *
C      *                                                                *
C      *         KPA      = Wavenumber.                                 *
C      *                                                                *
C      *         KSQ      = Square of the wavenumber.                   *
C      *                                                                *
C      *         MAXITER  = Maximum number of iterations used in        *
C      *                    Newton's method.                            *
C      *                                                                *
C      *         SEMIBAND = Range of search above and below             *
C      *                    the starting frequency, STRTFRQ.            *
C      *                                                                *
C      *         STRTFRQ =  Starting frequency used in Newton's         *
C      *                    method.                                     *
C      *                                                                *
C      *         X1       =  Maximum frequency in search.               *
C      *                                                                *
C      *         X2       =  Minimum frequency in search.               *
C      *                                                                *
C      *         XACC     =  Approximate number of significant          *
C      *                    digits of accuracy desired in Newton's      *
C      *                    method.                                     *
C      *                                                                *
C      ******************************************************************
C
       IMPLICIT DOUBLE PRECISION (A-H,O-Z)

       COMMON / WAVNUMBR / KPA
       COMMON / CLCT / DEL, DELSQ
       DOUBLE PRECISION KPA, KSQ, LASTKAPA, KAPPA
       DIMENSION IFLAG(2)
       EXTERNAL FDFS, FDFA
       PI = 3.14159265358979
       SEMIBAND = 2.0D0
C
C
       KPA = LASTKAPA
       DKPA = .1D0
C      Calculate frequency vs. wavenumber curve.
C
       DO 10 I = 1, 1000
C
C
          IF (KPA + .1D0 .GE. KAPPA) THEN
             DKPA = KAPPA - KPA
          END IF
C
C      Determine starting frequency to be used in Newton's method for the
C      next wavenumber, based on the current frequency and wavenumber.
C      The first expression, which applies when both frequency and wavenumber
C      are zero, is found in Achenbach's book, p. 229, eq. 6.82.
C
          KSQ = KPA ** 2
C
          IF (KPA .EQ. 0.D0 .AND. FRQS .EQ. 0.D0) THEN
             STRTFRQS = 2.D0 * DSQRT((DELSQ - 1.D0) / DELSQ) * DKPA
             STRTFRQA = 2.D0 * DSQRT((DELSQ - 1.D0) / (3.D0 * DELSQ)) *
     1                  DKPA ** 2
          ELSE
             STRTFRQS = FRQS - DKPA * DFDKPAS(FRQS) / DFDFRQS(FRQS)
             STRTFRQA = FRQA - DKPA * DFDKPAA(FRQA) / DFDFRQA(FRQA)
          ENDIF
C
```

Fig. 38. (continued)

```
C     Set limits on search range.
C
          X1S = STRTFRQS + SEMIBAND
          X2S = STRTFRQS - SEMIBAND
          X1A = STRTFRQA + SEMIBAND
          X2A = STRTFRQA - SEMIBAND
C
C     Update wavenumber.
C
          KPA = KPA + DKPA
*
*    Initialize max iteration exceed flag.
*
        IFLAG(1) = 0
        IFLAG(2) = 0
*
C
C     Find corresponding frequency.
C
          FRQATMP = del * kpa
          delfrqa1 = frqatmp - strtfrqa
          delfrqa = delfrqa1
          FRQS = RTNEWTDP(FDFS, X1S, X2S, XACC, MAXITER, iflag, 1)
  100     FRQA = RTNEWTDP(FDFA, X1A, X2A, XACC, MAXITER, iflag, 2)
*
*    This section of code recomputes starting frequency for antisymmetric
*    modes.  It is specifically designed for problems near the line
*    frqa = del * kpa.
*
          if (iflag(2) .gt. 0 .and. iflag(2) .le. 10) then
             if ((iflag(2) / 2) * 2 .eq. iflag(2)) then
                delfrqa = - dfloat((iflag(2) + 2)/ 2) * delfrqa1
             else
                delfrqa = - delfrqa
             end if
             strtfrqa = frqatmp - delfrqa
             X1A = STRTFRQA + SEMIBAND
             X2A = STRTFRQA - SEMIBAND
*c           WRITE(*, 1000) MODE, KPA, STRTFRQA
             go to 100
          else if (iflag(2) .gt. 10) then
             PAUSE 'Can''t seem to find the root!'
          end if
*
*
          IF (KPA .EQ. KAPPA) THEN
             LASTKAPA = KAPPA
             RETURN
          END IF
    10 CONTINUE
       RETURN
       END
C
C-------------------------------------------------------------------------------
C
       SUBROUTINE FDFS (X, FS, DFS)
C
C     This subroutine calculates the function fs(x) for symmetric
C     modes and its derivative with respect to x, both of which are
C     used by the subprogram RTNEWTDP.
C
C     This subroutine is called by RTNEWTDP.
C
       IMPLICIT DOUBLE PRECISION (A-H,O-Z)
C
       FS = FUNCS(X)
```

Fig. 38. (continued)

```
      DFS = DFDFRQS(X)
      RETURN
      END
C
C-------------------------------------------------------------------------------
C
      DOUBLE PRECISION FUNCTION FUNCS(X)
C
C     This routine calculates the function fs(x, y) for symmetric modes.
C
      IMPLICIT DOUBLE PRECISION (A-H,O-Z)
      COMMON / WAVNUMBR / KPA
      COMMON / CLCT / DEL, DELSQ
      DOUBLE PRECISION KPA, KSQ, KB, KBSQ
C
      XSQ = X ** 2
      KSQ = KPA ** 2
C
      IF (X .GT. DEL * KPA) GO TO 100
      IF (X .GE. KPA .AND. X .LE. DEL * KPA) GO TO 200
      IF (X .LT. KPA) GO TO 300
C
  100 A = DSQRT(XSQ / DELSQ - KSQ)
      B = DSQRT(XSQ - KSQ)
      BSQ = B ** 2
      F1 = (KSQ - BSQ) ** 2 * DSIN(B) * DCOS(A)
      F2 = 4.D0 * KSQ * A * B * DSIN(A) * DCOS(B)
      FUNCS = F1 + F2
      RETURN
C
  200 A = DSQRT(KSQ - XSQ / DELSQ)
      B = DSQRT(XSQ - KSQ)
      BSQ = B ** 2
      F1 = (KSQ - BSQ) ** 2 * DSIN(B) * DCOSH(A)
      F2 = - 4.D0 * KSQ * A * B * DSINH(A) * DCOS(B)
      FUNCS = F1 + F2
      RETURN
C
  300 A = DSQRT(KSQ - XSQ / DELSQ)
      B = DSQRT(KSQ - XSQ)
      BSQ = B ** 2
      F1 = (KSQ + BSQ) ** 2 * DSINH(B) * DCOSH(A)
      F2 = - 4.D0 * KSQ * A * B * DSINH(A) * DCOSH(B)
      FUNCS = F1 + F2
      RETURN
      END
C
C-------------------------------------------------------------------------------
C
      DOUBLE PRECISION FUNCTION DFDFRQS(X)
C
C     This routine calculates the partial derivative of the function
C     fs(x,y) with respect to x, for symmetric modes.
C
      IMPLICIT DOUBLE PRECISION (A-H,O-Z)
      COMMON / WAVNUMBR / KPA
      COMMON / CLCT / DEL, DELSQ
      DOUBLE PRECISION KPA, KSQ, KB, KBSQ
C
      XSQ = X ** 2
      KSQ = KPA ** 2
C
      IF (X .GT. DEL * KPA) GO TO 100
      IF (X .GE. KPA .AND. X .LE. DEL * KPA) GO TO 200
      IF (X .LT. KPA) GO TO 300
C
```

Fig. 38. (continued)

```
  100 A = DSQRT(XSQ / DELSQ - KSQ)
      B = DSQRT(XSQ - KSQ)
      BSQ = B ** 2
      KB = KSQ - BSQ
      KBSQ = KB ** 2
      F1 = - 4.D0 * KB * DSIN(B) * DCOS(A)
      F2 = (KBSQ / B + 4.D0 * KSQ * B / DELSQ) * DCOS(B) * DCOS(A)
      F3 = - (KBSQ / (DELSQ * A) + 4.D0 * KSQ * A) * DSIN(A) * DSIN(B)
      F4 = 4.D0 * KSQ * (B / (DELSQ * A) + A / B) * DSIN(A) * DCOS(B)
      DFDFRQS = X * (F1 + F2 + F3 + F4)
      RETURN
C
  200 A = DSQRT(KSQ - XSQ / DELSQ)
      B = DSQRT(XSQ - KSQ)
      BSQ = B ** 2
      KB = KSQ - BSQ
      KBSQ = KB ** 2
      F1 = - 4.D0 * KB * DSIN(B) * DCOSH(A)
      F2 = (KBSQ / B + 4.D0 * KSQ * B / DELSQ) * DCOS(B) * DCOSH(A)
      F3 = - (KBSQ / (DELSQ * A) - 4.D0 * KSQ * A) * DSINH(A) * DSIN(B)
      F4 = 4.D0 * KSQ * (B / (DELSQ * A) - A / B) * DSINH(A) * DCOS(B)
      DFDFRQS = X * (F1 + F2 + F3 + F4)
      RETURN
C
  300 A = DSQRT(KSQ - XSQ / DELSQ)
      B = DSQRT(KSQ - XSQ)
      BSQ = B ** 2
      KB = KSQ + BSQ
      KBSQ = KB ** 2
      F1 = - 4.D0 * KB * DSINH(B) * DCOSH(A)
      F2 = (- KBSQ / B + 4.D0 * KSQ * B / DELSQ) * DCOSH(B) * DCOSH(A)
      F3 = - (KBSQ / (DELSQ * A) - 4.D0 * KSQ * A) * DSINH(A) * DSINH(B)
      F4 = 4.D0 * KSQ * (B / (DELSQ * A) + A / B) * DSINH(A) * DCOSH(B)
      DFDFRQS = X * (F1 + F2 + F3 + F4)
      RETURN
      END
C
C-------------------------------------------------------------------------------
C
      DOUBLE PRECISION FUNCTION DFDKPAS(X)
C
C     This routine calculates the partial derivative of the function
C     fs(x,y) with respect to y, for symmetric modes.
C
      IMPLICIT DOUBLE PRECISION (A-H,O-Z)
      COMMON / WAVNUMBR / KPA
      COMMON / CLCT / DEL, DELSQ
      DOUBLE PRECISION KPA, KSQ, KB, KBSQ
C
      XSQ = X ** 2
      KSQ = KPA ** 2
C
      IF (X .GT. DEL * KPA) GO TO 100
      IF (X .GE. KPA .AND. X .LE. DEL * KPA) GO TO 200
      IF (X .LT. KPA) GO TO 300
C
  100 A = DSQRT(XSQ / DELSQ - KSQ)
      B = DSQRT(XSQ - KSQ)
      BSQ = B ** 2
      KB = KSQ - BSQ
      KBSQ = KB ** 2
      ABBA = A / B + B / A
      F1 = 8.D0 * KB * DSIN(B) * DCOS(A)
      F2 = - (KBSQ / B + 4.D0 * KSQ * B) * DCOS(A) * DCOS(B)
      F3 = (KBSQ / A + 4.D0 * KSQ * A) * DSIN(A) * DSIN(B)
      F4 = 4.D0 * (2.D0 * A * B - KSQ * ABBA) * DSIN(A) * DCOS(B)
```

Fig. 38. (continued)

```
      DFDKPAS = KPA * (F1 + F2 + F3 + F4)
      RETURN
C
  200 A = DSQRT(KSQ - XSQ / DELSQ)
      B = DSQRT(XSQ - KSQ)
      BSQ = B ** 2
      KB = KSQ - BSQ
      KBSQ = KB ** 2
      ABBA = - A / B + B / A
      F1 = 8.D0 * KB * DSIN(B) * DCOSH(A)
      F2 = - (KBSQ / B + 4.D0 * KSQ * B) * DCOSH(A) * DCOS(B)
      F3 = (KBSQ / A - 4.D0 * KSQ * A) * DSINH(A) * DSIN(B)
      F4 = - 4.D0 * (2.D0 * A * B + KSQ * ABBA) * DSINH(A) * DCOS(B)
      DFDKPAS = KPA * (F1 + F2 + F3 + F4)
      RETURN
C
  300 A = DSQRT(KSQ - XSQ / DELSQ)
      B = DSQRT(KSQ - XSQ)
      BSQ = B ** 2
      KB = KSQ + BSQ
      KBSQ = KB ** 2
      ABBA = A / B + B / A
      F1 = 8.D0 * KB * DSINH(B) * DCOSH(A)
      F2 = (KBSQ / B - 4.D0 * KSQ * B) * DCOSH(A) * DCOSH(B)
      F3 = (KBSQ / A - 4.D0 * KSQ * A) * DSINH(A) * DSINH(B)
      F4 = - 4.D0 * (2.D0 * A * B + KSQ * ABBA) * DSINH(A) * DCOSH(B)
      DFDKPAS = KPA * (F1 + F2 + F3 + F4)
      RETURN
      END
C
C*********************************************************************
C
      SUBROUTINE FDFA (X, FA, DFA)
C
C     This subroutine calculates the function fa(x) for antisymmetric
C     modes and its derivative with respect to x, both of which are
C     used by the subprogram RTNEWTDP.
C
C     This subroutine is called by RTNEWTDP.
C
      IMPLICIT DOUBLE PRECISION (A-H,O-Z)
C
      FA = FUNCA(X)
      DFA = DFDFRQA(X)
      RETURN
      END
C
C*********************************************************************
C
      DOUBLE PRECISION FUNCTION FUNCA(X)
C
C     This routine calculates the function fa(x, y) for antisymmetric
C     modes.
C
      IMPLICIT DOUBLE PRECISION (A-H,O-Z)
      COMMON / WAVNUMBR / KPA
      COMMON / CLCT / DEL, DELSQ
      DOUBLE PRECISION KPA, KSQ, KB, KBSQ
C
      XSQ = X ** 2
      KSQ = KPA ** 2
C
      IF (X .GT. DEL * KPA) GO TO 100
      IF (X .GE. KPA .AND. X .LE. DEL * KPA) GO TO 200
      IF (X .LT. KPA) GO TO 300
C
```

Fig. 38. (continued)

```
  100 A = DSQRT(XSQ / DELSQ - KSQ)
      B = DSQRT(XSQ - KSQ)
      BSQ = B ** 2
      F1 = (KSQ - BSQ) ** 2 * DCOS(B) * DSIN(A)
      F2 = 4.D0 * KSQ * A * B * DCOS(A) * DSIN(B)
      FUNCA = F1 + F2
      RETURN
C
  200 A = DSQRT(KSQ - XSQ / DELSQ)
      B = DSQRT(XSQ - KSQ)
      BSQ = B ** 2
      F1 = (KSQ - BSQ) ** 2 * DCOS(B) * DSINH(A)
      F2 = 4.D0 * KSQ * A * B * DCOSH(A) * DSIN(B)
      FUNCA = F1 + F2
      RETURN
C
  300 A = DSQRT(KSQ - XSQ / DELSQ)
      B = DSQRT(KSQ - XSQ)
      BSQ = B ** 2
      F1 = (KSQ + BSQ) ** 2 * DCOSH(B) * DSINH(A)
      F2 = - 4.D0 * KSQ * A * B * DCOSH(A) * DSINH(B)
      FUNCA = F1 + F2
      RETURN
      END
C
C*********************************************************************
C
      DOUBLE PRECISION FUNCTION DFDFRQA(X)
C
C     This routine calculates the partial derivative of the function
C     fa(x,y) with respect to x, for antisymmetric modes.
C
      IMPLICIT DOUBLE PRECISION (A-H,O-Z)
      COMMON / WAVNUMBR / KPA
      COMMON / CLCT / DEL, DELSQ
      DOUBLE PRECISION KPA, KSQ, KB, KBSQ
C
      XSQ = X ** 2
      KSQ = KPA ** 2
C
      IF (X .GT. DEL * KPA) GO TO 100
      IF (X .GE. KPA .AND. X .LE. DEL * KPA) GO TO 200
      IF (X .LT. KPA) GO TO 300
C
  100 A = DSQRT(XSQ / DELSQ - KSQ)
      B = DSQRT(XSQ - KSQ)
      BSQ = B ** 2
      KB = KSQ - BSQ
      KBSQ = KB ** 2
      F1 = - 4.D0 * KB * DCOS(B) * DSIN(A)
      F2 = - (KBSQ / B + 4.D0 * KSQ * B / DELSQ) * DSIN(B) * DSIN(A)
      F3 = (KBSQ / (DELSQ * A) + 4.D0 * KSQ * A) * DCOS(A) * DCOS(B)
      F4 = 4.D0 * KSQ * (B / (DELSQ * A) + A / B) * DCOS(A) * DSIN(B)
      DFDFRQA = X * (F1 + F2 + F3 + F4)
      RETURN
C
  200 A = DSQRT(KSQ - XSQ / DELSQ)
      B = DSQRT(XSQ - KSQ)
      BSQ = B ** 2
      KB = KSQ - BSQ
      KBSQ = KB ** 2
      F1 = - 4.D0 * KB * DCOS(B) * DSINH(A)
      F2 = - (KBSQ / B + 4.D0 * KSQ * B / DELSQ) * DSIN(B) * DSINH(A)
      F3 = - (KBSQ / (DELSQ * A) - 4.D0 * KSQ * A) * DCOSH(A) * DCOS(B)
      F4 = - 4.D0 * KSQ * (B / (DELSQ * A) - A / B) * DCOSH(A) * DSIN(B)
      DFDFRQA = X * (F1 + F2 + F3 + F4)
```

Fig. 38. (continued)

```
      RETURN
C
  300 A = DSQRT(KSQ - XSQ / DELSQ)
      B = DSQRT(KSQ - XSQ)
      BSQ = B ** 2
      KB = KSQ + BSQ
      KBSQ = KB ** 2
      F1 = - 4.D0 * KB * DCOSH(B) * DSINH(A)
      F2 = - (KBSQ / B - 4.D0 * KSQ * B / DELSQ) * DSINH(B) * DSINH(A)
      F3 = - (KBSQ / (DELSQ * A) - 4.D0 * KSQ * A) * DCOSH(A) * DCOSH(B)
      F4 = 4.D0 * KSQ * (B / (DELSQ * A) + A / B) * DCOSH(A) * DSINH(B)
      DFDFRQA = X * (F1 + F2 + F3 + F4)
      RETURN
      END
C
C*******************************************************************************
C
      DOUBLE PRECISION FUNCTION DFDKPAA(X)
C
C     This routine calculates the partial derivative of the function
C     fa(x,y) with respect to y, for antisymmetric modes.
C
      IMPLICIT DOUBLE PRECISION (A-H,O-Z)
      COMMON / WAVNUMBR / KPA
      COMMON / CLCT / DEL, DELSQ
      DOUBLE PRECISION KPA, KSQ, KB, KBSQ
C
      XSQ = X ** 2
      KSQ = KPA ** 2
C
      IF (X .GT. DEL * KPA) GO TO 100
      IF (X .GE. KPA .AND. X .LE. DEL * KPA) GO TO 200
      IF (X .LT. KPA) GO TO 300
C
  100 A = DSQRT(XSQ / DELSQ - KSQ)
      B = DSQRT(XSQ - KSQ)
      BSQ = B ** 2
      KB = KSQ - BSQ
      KBSQ = KB ** 2
      ABBA = A / B + B / A
      F1 = 8.D0 * KB * DCOS(B) * DSIN(A)
      F2 = (KBSQ / B + 4.D0 * KSQ * B) * DSIN(A) * DSIN(B)
      F3 = - (KBSQ / A + 4.D0 * KSQ * A) * DCOS(A) * DCOS(B)
      F4 = 4.D0 * (2.D0 * A * B - KSQ * ABBA) * DCOS(A) * DSIN(B)
      DFDKPAA = KPA * (F1 + F2 + F3 + F4)
      RETURN
C
  200 A = DSQRT(KSQ - XSQ / DELSQ)
      B = DSQRT(XSQ - KSQ)
      BSQ = B ** 2
      KB = KSQ - BSQ
      KBSQ = KB ** 2
      ABBA = - A / B + B / A
      F1 = 8.D0 * KB * DCOS(B) * DSINH(A)
      F2 = (KBSQ / B + 4.D0 * KSQ * B) * DSINH(A) * DSIN(B)
      F3 = (KBSQ / A - 4.D0 * KSQ * A) * DCOSH(A) * DCOS(B)
      F4 = 4.D0 * (2.D0 * A * B + KSQ * ABBA) * DCOSH(A) * DSIN(B)
      DFDKPAA = KPA * (F1 + F2 + F3 + F4)
      RETURN
C
  300 A = DSQRT(KSQ - XSQ / DELSQ)
      B = DSQRT(KSQ - XSQ)
      BSQ = B ** 2
      KB = KSQ + BSQ
      KBSQ = KB ** 2
      ABBA = A / B + B / A
```

Fig. 38. (continued)

```
      F1 = 8.D0 * KB * DCOSH(B) * DSINH(A)
      F2 = (KBSQ / B - 4.D0 * KSQ * B) * DSINH(A) * DSINH(B)
      F3 = (KBSQ / A - 4.D0 * KSQ * A) * DCOSH(A) * DCOSH(B)
      F4 = - 4.D0 * (2.D0 * A * B + KSQ * ABBA) * DCOSH(A) * DSINH(B)
      DFDKPAA = KPA * (F1 + F2 + F3 + F4)
      RETURN
      END
C
C*******************************************************************************
C
C
C       ****************************
C       *                          *
C       *     DOUBLE PRECISION     *
C       *                          *
C       ****************************
C
      FUNCTION RTNEWTDP(FUNCD,X1,X2,XACC,JMAX, iflag, ii)
C
      IMPLICIT DOUBLE PRECISION (A-H,O-Z)
      dimension iflag(2)
C
      IF (JMAX .LT. 20) JMAX = 20
      RTNEWTDP=.5D0*(X1+X2)
      DO 11 J=1,JMAX
       CALL FUNCD(RTNEWTDP,F,DF)
       DX=F/DF
       RTNEWTDP=RTNEWTDP-DX
       IF((X1-RTNEWTDP)*(RTNEWTDP-X2).LT.0.D0)PAUSE 'jumped out of brack
     *ets'
       IF(ABS(DX).LT.XACC) then
       iflag(ii) = 0
       RETURN
       end if
11    CONTINUE
      IF (ii .EQ. 2) WRITE(20, 5)
    5 FORMAT('RTNEWTDP exceeding maximum iterations')
      write(*, *) 'RTNEWTDP exceeding maximum iterations'
      iflag(ii) = iflag(ii) + 1
      RETURN
      END
```

APPENDIX H
PROGRAM NAME: MOMENTSPEC.M

Fig. 39. Program to calculate Mindlin's a_0 frequency spectrum.

```
% THIS M-FILE CALCULATED MINDLIN'S APPROXIMATE DISPERSION RELATION
% FOR THE FIRST ASYMMETRIC MODE IN AN INFINITE PLATE.  BOTH SHEAR AND
% ROTARY INERTIA WERE TAKEN INTO ACCOUNT.

% ASSIGN PELIMINARY PARAMETERS
% PARAMETERS DEFINED IN INPUT SECTION OF THIS PROGRAM
pnu=.34;
fqmax=10;
numomeg=701;
ct=3.1;
h=.14;

% FIT PARAMETERS TO EXPERIMENT
setup=1;
while setup == 1
   pnutxt=num2str(pnu);
   fqmaxtxt=num2str(fqmax);
   numomegtxt=num2str(numomeg);
   cttxt=num2str(ct);
   htxt=num2str(h);
   % DISPLAY CURRENT PARAMETERS
   disp(' ');
   disp(['PNU=',pnutxt,' ','FQMAX=',fqmaxtxt,' ','NUMOMEG=',numomegtxt]);
   disp(['CT=',cttxt,' ','H=',htxt]);
   disp(' ');
   % PROMPT FOR CHANGE IN PARAMETERS
   mm=menu('CHOSE PARAMETERS { 0=CONTINUE } ','PNU','FQMAX',...
         'NUMOMEG','CT','H');
   if mm==1
      pnu=input('ENTER VALUE FOR POISSON RATIO ');
   elseif mm==2
      fqmax=input('ENTER CUTOFF FRQUENCY (HZ) ');
   elseif mm==3
      numomeg=input('ENTER NUMBER OF INTEGRATION POINTS ');
   elseif mm==4
      ct=input('ENTER SHEAR WAVE VELOCITY ');
   elseif mm==5
      h=input('ENTER PLATE THICKNESS (mm) ');
   elseif mm== 0;
      setup=0;
   end;  %END IF
end; % END WHILE

% CALCULATE SHEAR CORRECTION COEFFICIENT SO THAT PHASE VELOCITY GOES TO
% RAYLEIGH VELOCITY IN THE LIMIT AS WAVENUMBER GOES TO INFINITY
% CTCL=RATIO OF SHEAR WAVE VELOCITY TO LONGITUDINAL VELOCITY
% ALPHA=RATIO OF SHEAR WAVE VELOCITY TO RAYLEIGH VELOCITY
ctclsq=(1-2*pnu)/(2*(1-pnu));
ctcl=sqrt(ctclsq);
coeff=[1,0,-8,0,(24-16*ctclsq),0,-16*(1-ctclsq)];
rts=roots(coeff);
alpha=rts(5);

% GENERATE FREQUENCY ARRAY
% (OMEG=FREQUENCY)
omegmax=fqmax*h/ct;
omeginc=omegmax/numomeg;
omeg=omeginc:omeginc:omegmax;

% GENERATE WAVE NUMBER ARRAY BY SOLVING MINDLIN FREQUENCY
% EQUATION FOR THE FIRST ASYMMETRIC MODE.
% (WAVENUMBER=K)
omeg2=omeg.^2;
omeg4=omeg.^4;
k1=omeg2*((1-pnu)/2 + 1/(alpha^2))/2;
k2=(3*(1-pnu)*omeg2)/2;
```

Fig. 39. (continued)

```
k3=((1-pnu)*omeg4)/(2*(alpha^2));
k4=k2-k3;
k=sqrt(k1 + sqrt(k1.^2 + k4));

% CALCULATE (DELTA K/DELTA OMEG)=DADO, THIS EXPRESSION IS USED TO
% CHANGE VARIABLES IN THE HANKEL IVERSION OF BOTH THE THERMOELASTIC AND
% ABLATIVE FORMULATION.
dado1=2*k1./omeg;
dado2=2*k2./omeg -4*k3./omeg;
dado=(dado1 + (2*k1.*dado1 + dado2)./(2*(k1.^2 + k4).^.5))./(2*k);

% PLOT WAVE NUMBER VS FREQUENCY
plot(k,omeg);
title(['DISPERSION RELATIONSHIP PNU=',pnutxt]);
xlabel('DIMESIONLESS FREQUENCY (K*H)');
ylabel('DIMESIONLESS FREQUENCY (OMEGA*H/Ct)');
```

APPENDIX I
PROGRAM NAME: PLOTFRQ.M

Fig. 40. Program that plots frequency spectrum generated by MLABRT.MEXG.

```
%  THIS MFILE PLOT DIMENSIONLESS FREQUENCY VS DIMENSIONLESS
%  WAVENUMBER
%
%  THIS M FILE CALLS MLABRT, A MEXG FILE THAT CALCULATES THE ROOTS OF THE
%  RAYLEIGH LAMB FREQUENCY EQUATION USING MLABRT.FOR, A FORTRAN ROUTINE
%  CREATED BY DR CONANT.
%
%  LAST UPDATED 6/3/91

%  FRQA=ASYMMETRIC FREQUENCY
%  FRQS=SYMMETRIC FREQUENCY
%  KAP=WAVENUMBER
%  ALL REMAINING VARIABLES ARE DEFINED IN THE INPUT STATEMENTS GIVEN BELOW.

pnu=input('ENTER POISSONS RATIO ')
nmode=input('ENTER NUMBER OF MODES YOU WANT PLOTTED ')
delk=input('ENTER STEP SIZE ')
ngq=input('ENTER NUMBER OF INTEGRQTION POINTS ')
skpa=input('ENTER STARTING WAVE NUMBER ')
xmax=ngq*delk;

[frqs,frqa,kap]=mlabrt(pnu,nmode,delk,ngq,skpa);  %CALL MEX FILE CONTAINING ROOT
.FOR
frqs=frqs';
frqa=frqa';
kap=kap';

for n=1:nmode
    if n==1
       hold off;
    else
       hold on;
    end  %END IF
    plot(kap(1:ngq,n),frqs(1:ngq,n),kap(1:ngq,n),frqa(1:ngq,n))
end  %END FOR

xlabel('DIMENSIONLESS WAVE NUMBER (KD)');
ylabel('DIMENSIONLESS FREQUENCY (OMEGA)');
title(['DISPERSION RELATIONSHIP (PNU=',num2str(pnu),')']);
grid;
```

APPENDIX J
PROGRAM NAME: PNNNU.M

Fig. 41. Program to calculate Poisson's ratio from Ce and Cr.

```
% THIS M FILE CALCULATES POISSON'S RATIO IF CE (THE SYMMETRIC GROUP
% VELOCITY AT ZERO WAVENUMBER) AND CR (RAYLEIGH VELOCITY) ARE KNOWN
%
% THIS M FILE WAS USED TO GENERATE TABLES 1 THROUGH 4
%
% LAST UPDATED 6/3/91

% PNU=POISSON'S RATIO
% CTCL=RATIO OF CT (SHEAR WAVE VELOCITY) TO CL (LONGITUDINAL VELOCITY)
% RMDR=REMAINDER OF EQUATION 5.6
% ALPHA=RATIO OF CR/CT

ce=input('ENTER SYMMETRIC WAVE VELOCITY ');
ca=input('ENTER ANTISYMMETRIC WAVE VELOCITY ');
pnu=.5;
rmdr(1)=.2;
lk=1;
while rmdr(lk) > .01
   pnu=pnu-.001;
   lk=lk+1;
   ctclsq=(1-2*pnu)/(2*(1-pnu));
   ctcl=sqrt(ctclsq);
   coef=[1, 0, -8, 0, 24-16*ctclsq, 0, -16*(1-ctclsq)];
   rtss=roots(coef);
   alpha=rtss(5);
   rmdr(lk)=-ce*alpha+2*ca*sqrt(1-ctclsq);
   rmdr(lk)=abs(rmdr(lk));
end
```